Strojniški vestnik
Journal of Mechanical Engineering

no. 10
year 2022
volume 68

Strojniški vestnik – Journal of Mechanical Engineering (SV-JME)

Aim and Scope
The international journal publishes original and (mini)review articles covering the concepts of materials science, mechanics, kinematics, thermodynamics, energy and environment, mechatronics and robotics, fluid mechanics, tribology, cybernetics, industrial engineering and structural analysis.
The journal follows new trends and progress proven practice in the mechanical engineering and also in the closely related sciences as are electrical, civil and process engineering, medicine, microbiology, ecology, agriculture, transport systems, aviation, and others, thus creating a unique forum for interdisciplinary or multidisciplinary dialogue.
The international conferences selected papers are welcome for publishing as a special issue of SV-JME with invited co-editor(s).

Editorial Office
University of Ljubljana, Faculty of Mechanical Engineering
SV-JME, Aškerčeva 6, SI-1000 Ljubljana, Slovenia
Phone: 386 (0)1 4771 137
Fax: 386 (0)1 2518 567
info@sv-jme.eu, http://www.sv-jme.eu

Print: Demat d.o.o., printed in 250 copies

Founders and Publishers
University of Ljubljana, Faculty of Mechanical Engineering, Slovenia
University of Maribor, Faculty of Mechanical Engineering, Slovenia
Association of Mechanical Engineers of Slovenia
Chamber of Commerce and Industry of Slovenia, Metal Processing Industry Association

President of Publishing Council
Mihael Sekavčnik
University of Ljubljana, Faculty of Mechanical Engineering, Slovenia

Vice-President of Publishing Council
Bojan Dolšak
University of Maribor, Faculty of Mechanical Engineering, Slovenia

Cover:
Blockchain technology enables interaction between otherwise competing manufacturing entities to satisfy increasing customer demands in a trustful way. However, existing blockchain networks are facing limitations, which are defined by the trade-off between scalability, decentralization, and security. The scalability of the blockchain network is defined as the ability of the network to support an increasing load of transactions and it is lower compared to the non-blockchain systems.

Image Courtesy:
Photo by NASA on Unsplash, from https://unsplash.com/s/photos; Blockchain Logo Vectors by Vecteezy, from *https://www.vecteezy.com/free-vector/blockchain-logo*

ISSN 0039-2480, ISSN 2536-2948 (online)

General information
Strojniški vestnik – Journal of Mechanical Engineering is published in 11 issues per year (July and August is a double issue).

Institutional prices include print & online access: institutional subscription price and foreign subscription €100,00 (the price of a single issue is €10,00); general public subscription and student subscription €50,00 (the price of a single issue is €5,00). Prices are exclusive of tax. Delivery is included in the price. The recipient is responsible for paying any import duties or taxes. Legal title passes to the customer on dispatch by our distributor. Single issues from current and recent volumes are available at the current single-issue price. To order the journal, please complete the form on our website. For submissions, subscriptions and all other information please visit: *http://www.sv-jme.eu*.

You can advertise on the inner and outer side of the back cover of the journal. The authors of the published papers are invited to send photos or pictures with short explanation for cover content.

We would like to thank the reviewers who have taken part in the peer-review process.

The journal is subsidized by Slovenian Research Agency.

SV-JME is indexed / abstracted in: SCI-Expanded, Compendex, Inspec, ProQuest-CSA, SCOPUS, TEMA. The list of the remaining bases, in which SV-JME is indexed, is available on the website.

Strojniški vestnik - Journal of Mechanical Engineering is available on *https://www.sv-jme.eu*.

Contents

Strojniški vestnik - Journal of Mechanical Engineering
volume 68, (2022), number 10
Ljubljana, October 2022
ISSN 0039-2480

Published monthly

Papers

Nejc Rožman, Marko Corn, Gašper Škulj, Janez Diaci, Primož Podržaj: Scalability Solutions in Blockchain-Supported Manufacturing: A Survey 585
Mateusz Wrzochal, Stanisław Adamczak, Ryszard Domagalski, Grzegorz Piotrowicz, Sylwester Wnuk: A New Device Proposed for the Industrial Measurement of Rolling Bearing Friction Torque 610
Marcin Trajer, Łukasz Pyclik, Jerzy Robert Sobiecki: The Nickel Aluminide Coatings Obtained on Small Holes Produced with the EDD Method 623
Volodymyr Brazhenko, Yibo Qiu, Jiancheng Cai, Dongyun Wang: Thermal Evaluation of Multilayer Wall with a Hat-Stringer in Aircraft Design 635
Hla Gharib, György Kovács: Development of a New Expert System for Diagnosing Marine Diesel Engines Based on Real-Time Diagnostic Parameters 642

Strojniški vestnik - Journal of Mechanical Engineering 68(2022)10, 585-609
DOI:10.5545/sv-jme.2022.355
Review Scientific Paper
Received for review: 2022-09-02
Received revised form: 2022-09-26
Accepted for publication: 2022-09-26

Scalability Solutions in Blockchain-Supported Manufacturing: A Survey

Nejc Rožman* – Marko Corn – Gašper Škulj – Janez Diaci – Primož Podržaj[1]
University of Ljubljana, Faculty of Mechanical Engineering, Slovenia

Researchers in the field of smart manufacturing have recognized the benefits of blockchain technology, which solves the trust problem in the open network without relying on any trusted third party. Blockchain technology enables interaction between otherwise competing manufacturing entities to satisfy increasing customer demands in a trustful way. However, existing blockchain networks are facing limitations, which are defined by the trade-off between scalability, decentralization, and security. The scalability of the blockchain network is defined as the ability of the network to support an increasing load of transactions and it is lower compared to the non-blockchain systems. In order to omit the effects of the limitations, scalability solutions are being presented. This research reviews the literature in the field of blockchain-supported manufacturing concerning scalability solutions. The selected literature has been reviewed and classified according to the type of scalability solution. For each type of scalability solution, the main features of the concepts and connection between blockchain technology and manufacturing system are highlighted and discussed. The main findings of the study are that Layer 1 scalability solutions are better represented in the literature and are predominating in the case of general smart manufacturing systems, whereas Layer 2 scalability solutions are better represented in the case of specific smart manufacturing systems. Based on insights obtained from the presented analysis, future directions and open issues regarding the scalability limitations and solutions in blockchain-supported manufacturing are presented.
Keywords: blockchain, manufacturing, scalability, trilemma

Highlights
- *The literature on scalability solutions in blockchain-supported manufacturing does not follow the trends of publications in the field of scalability solutions.*
- *Most solutions employ the consensus mechanism, off-chain solutions, or optimize blockchain structures.*
- *Layer 1 scalability solutions are better represented than Layer 2 solutions. Layer 1 solutions are predominating in the case of general smart manufacturing systems and Layer 2 in specific smart manufacturing systems.*
- *The research on scalability limitations in blockchain-supported manufacturing is increasing and improving over time.*
- *Major open issue with the literature proposed solutions is a lack of implementation in the industry and insufficient analysis of the scalability trilemma in connection with practical limitations.*

0 INTRODUCTION

In recent years, we have witnessed an increase in the literature introducing blockchain technology in the field of manufacturing [1]. Technological advances and the stringent requirements of Industry 4.0 have resulted in new concepts of smart manufacturing systems. Manufacturing systems are formed into complex organizational networks that take advantage of a high level of digitized manufacturing segments to meet as many diverse customers' needs as possible [2]. Individual manufacturing activities are packaged in services that are available on shared virtual platforms (service-oriented architecture) [3]. By connecting through such organized networks, manufacturers can meet a larger number and more diverse market requirements. As there are interactions between production entities that have different owners, the problem of trust in the operation of the system arises. Typically, centrally managed platforms that allowed the integration of production entities were identified as weaknesses in the system, mainly from a security perspective [4].

Blockchain technology, which was implemented in response to the manipulations of centralized organizations in the banking system, is presented as an answer to the problem of ensuring trust between competing entities participating in global networks [4]. In conjunction with smart manufacturing networks, it can ensure that interactions between individual entities in the system are recorded, in a self-executing manner, in a transparent and immutable blockchain maintained by a decentralized network [5]. So far, these features have been used in manufacturing to address various cyber security issues in smart manufacturing systems (SMS) to increase trust in the system [6].

However, blockchain technology also has certain limitations. The limitations of blockchain technology are represented by the scalability trilemma [7]. Similar to the consistency, availability, and partition tolerance (CAP) theorem [8] in the traditional field of the distributed system, a trade-off occurs between three blockchain network properties, namely:

*Corr. Author's Address: University of Ljubljana, Faculty of Mechanical Engineering, Aškerčeva 6, 1000 Ljubljana, Slovenia, nejc.rozman@fs.uni-lj.si

scalability, security, and decentralization. In the currently existing major public blockchain networks (e.g. Bitcoin, Ethereum), it has repeatedly happened that the network failed to process a large increase of transaction requests resulting in much longer waiting times than usual for transactions to be processed. Scalability limitations of blockchain technology thus affected the operation of the blockchain-supported systems [9]. Due to the limited transaction throughput, pending transactions are waiting longer in line to be confirmed. Priority in line is defined by a set transaction fee, therefore, the transaction fee increases due to the competition for faster confirmation. The reduced number of nodes storing the whole ever-growing blockchain results in delays when querying data from the blockchain.

Global manufacturing networks are big and a large number of interactions between entities can be assumed. This, in turn, means that the traditional approach of implementing blockchain technology in manufacturing systems would not satisfy the performance requirements and at the same time ensure decentralization and security (which creates the trust). For example, if the frequency of incoming transactions from the manufacturing system exceeds the frequency of transaction confirmation of the blockchain network (e.g. Ethereum confirms 15 transactions per second), the manufacturing system would be affected by the scalability limitations of the blockchain technology. However, scalability solutions have already been presented in the field of blockchain technology, which can increase scalability or enable the change of blockchain network properties according to the trilemma and thus offer different properties according to user requirements.

There are already several published literature reviews on the topic of integrating blockchain technology into manufacturing. A survey was made regarding different aspects of the engineering and manufacturing processes where researchers or developers have already proposed or applied blockchain [1]. Similar research was conducted regarding the existing blockchain applications in Industry 4.0 and industrial internet of things (IIoT) settings [10]. Another survey discusses the research progress of blockchain-secured smart manufacturing and how blockchain technology is applied to address cybersecurity issues in the smart manufacturing system [6]. The research was also presented regarding the literature on achieving sustainability by employing blockchain technology in manufacturing systems and product lifecycle management [11].

However, so far no one has discussed how the presented concepts of blockchain-supported manufacturing take into account the constraint on scalability that blockchain technology introduces into manufacturing. In this paper, a review of the literature on the scalability solutions applied in blockchain-supported manufacturing is presented. The main contributions of the paper are summarized as follows:

- Literature addressing the problem of scalability and scalability solutions in blockchain-supported manufacturing is identified and classified according to existing scalability solutions. The main features of emerging concepts are presented.
- The literature is analyzed regarding the type of scalability solutions, the type of manufacturing system, and the extent of concept presentation.
- Based on the analysis, future directions and open issues in research regarding the scalability limitations in blockchain-supported manufacturing are given.

1 BLOCKCHAIN TECHNOLOGY IN MANUFACTURING

1.1 Blockchain Technology

A blockchain is a distributed database where an ordered list of various records is stored on. Records are stored in blocks connected through links in form of a chain [12]. The links between blocks are made with the use of asymmetric cryptography [13]. Each record in the blockchain made by a user is signed with a set of encryption keys that are self-managed and unique [14]. Nodes in the blockchain network are communicating with each other to establish synchronization of the written data in the blockchain.

The key properties of the blockchain network are:

- decentralized consensus,
- immutability of the records,
- transparent database,
- self-executing environment.

The first key property of the blockchain network is its ability to reach a consensus among the nodes in the network (solving Byzantine generals problems [15]). Consensus must be reached for every change of data written on the blockchain (e.g. new transaction). The consensus mechanism represents democratic voting on the changes of the written records on the blockchain and it further means that all of the written changes of the blockchain were made in agreement of the majority of the participants in the transaction confirmation on the blockchain network. This coordination between nodes in the network instills trust that the data in the blockchain was written correctly and without

tempering, [16]. There exist two types of blockchain networks that are distinguished according to how openness to participation in the consensus mechanism is defined, namely: permissioned and permissionless [17]. Permissioned networks allow only selected confirmators to join the consensus mechanism and permissionless allow anyone to join the consensus process in the network.

Because of the decentralized consensus, tampering with existing data written on the blockchain is almost impossible. It is only possible if the majority of the nodes in the network agree to the changes. Therefore, blockchain technology offers immutability of the records [18]. Again, there exist two types of blockchain networks regarding access to the usage of the blockchain network and the access to the data written on the blockchain, namely: private and public [19]. Private blockchain networks have a strictly defined list of users that can create new transactions and have access to the written transactions on the blockchain. Public blockchain networks on the other side enable anyone to create transactions and the whole blockchain is publicly accessible. In both types of blockchain networks, users that have access to the blockchain can verify which blockchain data was written and when it was written on the blockchain, meaning that blockchain technology provides a transparent database.

The last key property of blockchain technology is that it enables a self-executing environment. By providing a virtual environment on the blockchain network, developers can code an assortment of automated procedures into digital transactions [20]. These programs are named smart contracts and are digital contracts allowing terms contingent on the decentralized consensus that is tamper-proof and typically self-enforcing through automated execution [21]. By employing smart contracts, different procedures directly related to the change of written data on the blockchain can be executed automatically.

Observing diverse blockchain networks leads to the conclusion that blockchain networks are unable to scale effectively [22], the networks are susceptible to various security vulnerabilities [18], and are prone to centralization [23]. These observations and research conclusions about the current state of blockchain networks were being joined into a single idea named the scalability trilemma (Fig. 1) [24] and [25]. One definition of the Trilemma states that when someone is trying to optimize a blockchain-supported system, there exists a trade-off between three important properties: scalability, decentralization, and security [7].

Table 1. *Definition of blockchain network properties terms*

Term	Definition
Scalability	The ability of the blockchain network to support an increasing load of transactions [26].
Decentralization	The number of nodes in the blockchain network participating in the process of transaction confirmation [27].
Security	The ability of the blockchain network to defend itself against attackers with a certain amount of resources [28].

For example, adding a centralized coordinator into the system to increase the speed of the consensus process would result in a more centralized system. Another example, shortening the block interval can increase the transaction throughput but also affects the security of the whole system because nodes are not synchronized. Therefore, balancing or even achieving these three aspects of the blockchain system well is essential for the future development of blockchain that is suitable for more complex and larger-scale scenes in our daily lives [29].

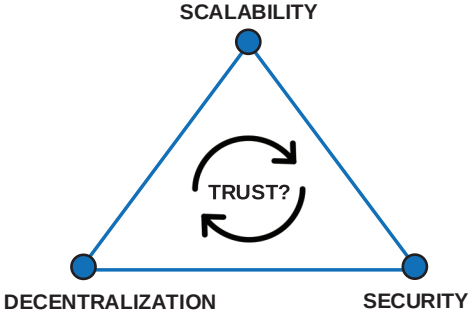

Fig. 1. *The scalability trilemma*

Where an individual blockchain network is positioned according to its characteristics affects users' trust in the operation of that network [30]. Trust is a psychological state comprising the intention to accept vulnerability based upon positive expectations of the intentions or behavior of another [31]. Trust in the correct execution of the consensus mechanism and recorded data on the blockchain increases with decentralization and security. Mainly because a stronger consensus has been established among a larger number of entities involved in the validation of new blocks. This, in turn, means that if we move towards a more scalable system with the properties of blockchain technology, trust in the system reduces. However, it is difficult to define how exactly is trust dependent on the three properties of the blockchain network (Fig. 1).

1.2 Blockchain-Supported Manufacturing

The four key properties of blockchain technology (decentralized consensus, immutability of the records, transparent database, and self-executing environment) are enabling a trusted environment for cooperation and interaction between users who do not trust each other [32]. Based on this fact, researchers have recognized blockchain technology as a solution to the problem of trust between participants in global smart manufacturing networks [6].

The existing networked manufacturing models (not blockchain supported) make significant progress in information and resource sharing. However, the shortcomings of networked manufacturing regarding information and resource sharing are considerable including delays, asynchronous data between multiple parties, multitudes of sharing approaches, irregularity in monitoring mechanisms, and the possibility of shared data being tampered with or concealed. The asymmetric nature of information puts the downstream manufacturers' product quality and credibility at risk. In contrast, due to the properties of the blockchain technology described in the previous section, the blockchain-based approach improves the quality of information sharing, reduces operational costs (due to intermediation), enables dynamic production resource allocation, and enables peer credit evaluation [33]. Therefore, blockchain provides an online environment for enabling decentralized self-organization and thus offloading and accelerating the optimization of upper-level manufacturing planning [34].

In the general blockchain-supported manufacturing model, the blockchain network represents an additional sublayer of the infrastructure layer [35], which supports the establishment of the entire framework by providing the hardware and software infrastructure for the ecosystem (Fig. 2). Blockchain sublayer is structured to support various functions such as manufacturing production, materials and inventory management, smart supply chain, and security and identity management [36]. Blockchain technology provides methods and tools, which include application program interfaces, protocols, and software development kits to support the exchange of data, resources, and knowledge in a transparent, safe, and decentralized way [37]. The Internet of things (IoT) infrastructure of the manufacturing resources is connected directly to the blockchain network through extensible embedded software components [38]. The manufacturing activities in the smart factory are recorded in the blockchain and then retrieved by the enterprise applications for monitoring, planning, and control [36].

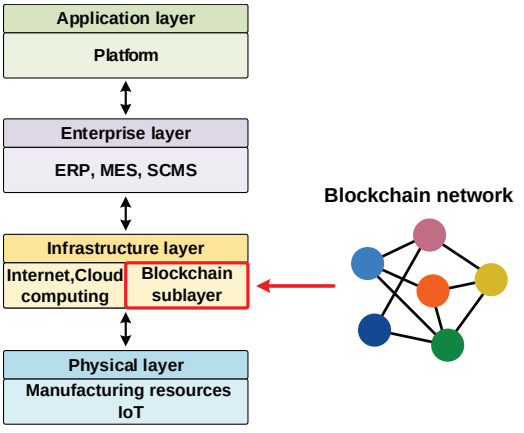

ERP - Enterprise Reource Planning, MES - Manufacturing Execution Syster
SCMS - Supply Chain Management System

Fig. 2. *General blockchain-supported manufacturing model*

Smart contracts are employed to write complex data on the blockchain network and to enable the self-execution of automated procedures. Issued smart contracts on the blockchain are containing information on the available time for processing, processing capabilities, and expected compensation for utilization of the manufacturing resources [39]. The personalized manufacturing tasks/demands are published on the smart contracts and each manufacturing service matching between the demander and provider is recorded as a transaction in the blockchain [38]. Furthermore, smart contracts are used to provide membership registration, certification authority, and security and privacy verification [36]. The captured manufacturing data from the sensors/controllers is directly written on the smart contract and consumers who are calling for manufacturing services can verify the capabilities or past actions of providers on the blockchain network [38]. The data written on the transparent and immutable blockchain is signed by the public key of the source, which increases data reliability and trustfulness.

The differences in the concepts presented in the literature on the implementation of blockchain technology in manufacturing systems are mainly twofold, namely: the level at which blockchain technology connects to the manufacturing system is different, and different manufacturing processes are being executed using blockchain technology. In the case of cloud manufacturing, blockchain technology is used only as a storage layer where interactions between providers and consumers are recorded, and

the cloud platform still ensures that data is published and classified in the cloud [40]. The manufacturing resources are packed in services, which are then posted on the platform and are not necessarily written on the blockchain. Similarly, individual manufacturers offer their services in the case of social manufacturing (Fig. 3), where the need and supply are advertised in a peer-to-peer (P2P) way via social networks [38]. In the case of Shared manufacturing, individual production units and manufacturing resources are directly connected to the blockchain network and are also interacting with other entities on the blockchain network [41]. The direct connection of individual manufacturing resources results in a high amount of interactions that are written on the blockchain. This in turn means that blockchain-supported Shared manufacturing systems are more dependent on the performance properties of the blockchain technology.

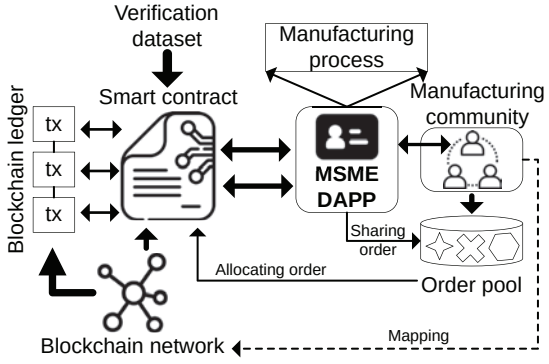

Fig. 3. *The concept of blockchain-supported social manufacturing, adapted from* [42]

2 SCALABILITY SOLUTIONS IN BLOCKCHAIN TECHNOLOGY

Applications built on blockchain technology have in the past encountered limitations of blockchain technology [43]. The main limitations of scalability have severely affected the performance of the applications on the blockchain network and have degraded the user experience. Scalability limitation is the main reason why blockchain technology is not more widely adopted in real-world applications [9]. For this reason, general-purpose solutions for increasing scalability have appeared, which are supposed to solve the scalability problem of blockchain technology. General-purpose solutions represent network organization mechanisms, methods of recording data in the blockchain, and topological upgrades of the blockchain network. For specific applications, the implementation of these solutions is adapted and upgraded according to the characteristics of the applications.

2.1 Scalability Limitations

Nodes in a blockchain network are communicating to update distributed database of data records in a coordinated manner. To update distributed database, each node must store the whole data by itself. New data emerging at one point of the network must propagate through the network and nodes must agree to update records. These properties of the blockchain network are the main reason for the scalability limitations of blockchain technology. The major scalability limitations (Table 2) of the blockchain technology are recognized in transaction throughput, storage size, and read throughput [30].

Table 2. *Scalability limitations of the blockchain technology*

Scalability limitations	Reason	Consequences
Transaction through-put	Information propagation, network synchronization	Congestion of the blockchain network, pending time increases, transaction fee increases
Storage size	The constant growth of the distributed database	Large storage requirements, fewer nodes are able (blockchain) to run a full node
Read through-put	Lack of full nodes in the network, high amount of requests from users	Longer waiting time for requested data

Transaction throughput is the main scalability limitation of blockchain technology as it affects all the users of blockchain technology [29]. Due to the technological limitations of information propagation in the network, blockchain networks cannot confirm new transactions faster in a decentralized way. If we increase the size of the data, being sent through the network the information propagates slower through the network [44]. In addition, the larger the network the longer it takes for the information to propagate through the network. Blockchain networks intentionally increase the period of new transaction confirmation to enable better synchronization of the nodes in the network and thus reduces opportunities for malicious acts [24]. The consequences of limited transaction throughput are congestion of the blockchain networks. When the number of pending transactions exceeds the maximum block size, some of the transactions will have to wait for another block to be included in the blockchain [46]. Such congestion of pending transactions for confirmation causes

competition between users for the execution priority of their transactions. Transaction priority increases by higher transaction fees and therefore such blockchain congestions results in an overall increase in transaction fee on the blockchain network [47].

The storage size limitation of blockchain technology emerges due to the constant growth of the blockchain and the fact that each node participating in the confirmation of transactions must keep a complete record of the data on the blockchain [47]. All participating nodes must have large storage capacities at their disposal to ensure the security of the written data on the blockchain. As blockchains are growing, fewer and fewer nodes are capable to store the whole blockchain on its hardware and the decentralization of the network is reducing [48]. Consequently, due to the storage size limitations, many of the nodes in the network are not storing the whole blockchain (are not full nodes) but are storing only parts of the blockchain that are relevant to them (light nodes) [49]. However, when users who do not run blockchain nodes are querying for the data written on the blockchain, light nodes cannot provide all the data. This is the reason for the read-throughput limitation of blockchain technology. The consequences of limited read throughput of the blockchain network are longer data queries and a longer synchronization period for new full nodes joining the network or for nodes who missed a message.

Compared with the centralized payment system like banks, performance (scalability) cannot be improved easily in blockchain, a self-regulating system, that needs more consideration to maintain decentralization [29].

2.2 Scalability Solutions

In response to the problem of scalability, new solutions are being presented that seek to increase the scalability of the blockchain network while maintaining the same degree of decentralization and security. Most of these solutions do not ensure this, but they do enable the change of blockchain properties regarding the trilemma (increase scalability and reduce security or decentralization) according to the requirements of the blockchain network users. Solutions that would allow for greater scalability while maintaining the same level of security and decentralization are mainly solutions based on technological leaps (e.g. quantum computers). One such example is improving the speed of data propagation across the distributed network [50]. By allowing nodes to process and transmit messages faster in a distributed network, new blocks could be confirmed faster or they can be bigger, in an equally secure and decentralized blockchain network.

Other scalability solutions thus in most cases suggest the use of new innovative methods in the implementation of the blockchain network, while with such an approach they merely position the blockchain network properties elsewhere within the trilemma. Some of these solutions even allow for dynamic trilemma positioning. The point is that with the help of these scalability solutions, the trilemma surface can be filled with different properties of blockchain networks, and then users can choose the network that has the appropriate properties, depending on their needs. This work focuses on these types of scalability solutions that result in a change of trilemma properties. They can be divided into solutions that focus on the first layer design of blockchain (L1) and second layer solutions (L2) [51]. Table 3 presents the scalability solutions presented in the literature.

Table 3. *Scalability solutions in blockchain technology*

Solution		What	How
Layer 1	Block data	TT, SS, RT	Block compression, data reduction
	Consensus mechanism	TT, SS, RT	Improved consensus mechanism
	Blockchain structure	TT	Different database structure
	Sharding	TT, SS, RT	Partitioning of the network
Layer 2	Payment channels	TT, SS	Channels offload transactions from the blockchain
	Sidechains	TT, SS, RT	Additional blockchain network connected to the main network
	Cross-chain	TT, SS, RT	Multiple connected blockchain networks

TT - transaction throughput, SS - storage size, RT - read throughput

L1 solutions include optimizing the process of block generation, consensus mechanisms, and blockchain structure. L2 solutions focus on relieving the main blockchain network by performing part of the transactions from the blockchain network or by transferring part of computationally demanding tasks to platforms that are not set on blockchain networks. First L1 solutions were optimizing the size of the block in the blockchain. Block compression and data reduction are used in this kind of scalability solution to increase transaction throughput. Segregated witness (SegWit) is one implementation of this solution, where transactions are split into two segments [52]. The unlocking signature is removed from the block creating more space for other transactions to be added to the same block. Various solutions related to block

compression have been also proposed (e.g. Txilm [53]). The idea is to reduce some redundant data of a block that has been already stored in the Mempool of receivers [29].

L1 scalability solutions also optimize consensus mechanisms in the blockchain network. Many different mechanisms have been proposed and the main difference is usually regarding the process of candidate selection for block creation or in the process of block acceptance in the blockchain. The first consensus mechanism proposed in the bitcoin network was proof of work (PoW) [54]. Compared to pow, an example of alternative consensus mechanism proof of stake (PoS) avoids the computational overhead in the process of candidate selection for block creation. The basic idea of PoS is that nodes with more currencies in the system are less likely harm the system and therefore candidate selection is done based on the owned funds in the blockchain network [55]. Delegated PoS extends the idea, that stake is used for voting of delegation nodes that are fulfilling technological requirements (enough storage and computational power) [56]. Only delegated nodes are participating in transaction confirmation and only they are storing the whole blockchain. Therefore, communicational overhead in the network is reduced as well as storage requirements are justified. Practical Byzantine fault tolerance (PBFT) is another voting-based consensus mechanism [57]. It reduces the complexity of consensus to the polynomial level but requires more communication overhead. Due to the overhead, the PBFT works efficiently only when the number of nodes in the distributed network is small. For that reason, usually only selected nodes in the network are a part of the transaction confirmation process.

Transactions in a traditional blockchain network are written in blocks that are organized in a single chain. To enable concurrent block generation a different blockchain structure has been proposed. An example of a different blockchain structure is the directed acyclic graph (DAG). In the case of DAG, several blocks can be connected to a previous block. This results in a parallel creation of blocks which increases transaction throughput. As opposed to traditional blockchain technology where dedicated validators must exist to generate and order blocks, transaction ordering in DAG is done asynchronously by the account owner in charge of the ordering. A transaction is valid if the majority votes are in favor of that transaction. Storage limitations are not omitted by this kind of scalability solution [58].

The idea of the sharding scalability solution is to divide the blockchain network into several smaller networks that process transactions internally, however, all shards are connected in a larger network [7]. Validators in each shard only need to process a small part of arriving transactions and different shards can process transactions in parallel. This results in higher transaction throughput, transaction confirmators are relieved of storing the whole blockchain and reading throughput is increased [59]. On the other side, cross-shard transactions cause communication overhead and increase confirmation latency.

First L2 solutions appeared in the form of payment channels, in which a temporary off-chain trading channel is established. Any number of transactions between participants is performed via the private channel. If participants want to close the payment channel at any point, they can broadcast the most recent signed transaction message to the blockchain network to finalize their transfer of funds [51]. Therefore, multiple transactions can be executed on parallel channels, and only final states are written on the blockchain, which results in better transaction throughput and reduces storage requirements.

Another L2 solution is sidechains, which are separate blockchain networks that are pegged to the main blockchain (mainchain). Funds can be freely transferred from the mainchain to the sidechain and vice versa. The first concept of sidechains was proposed in 2014 [60]. The concept defined a general notion of a 2-way peg and described two operational modes of interactions between pegged chains – asynchronous and synchronous. The asynchronous mode assumes that the mainchain is agnostic to all sidechains, but it is necessary to rely on sidechain validators in the process of validating transfer transactions between chains. One of the sidechain solutions that enables asynchronous mode is Plasma [61] on the Ethereum network, which acts as the mainchain. ZK-Rollup is another technology, which enables the construction of sidechains. ZK-Rollups bundle hundreds of transfers on the sidechain into one transaction on the mainchain by employing the cryptographic tool of zero-knowledge proofs [62]. Synchronous mode assumes that the mainchain and sidechain are aware of each other's existence and can directly verify the validity of transfer transactions between chains. This concept is further explored in cross-chain scalability solutions where two separate blockchain networks can be connected with cross-chain transactions, however, both networks can operate even if the connection is cut between blockchains. One implementation of the cross-chain scalability solutions is the Polkadot ecosystem [63]. Both of the scalability solutions are improving transactional throughput,

storage limitations, and read throughput by dividing blockchain network into smaller networks, which enables better information propagation. In addition, less strict requirements are posed to nodes who participate in the transaction confirmation process.

Off-chain solutions exploit the possibility to relay computational or storage tasks to capacities or networks that are not organized as a blockchain network. A multi-party computation network or distributed data storage network such as is InterPlanetary File System (IPFS) [64] can be employed as an off-chain solution. A distributed hash table (DHT) is used to store blockchain raw data on an off-chain data storage while the hash of the raw data is stored on the blockchain. There are different protocols, which define what part of the computation is done off-chain and how computation is organized. Truebit is an example of a system that outsources complex computing tasks to an off-chain market [65].

3 SCALABILITY SOLUTIONS IN BLOCKCHAIN-SUPPORTED MANUFACTURING

Given the features of blockchain-supported manufacturing systems, it seems inevitable that such large global systems will eventually encounter a limit to the scalability of blockchain technology. Scalability solutions enable blockchain technology to be a trust-ensuring solution among users in large-scale systems. Due to the high volume of the presented scalability solutions in the literature, this paper focuses on the implementations of scalability solutions in the presented blockchain-supported manufacturing concepts in literature. This section discusses in detail how are general-purpose scalability solutions applied and modified for specific problems in the field of manufacturing.

3.1 Methodology

A literature search was conducted in the Google Scholar database, where a broad range of literature on blockchain-supported smart manufacturing can be identified. The searches were conducted using the following keywords in all possible combinations: blockchain, manufacture (ing), scalability, and scalability trilemma. Review articles were omitted from the analysis. The focus was on works that are aware of the limitations of scalability of blockchain technology (works that do not address scalability were omitted).

The selected literature was arranged according to the type of scalability solutions mentioned in connection with the limitation of the scalability of blockchain technology. Further identification of whether the concept is designed specifically for any of the specific paradigms of smart manufacturing (e.g. cloud manufacturing) or just for general manufacturing systems was made. Then assessments were made to what extent scalability limitations and the proposed solution was described in each of the screened papers. The evaluation criteria divided literature into three categories.

1 category Articles that merely identify the scalability limitations of the blockchain technology and suggest one of the general-purpose solutions as potential (citing other literature) in connection with the proposed concept.

2. category Papers that in addition to stating the solution, also explain in more detail why this selection is justified according to the proposed concept. The implementation of a scalability solution in a manufacturing environment is more clearly defined (e.g. discussing how manufacturing-specific properties affect the integration of the scalability solution in the concept).

3. category Literature that describes in detail how this solution would be included in the proposed concept, and may even further adapt the proposed scalability solution according to the proposed concept. The papers in the third category extend general-purpose scalability solutions with manufacturing-specific functionalities.

Table 4. *Literature classification according to the scalability solution*

Scalability solutions		In manufacturing
Layer 1	Block data	[66], [67]
	Consensus mechanism	[68], [69], [70], [71], [72], [73], [74], [75], [67], [76]
	Blockchain structure	[77], [78], [79], [80], [81], [53], [82]
	Sharding	[83], [84], [85]
Layer 2	Payment channels	[86], [87]
	Sidechains	[41], [88]
	Cross-chain	[89], [90], [91], [92], [93], [94], [69], [70]
	Off-chain	[71], [95], [96], [97], [98], [99]

3.2 Selected Literature

According to the described methodology, 36 papers were found in the literature that addresses the problem of scalability in blockchain-supported manufacturing

and suggests one of the scalability solutions. Table 4 shows the reviewed literature, which is classified according to the type of considered scalability solution in connection with the manufacturing system. First L1 scalability solutions in blockchain-supported manufacturing are presented and analyzed. Most concepts are proposing the improvement of the consensus mechanism and blockchain structure, where mainly alternatives to the PoW consensus mechanism are modified for specific use in manufacturing, and the DAG structure in connection with IoT devices is discussed. Then L2 scalability solutions are presented and analyzed. Most authors are proposing off-chain solutions and cross-chain solutions where the IPFS approach is the most common one and different relay protocols for cross-chain interactions are second.

Fig. 4 shows a comparison between the emergence of literature in the field of scalable solutions in blockchain technology and the field of blockchain-supported manufacturing over time. The figure shows that the literature in the field of blockchain-supported manufacturing does not exactly follow the trend in the field of blockchain technology. There can be several reasons for this. It may mean that researchers in the field of smart manufacturing are unaware of the importance of the scalability limitation of blockchain technology. One of the explanations may be that the solution used in the global manufacturing system has not yet been implemented and that this limitation of scalability has not yet been observed in the existing manufacturing system. In the case of Bitcoin, which is the world's first blockchain network, scalability limitations have been identified after several years of operation.

Another possible explanation is that researchers in the field of smart manufacturing simply assume that the operation of blockchain technology will be perfected in the future and that such systems will come to life when the technology is ready for it. Until then they leave the solution to the scalability problem to researchers in the field of blockchain. However, because of the trilemma, we see that this limitation will always exist and it is necessary to explore what properties of the blockchain network regarding the trilemma are beneficial for the manufacturing system.

The reviewed literature was also divided into three categories according to the criteria described above. Fig. 5 shows the proportions of literature according to the assessed extent of addressing the problem. Almost half of the reviewed literature belongs to the second category, and the least literature belongs to the first category. The latter is surprising, as the word blockchain has been of interest to publications in recent years, and as a result, quite a bit of lower-quality literature has been published. Thus, the literature prevails, in which the authors have a good understanding of the problem of scalability of blockchain technology and, consequently, the concepts are well described. However, most of the papers struggle to present manufacturing-specific solutions and are sometimes exploiting the concept of blockchain-supported manufacturing to present general-purpose scalability solutions. Fig. 5 also shows a graph showing how the extent of addressing the problem in the reviewed literature changes over time. There is a growing number of literature in time that describes the use of scalability solutions in blockchain-supported manufacturing in dept and with a lot of effort.

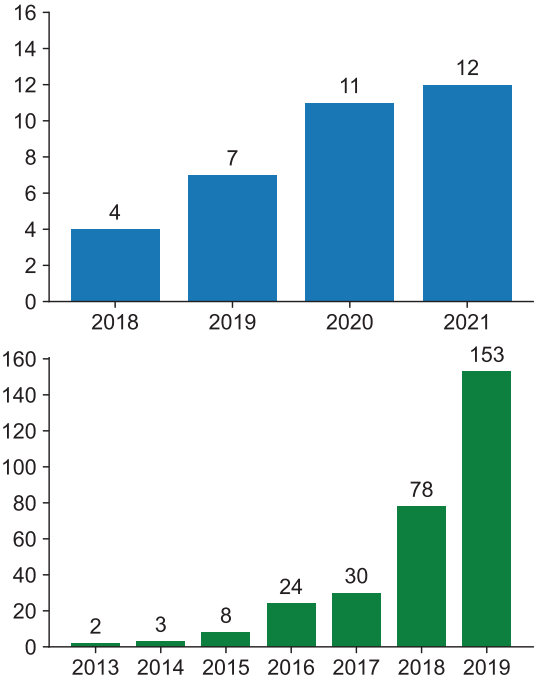

Fig. 4. *Emergence of literature in time; a) scalability solutions in blockchain-supported manufacturing; and b) scalability solutions in blockchain technology, adapted from* **[30]**

3.3 Reviewed Solutions

In the next subsections, reviewed literature is presented in detail for each group of scalability solutions and manufacturing-specific properties are highlighted for each solution.

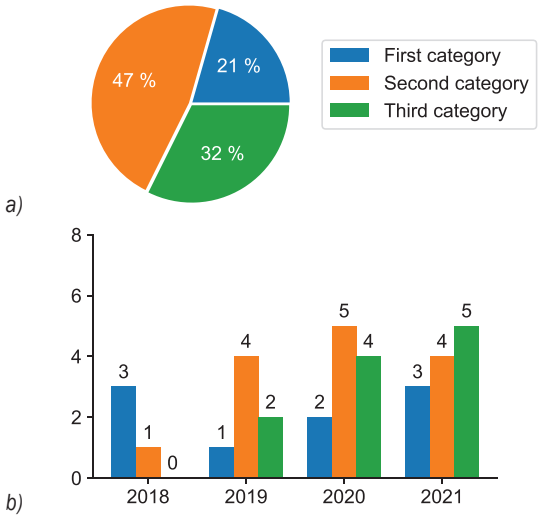

Fig. 5. *a) Proportions of reviewed literature quality; and b) extent of addressing scalability problem in time*

3.3.1 Block Data

In the case of the L1 solutions related to block data optimization, two solutions related to manufacturing have been presented so far. The first proposes to upgrade the Merkle Patricia tree (MPT) specifically for IIoT devices in SMS [66]. The new approach optimizes the storage mode of the blockchain and accelerates the speed of the data query. The solution also supports thread-safe and parallel data operations, speed up block verification or construction, and further improves the transaction throughput. A tree structure called the concurrent Merkle-Patricia tree, which supports concurrent insertion and lock-free search, is a general scalability solution that can be applied to any blockchain-based system with many blockchain queries and high data volume scenarios. In the paper, the solution is used to expand traditional blockchain so that, via limited hash computing, it can rapidly locate the manufacturing equipment or products from intelligent manufacturing systems. The second concept is trying to optimize the blockchain settings (block size, block interval, selection of the block producers) using the deep reinforced learning (DRL) technique [67]. A deep reinforcement learning approach is adopted to handle the dynamic and large-dimensional characteristics of the IIoT systems. For optimization, this solution takes into account the trade-off defined by the scalability trilemma. The authors proposed metrics that, in their opinion, should characterize the blockchain network's scalability, decentralization, and security. The presented design of a modulable blockchain where properties of the blockchain are adjusted using DRL is well adapted to the dynamics of the manufacturing systems. However, the presented solution is general purpose and can be used also on other blockchain-based applications (e.g. any blockchain network can apply presented a framework to improve performance).

3.3.2 Consensus Mechanism

The above-described concept also optimizes the choice of consensus mechanism, so it is also included in the group of solutions that use the improved consensus mechanism as a scalability solution. Another solution has been presented in the literature that similarly optimizes the consensus algorithm of blockchain-supported manufacturing using deep reinforcement learning [75]. This solution is only optimizing the selection process of the validator in terms of performance and the trilemma is not taken into account in terms of decentralization and security. The proposed deep reinforcement consensus mechanism is trained by a DRL training set and is adapted to the smart manufacturing business model. Applying the DRL-optimized consensus mechanism to manufacturing based on an IoT environment generates simpler operations, faster response, and higher accuracy and security than the traditional consensus mechanism. However, the presented approach did not take into account any specific properties of manufacturing systems that would affect the design of the consensus mechanism. This approach can be used in any kind of blockchain-based application where optimization of blockchain scalability is necessary.

Most of the other concepts that include consensus mechanism solutions, suggest the use of an alternative consensus mechanism as implemented in the case of the bitcoin network PoW. A blockchain architecture that uses a dynamic PoW consensus with a block checkpoint mechanism for IIoT was proposed [72]. The dynamic PoW consensus mechanism upgrades the traditional PoW mechanism by introducing a sliding window algorithm, which defines how many preceding blocks need to be included in the newly mined block. The authors also discussed the security aspect of the proposed more scalable consensus mechanism. The consensus offers different mining difficulty levels for different transaction arrival rates of IIoT devices, while the checkpoints define how to generate the next block hash. Instead of constant mining difficulty, the solution introduces four different levels (Table 5) where each level is triggered for a certain rate of incoming communication traffic generated by the IIoT devices. The authors have shown

that for low arrival rates, the security is high, while for high arrival rates, the throughput is high, which makes the proposed protocol scalable to meet the high concurrency and security requirements of blockchain-supported IoT manufacturing networks.

Table 5. *Difficulty levels in the DPoW consensus mechanism, adapted from* **[72]**

	Tx arrival rate	Difficulty	Size (bits)	Target hash
1	High	Level 01	4	SHA256[0:1]
2	Medium-high	Level 02	8	SHA256[0:2]
3	Medium-low	Level 03	12	SHA256[0:3]
4	Low	Level 04	16	SHA256[0:4]

The proposed concept of a decentralized manufacturing network addressed a comparison of performance between PoW and the proof-of-authority (PoA) consensus mechanisms **[68]**. The proposed PoA consensus mechanism implements a general-purpose PoA consensus mechanism named Clique. The authors emphasize that a different type of consensus mechanism is appropriate for different uses. They highlight the better decentralization and security features of the PoW mechanism compared to bad scalability as it is in line with the scalability trilemma. The authors discuss that the PoW mechanism would be more appropriate in the case of provenance tracking across a large supply chain, which requires higher trust and security. However, if a blockchain system is implemented for the verification of machine states such as states of the computer numerical control (CNC) machine, the PoA will be sufficient. The proposed solution does not provide any additional manufacturing-specific insights on how different consensus mechanism affects the integration into the manufacturing system.

A consortium PoA consensus mechanism is proposed in the case of the smart contract platform for the machine servitization blockchain network **[71]**. The proposed system of three-dimensional (3D) printing servitization is not public and it is a system provided by a known platform provider to known machine providers. Therefore, there is no need for a public network. The employed PoA consensus mechanism is a general PoA mechanism (not manufacturing specific) where only a set of known trusted entities is allowed to set up confirmation nodes. It supports arbitrary block times and sizes, increasing network performance and decreasing transaction latency. A free transaction environment is an important feature of PoA that is especially valuable for manufacturing use cases. This means that the gas price is set to zero, and the blockchain network imposes no transaction costs. Another benefit of free transactions is that the native cryptocurrency can now be easily used for manufacturing service payments. The currency can serve as a voucher (namely an Ethereum Request for Comment (ERC) token without smart contracts), and its value can be mapped to FIAT at a fixed price. PoA consensus mechanism was also selected in the case of the proposed architecture for fast certification of manufacturing data, compatible with current industrial landscapes **[76]**. A general-purpose PoA consensus mechanism is employed due to the permissioned nature of the certification system. There are two types of nodes, namely administrator nodes and mining nodes. Administrator nodes are reserved for the sovereign entity that fundamentally holds legislative power over the network. Mining nodes are responsible for creating (mine) blocks and can be deployed across multiple cells in a production line, different production lines, departments, factories, or even organizations.

A consensus mechanism that supports a permissioned blockchain network was proposed to satisfy scalability requirements regarding the ISA95 compliance of SMS **[69]**. The ISA95-CTS and SMS ecosystem constitute a broad scope of devices and systems with varying computational capabilities where scalability becomes a crucial design requirement. The reference architecture design specification requires 300 ms maximum latency with a throughput of 6000 to 8000 transactions per second (TPS). These requirements can be met with a permissioned blockchain network employing a trivial consensus protocol Raft, which is a general-purpose blockchain consensus mechanism. A similar proposal of permissioned blockchain architecture was presented regarding the manufacturing blockchain of things concept. The authors have suggested the use of a simple crash fault-tolerant (CFT) consensus protocol to achieve higher throughput and lower latency **[74]**. The proposed CFT protocol is also a general-purpose consensus mechanism that can be employed in blockchain networks for arbitrary use cases.

Two concepts in the literature suggest the use of the practical Byzantine fault tolerance (PBFT) consensus mechanism, stating that it has better performance than the traditional blockchain network (e.g. Ethereum) **[70]**, and **[73]**. However, the proposed concepts are not considering the deterioration of privacy and decentralization in the system according to the scalability trilemma. PBFT consensus mechanism is a general-purpose blockchain consensus mechanism that is already employed in other general blockchain networks (e.g. Hyperledger). None of the concepts are

extending the solution according to the requirements of manufacturing systems. For example, the authors recognize that stability of the throughput (fluctuation) is one of the problems of the PBFT mechanism, which can severely affect the processes in manufacturing planning that require synchronization. However, the proposed solutions do not provide any solution which would mitigate this manufacturing-specific problem.

3.3.3 Blockchain Structure

All the concepts that implement blockchain structure scalability solutions with blockchain-supported manufacturing are based on the use of DAG structure, with the implementation on the IOTA network being the most prominent. In four cases [77], [79], [53], and [78], this technology is only mentioned as a way to improve the scalability limitations of blockchain technology in connection with manufacturing. In all four concepts of blockchain-supported manufacturing is a physical layer directly connected to the blockchain network and the authors are expecting a high number of activities and interactions between entities that would require high transactional throughput. One of the concepts presents the implementation of the proposed architecture using STM32 IoT devices. The scalability evaluation of the implemented system suggests improved scalability and that the proposed architecture is feasible in SMS [82]. However, all of the above concepts do not provide any specific details on how a general-purpose DAG blockchain structure would be implemented in connection with the manufacturing system.

Some authors have described in more detail the implementation of the masked authentication messaging (MAM) protocol defined by the IOTA network in the case of communication between IIoT devices in SMS [80] and [81]. In the case of blockchain-supported cloud manufacturing the MAM, communication protocol is employed to realize flexible data access management [81]. The restricted mode of privacy and encryption is proposed for data sharing to control the visibility and access of a channel. Besides connections between entities in form of contracts (smart contracts), the DAG blockchain structure provides an infrastructure for an additional data layer. The data layer provides information for participants in the system with variable frequencies and does not require previous agreements or data access. MAM communication channel can regularly deliver information about relevant key performance indicators of cloud manufacturing, by the previously required constraints. In the system architecture of smart factories, which requires real-time data collection, the DAG structured blockchain is employed for a distributed traceability system and the MAM protocol enables a communication channel [79]. Each device in the smart factory is capable of publishing its messages and broadcasting them to other machines. MAM protocol is modified to enable different types of complex tree-like workflows of manufacturing processes. The modified protocol enables channels to merge and backtrace paths, which is important as multiple assembly lines merge leads to channel switching issues and source traceback is important for traceability.

In none of the above describes concepts the authors do not consider the limitation of the trilemma. Security problems and poor decentralization of the IOTA network [100] have already been identified in the literature, which may suggest that this technology is not optimal in the case of global SMS.

3.3.4 Sharding

Concepts that include sharding as a scalability solution describe the implementation of the sharding mechanism in SMS in much more detail. One of the solutions is not implementing a strict sharding mechanism but scalability is improved in a similar matter. A clustering algorithm has been used to group the overlay network participants into clusters and that results in low latency, and higher throughput [83]. The participating nodes of the clusters also select a cluster header as well as a co-leader of the cluster in the case the cluster header becomes malicious or leaves the network due to a sudden loss of connectivity. These cluster heads are responsible to maintain and manage the blockchain-supported overlay network of the manufacturing system. The industrial production line is equipped with randomly placed IIoT-enabled machines and devices. Such an unstructured environment creates overlapping network topology, which is not suitable. The proposed algorithm in a distributed manner discovers network nodes by exploiting local network topology knowledge and forms clusters in random geometric graphs. This facilitates covering the whole network with a minimum number of nodes and further reduces processing and packet overhead on IoT devices.

Another concept proposes a sharding hashgraph consensus mechanism (Fig. 6) and introduces a node evaluation mechanism based on the state of the node, which is applied to divide a large number of nodes into many shards dynamically [85]. This mechanism comprehensively considers the node's

geographic location, credit score, network status, and CPU resources and divides all nodes in the network into multiple shards. The nodes in each shard are geographically close, the network status is generally good, and the credit rating is similar. Each full node is responsible for a group of lightweight IIoT devices (sensor network) in a certain area, receiving all data uploaded by the sensor network and storing these data. The simulation results demonstrate that the proposed algorithm demonstrates better scalability performance in comparison to the PBFT consensus mechanism. Both of the described sharding solutions are considering the low capabilities of the IIoT devices in manufacturing networks, which are the end users in the blockchain network, and are proposing solutions that would increase the scalability of the blockchain network specific for blockchain-supported manufacturing.

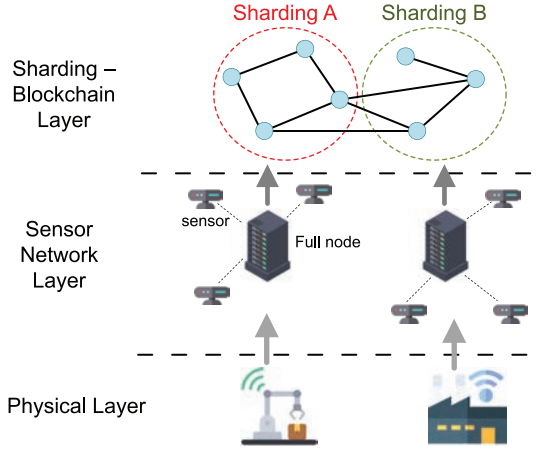

Fig. 6. *The IIoT data management system architecture based on blockchain and sharding, adapted from* [85]

However, the effectiveness of sharding is still challenging due to the uneven distribution of malicious nodes, Fig. 7. In IIoT user data and computing tasks are generally transferred to edge nodes (EN) from user equipment (UE) using distributed units (DU). A UE is set in a harsh environment for a long time and it is impossible to ensure that the task to be migrated for each device has not been tampered with. The blockchain technology approach prevents tampering with computing tasks across the entire network. The blockchain nodes are composed of all UE and DU. The UE layer consists of ordinary nodes, and the DU layer contains consensus nodes. Potential malicious consensus nodes can tamper with the data, causing excessive computing overhead and even paralysis of the IIoT.

The authors in their paper assume that each attacked UE will send the wrong calculation task to the DU. Therefore, a many-objective optimization algorithm based on the dynamic reward and penalty mechanism has been proposed to optimize the shard validation validity model [84]. The dynamic reward and penalty mechanism dynamically combine the diversity function and the convergence function to increase the selection pressure and make the population closer to the real Pareto frontier (PF). At the same time, the weights of the two functions are dynamically set to classify individuals in the population, thereby making individuals with different performances evolve iteratively. The proposed optimization algorithm is general-purpose and can be applied to any sharding solution in the general-purpose blockchain network. However, the possibility for malicious nodes seems to be greater in the case of IIoT networks due to a large number of devices with limited capabilities and the high impact (the whole manufacturing system can be obstructed) of such malicious attacks. The presented sharding solutions mention the limitation of the scalability trilemma but do not provide any discussion or analysis of how the proposed concepts would affect the relationship between scalability, decentralization, and security in blockchain-supported manufacturing.

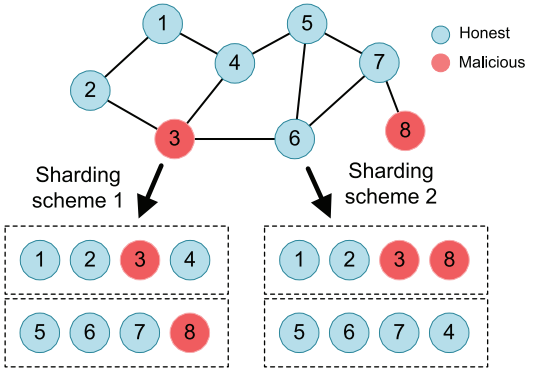

Fig. 7. *Sharding scheme leads to the aggregation of malicious nodes, adapted from* [84]

3.3.5 Payment Channels

Payment channels in blockchain-supported manufacturing are poorly addressed. Only in two concepts, are payment channels proposed as one of the possible scalability solutions. In the proposed blockchain protocol for manufacturing and supply chain management of integrated circuits, the authors have recognized the scalability limitations of blockchain technology and they have also proposed

possible scalability solutions to be implemented in the concept [86]. The implementation of the state channel was described in three parts. First, a part of the blockchain would be locked and updates can be made if a specific set of participants agrees to it. Second, the participants update themselves by constructing and signing transactions without submitting them to the blockchain network. Third, participants would submit the final state to the blockchain network after the interactions are finished to close the channel.

Payment channels in the form of a lightning network were proposed similarly in the blockchain model for industrial internet [87]. For low transaction speed, a lightning network could process high-frequency but small-sum transactions in an off-chain way. However, none of the above works provides any kind of detailed explanation of how this scalability solution would be connected to the manufacturing systems. The lack of interest in this L2 solution is probably because other L2 solutions provide better functionality and interoperability of the system. Both of the papers addressing payment channels were written in 2018 when other L2 solutions were still being explored and developed.

3.3.6 *Sidechains*

In contrast to the payment channels, the literature discusses the L2 solution of sidechains and blockchain-supported manufacturing in more detail. Both of the concepts are proposed for a specific type of SMS, namely Cognitive manufacturing and Shared manufacturing. The first paper proposes atopic mining process in blockchain-network-based cognitive manufacturing [88]. The proposed method exploits the highly universal Fourier transform algorithm to analyze the context information of equipment and human body motion based on a variety of sensor input information in the cognitive manufacturing process. Because of its primitive management, a cognitive manufacturing process can have problems including the absence of efficient statistical information, negligence of supervision, and inconsistency of physical and soft data. The conventional physical Cognitive manufacturing system has unclear information in the manufacturing process, whereas the proposed cognitive manufacturing process supports end-to-end trace based on the transaction data saved in the blockchain in order to prevent data loss in each step. The blockchain-supported cognitive manufacturing process exploits the information exchange of the data collected in real-time to analyze a variety of data related to the traceability system, extension infrastructure in each base, and worker's work system. Such an approach in manufacturing results in the collection of massive amounts of data. Because of the structural problem of the blockchain (scalability limitations), it is difficult to include massive data on the general-purpose blockchain. Therefore, sidechains are used to store a large amount of data collected by smart devices in the system. The mapping between the specific data on the sidechain and the mainchain is done by writing the hash of the block on the mainchain. However, the proposed solution employs general-purpose sidechains and does not provide any specific reason why another scalability solution is not viable to provide better scalability in the case of blockchain-supported cognitive manufacturing.

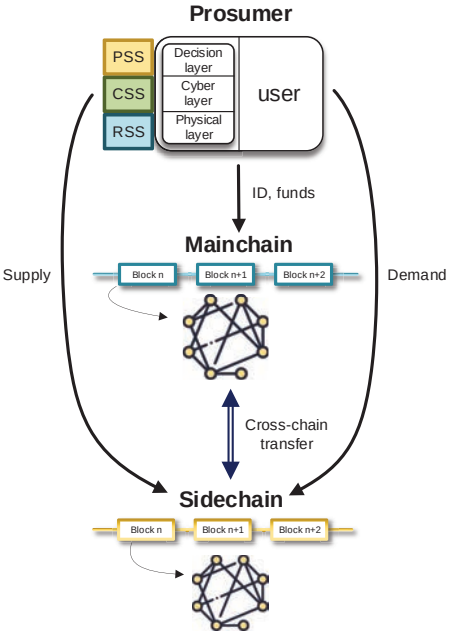

Fig. 8. *Sidechain solution in blockchain-supported manufacturing, adapted from* [42]

The second paper presents a scalable framework for blockchain-supported Shared manufacturing (Fig. 8) that preserves the transparency and immutability characteristics of transaction records, which is critical to building trust between entities in blockchain-supported systems [41]. The concept proposes that authentications of the manufacturing resources in the system are done on the mainchain and all the interactions between providers and consumers of the manufacturing services are done on the sidechains. The authors further discuss what cross-chain technology should be used to relay data from sidechains to the mainchain, and a hybrid solution is proposed. It allows a more configurable setup of sidechain networks,

which means that it can provide greater scalability and interoperability according to users' needs. When users determine that they need a blockchain network with different properties, they can open a new network (sidechain) with custom settings or connect an existing network with a preferred setting. There are two types of connection between blockchains in the proposed concept, namely information and financial. Financial is provided by the general-purpose sidechains scalability solutions. The information connection is provided by the appropriate implementation of the proposed protocol using smart contracts both on the sidechains and on the mainchain. Upon entering the system on the mainchain, prosumers create a digital identity with which they then carry out transactions on various blockchain networks. Thus, prosumers can track other prosumers throughout the tree of sidechains and obtain information about their business history, and use this information when deciding to do business with a particular prosumer. The authors also discuss that sidechain networks would be organized by manufacturers in the system who have computer hardware and resources to support this kind of system that benefits them. They compare implementations of the proposed framework on the main public blockchain network and sidechain network, which results in better scalability by the sidechain solution.

3.3.7 Cross-Chain

Cross-chain scalability solutions present variable cross-chain protocols to relay data between two blockchain networks and many of them were connected to blockchain-supported manufacturing. A concept for enabling the traceability of manufacturing processes was presented, where manufacturing products are represented by non-fungible tokens on the blockchain network [89]. In order to reduce the overhead involved, a lightweight contract is implemented as an alternative to the more general ERC-721 compliant version. The authors are further aware of the scalability limitations of blockchain technology, therefore, they propose the use of scalability solutions. The tests on the implemented system showed that varying batch sizes of manufacturing products influence the system's scalability in terms of throughput, ledger size, and potential gas costs. Consequently, small batch sizes, as required for tracing single goods, negatively affect the system's performance. The authors propose cross-chain solutions over L1 solutions because cross-chain solutions provide better interoperability, which is required in the case of the proposed concept. The authors argue that the intersection of industries and bidirectional dependencies requires different environments that should be connected. However, only general-purpose existing cross-chain scalability solutions are proposed, without further explanation of how the proposed concept should be integrated with cross-chain solutions.

Manual asset exchange as a cross-chain protocol is selected in the concept of the infrastructure of decentralized collaborative manufacturing [93]. To satisfy high-performance requirements, the matching layer relies on atomic swaps to enable automatic pricing. The protocol allows the trade of arbitrary crypto-assets, like cryptocurrencies (value tokens) and ERC-20 tokens (capacity tokens) through different blockchain networks. Free capacities of manufacturing machines in the system correspond to a number of capacity tokens on the token layer. However, the cross-chain scalability solution in this concept is an existing general-purpose solution for transferring funds over any general-purpose blockchain network. No additional insights are provided on how manufacturing-specific properties of collaborative manufacturing affect the integration of the proposed scalability solution into the system.

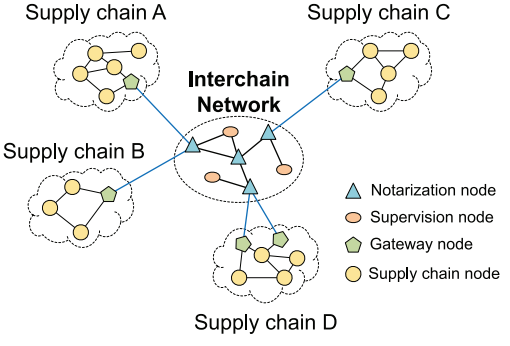

Fig. 9. *Cross-chain architecture for manufacturing supply chain system, adapted from* [90]

Another concept presents a design scheme of an integrated platform for information exchange services provided by participants in a manufacturing supply chain based on blockchain technology [90]. In order to reduce the scalability limitations of blockchain technology and due to the requirements of the global manufacturing supply chain, cross-chain architecture is proposed. An interaction chain is defined as the coordinator in the system and the notary scheme is selected as the cross-chain protocol between different blockchain networks. An interaction chain is managed by authorities and is organized like other blockchain networks. The nodes in the interaction chain are notarization nodes that are ensuring cross-

chain communication and global consensus between different networks (Fig. 9). There are four types of nodes in the system. Supply chain nodes are taking care of executing supply chain services. Gateway nodes are in charge of collecting cross-chain transactions and transmitting them to the interaction chain to be verified. Notarization nodes are the nodes implementing notary schemes to validate cross-chain transactions. Supervision nodes are operated by the authorities and are in charge of monitoring the notarization nodes.

A notary scheme is the selected cross-chain protocol also in the algorithm for the blockchain-supported system on multi-chain storage for cyber, physical, and social (CPS) under edge cloud computing [91]. Blockchain-supported CPS systems are generating a huge amount of similar data that occupies the storage of the devices in the system. In addition, the traditional blockchain approach without scalability solutions leads to the mismatch between the communication speed of nodes and the requirements of high concurrency and high response speed in CPS. Data storage and parallel processing become the key factors that restrict system performance. The algorithm divides nodes of the system into separate blockchain networks according to the relationship of communication tightness. A partitioning algorithm based on node community clustering minimizes time for cross-chain communication, resulting in improved speed of data processing and reduced communication load in the system. A similar approach can be employed in other blockchain-supported applications where storage and communication limitations are the main problem.

The above-presented concepts are well presented, however, none of them are discussing how the improved scalability of the system will affect the property of security and decentralization. The trilemma is discussed in a proposed cross-chain protocol of interoperable blockchains for collaborative manufacturing [92]. Existing cross-chain protocols are being extended using a trusted execution environment to increase the security of the solution. A relay scheme is proposed as a cross-chain communication technology. The authors have shown that negligible additional communicational overhead emerges due to the cross-chain interaction, however, security and interoperability are increased.

3.3.8 Off-Chain

Most blockchain-supported manufacturing concepts involve huge amounts of captured data and cannot be stored all on one network, so data storage on a distributed storage system that is not part of the blockchain (off-chain) appears to be the main solution to this problem. The proposed solutions define which data is written on the blockchain and which is off-chain. In the case of the industrial blockchain-supported framework for product lifecycle management (PLM) in Industry 4.0, the authors suggest that some raw data is written off-chain, whereas the hash of raw data is on the blockchain [70]. PLM aims to seamlessly manage all product information, and knowledge generated throughout the product lifecycle for achieving business competitiveness. The information of PLM is difficult to be integrated and shared among the cooperating parties due to the amount of data and privacy reasons. The authors propose that design schemes and certificates are written off-chain, however, manufacturing quality information, recall data, and supply chain traceability data are written on the blockchain (Table 6). Off-chain data is stored in the cloud storage environment, which is employed also for data validation, data cleaning, and data broadcasting.

A similar way of recording generated data is presented in the case of 3D printing as a service in a decentralized manufacturing concept where important data about the service is written on the blockchain network, and additional digital content, such as stereolithography (STL) files, is stored off-chain [71]. The off-chain cloud storage is an add-on integrated into the on-chain logic. The authors define the data and event models for a hybrid on-chain and off-chain decentralized application. On blockchain are stored JavaScript object notation (JSON) structures with hash values, uniform resource locators (URLs), and metadata. URLs are pointing to the 3D printing specification in STL files that are stored off-chain.

Table 6. *Data in the industrial blockchain-supported framework for PLM, adapted from* [70]

Data type	Privacy	Amount	On or off-chain
Design schemes	High	Medium	Off-chain
Quality information	Medium	High	On-chain
Logistics traceability	Low	High	On-chain
Recall data	Low	High	On-chain
Contracts	Null	Medium	On-chain
Certificates	Low	Low	Off-chain

The data sharing framework for IIoT was presented in the literature, where the authors propose an off-chain procedure for participants to compress and encrypt product data before being submitted to the blockchain [99]. The concept proposes two types

of transactions named point transactions and data transactions. Point transactions are indicating the place of the written data on the off-chain and data transactions store encrypted data on the blockchain. When a product id is processed through a path of participants, each of them transfers its product record to a dedicated participant for compression. The dedicated participant then encrypts the compressed product data with a policy and submits it to the blockchain. In the off-chain procedure, participants transferring product records also submit point transactions to store the off-chain storage address of the data of id. At the end of the procedure, the dedicated participant submits a data transaction to carry the encrypted compressed data of the id. To access the data of the id, a data user can send a request to the blockchain. If a point transaction is returned, the user extracts the off-chain address from it and interrogates a certain participant according to the address. The participant encrypts the data of the id with a policy and returns the ciphertext. The user then decrypts the ciphertext according to the policy to acquire the data of the id. If a data transaction is returned, the user directly extracts the encrypted product data from it and decrypts it according to the policy to acquire the data of id. The evaluation results show that compared with the baseline approach, the proposed concept achieves a 4 to 9 times improvement in storage efficiency and a 5 to 20 times improvement in data access efficiency, respectively.

Several solutions suggest using the inter-planetary file system (IPFS) as a distributed storage system. In the case of traceability and management in additive manufacturing systems, IPFS is used to store design files, IoT device records and additional product specifications [94]. When a customer submits an order, the smart contract connects to the product manufacturer and the 3D printing workshop. Once the product manufacturer and the 3D printing workshop confirm accepting the order, the product designer is in a heterogeneous environment with many actors. Thereby, the IPFS-based enterprise file share should be protected from unauthorized users. The authors propose OAuth, Security Assertion Markup Language, Kerberos-based single sign-on (SSO), and authentication schemas to preserve privacy.

Excessive data gathered to satisfy the requirements of the ISA95 standard must also be relayed through the IPFS to reduce the amount of data being written on the blockchain [69]. Various actors in the system can directly read and write to IPFS via P2P network protocols, given that relevant access rights are granted (Fig. 10). The suggested policy can define thresholds, and if a file or transaction content is above the limit, then the blockchain operating system makes the actor write the file content to IPFS. Next, the file hash (acting as the pointer to the original file) is generated and inserted as a new block content to the blockchain. When an actor needs to access the file, first gets the file address on IPFS from the blockchain, and then the actor accesses the address location to read the file content. The reference architecture attempts to address location restrictions by preserving the sensitive data on IPFS-based network storage that is geographically situated as per regulatory requirements. However, to add an extra layer of protection, individual data elements are encrypted, and the hashes of the files are distributed through the ledger. Large files are distributed through IPFS over the P2P network. IPFS does not dictate any access control by default. The ISA95 enterprise uploads the digital design on the IPFS, and the hash of the file is transmitted to the 3D printing workshop. All interactions and transactions between the stakeholders are stored in the blockchain ledger. Due to storage limitations and size restrictions, larger files are stored in IPFS and their hash is sent to respective participants and stored in the blockchain ledger. Once printing is completed, all IoT devices and camera records will be uploaded to the IPFS and hashed in the blockchain ledger. The hash for the control measures recorded during the printing process is transmitted to the Attestation and Certification Authority accessed via IPFS to verify quality control measures.

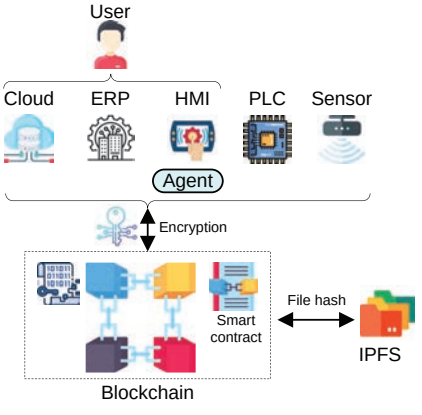

* ERP – Enterprise Resource Planning, HMI – Human Machine Interface, PLC – Programmable Logic Controller

Fig. 10. *On-chain and off-chain transaction encryption, adapted from* [70]

In the case of the blockchain-based service architecture for Cloud manufacturing, the authors proposed to relay the dynamic elliptic curve certificate data on a distributed storage system (IPFS) to increase

the storage scalability of the proposed architecture [95]. Dynamic certificates and elliptic curve integrated encryption schemes are proposed to enable blockchain-based security services for trust establishment. Diffie–Hellman key exchange is used for the establishment of a symmetric key between IoT–Fog–Cloud channel to encrypt the manufacturing-related message traffic. Non-interactive zero-knowledge proofs are used for verification in the security service to ensure anonymity and unlinkability on dynamic identities stored in the ledger. Additional data used for encryption procedures is offloaded to the extended storage off-chain. The extended storage record is linked to the ledger record with the extended storage key, which is the hash of the multiple data elements. The data consists of the key of storage, certificate, counter data, auxiliary data for private key generation, curve point of zero-knowledge proof, and data set. The experiment showed that the blockchain storage utilization is significantly reduced in the proposed architecture compared to storing all data on the blockchain.

To reduce the load and delay of the network, the blockchain-based platform for IIoT is designed as a light-weighted network architecture (Fig. 11) consisting of an on-chain network and an off-chain network [96]. Under the conditions of the IoT, the computing power of each intelligent device is very limited. Compared with the traditional blockchain mining nodes, the hash computing capability is even less than one-thousandth of the graphics processing unit (GPU) system. The off-chain network handles problems that cannot be solved by blockchain technology, such as storage and complex data processing. The off-chain network has a decentralized off-chain database, namely DHT, which can be accessed by the blockchain. The data is encrypted in the blockchain and stored in the DHT, the access control protocol is written on the blockchain to ensure security, and the off-chain network provides an API interface to read the data in the DHT. The proposed off-chain network further implements a multi-party computation protocol, which allows multiple nodes to perform computing tasks on a common problem in a secure way. In the use case of the proposed concept for manufacturing equipment data sharing, the authors discuss that the shared data is organized into a standardized readable, and writable data format by big data and AI technology on the off-chain network. The shared data is also stored in the off-chain database, while a summary index is generated and stored in the on-chain network. However, the proposed concept is employing general-purpose blockchain solutions and can be implemented on any other blockchain application. The authors do not provide any additional insights into what manufacturing-specific data is written on or off-chain.

In the case of the architecture for secure management of manufacturing data, the off-chain data is stored on the cloud storage system [97]. For the high volume of shared data, the authors present a hybrid approach where a token and conditions on when the token can be used are written on the blockchain, and when the conditions are met the token grants access to particular data on cloud storage. The data itself can go on low-cost cloud-based Write Once, Read Many (WORM) storage owned by the manufacturer, while a token corresponding to the data can be included on the blockchain. The token leaks minimal information about the manufacturing process, allaying potential confidentiality concerns. Upon conditions that can also be spelled out in the blockchain, certain parties have the contractual right to present the token to the manufacturer and be given access to the data.

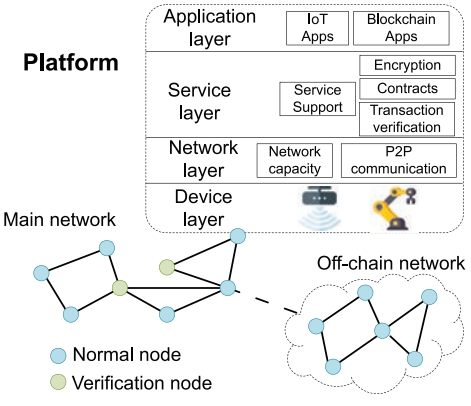

Fig. 11. *Light-weighted blockchain-based network architecture for IIoT, adapted from* [96]

The WORM layer includes a blockchain element because even if data has been placed on WORM storage, there is no guarantee that anyone can find it. The WORM-blockchain combination overcomes this problem by placing the relevant lookup information on the blockchain. The authors, however, do not discuss in detail what kind of manufacturing data is stored off-chain and do not elaborate on how tokens would be implemented (using cryptography or any other tools).

Another concept of blockchain architecture for Cloud manufacturing proposes that a large volume of manufacturing data is stored in decentralized and immutable bid data storage platform like the BigchainDB [98]. Compared to IPFS and cloud platforms proposed decentralized storage is including some parts of blockchain technology such as the

consensus mechanism, however it omits safety measures like full replication of the database in each node to provide better scalability. Communication between layers L1 and L2 is established by a new addition to the client middleware as the BigchainDB interface layer. This layer is primarily a middleware software module that resides within the client middleware software architecture and houses event subscribers that subscribe to specific transaction events. These transaction events are emitted by the oracles designed as a part of the smart contracts. Once the manufacturing service is executed an ERC-721 token is created on the L1 network. The oracles on the issuance of these tokens in turn emit their own events which trigger subscribers in the BigchainDB layer to complete the collection of data. The BigchainDB layer collects a large volume of metadata on manufacturing services. The data includes a cryptographically hashed signature of the design file of the final part, detailed dimensional metadata of the part, and necessary information about both the client and the CMaaS platform in terms of their Ethereum identities i.e., wallet addresses. Most of this information quite naturally would involve data of different types and precision. Due to the restrictive nature of the Ethereum ecosystem, there is no default support for many complex data types like variable length strings which have to be used to record modalities like product name or description. BigchainDB as an off-chain solution provides better scalability and enables the storage of complex data types.

3.4 Comparison of the Literature

It is noticeable from the presented literature that a few more concepts propose L1 solutions than L2 and some authors propose a combination of both types of solutions (Fig. 12a). In the case of L1 solutions, the concepts in the literature are mainly proposing the use of scalability solutions that change the consensus mechanism and solutions that change the blockchain structure. For the consensus scalability solution, this is mainly because using alternative consensus mechanisms (e.g. PBFT) can implement a more scalable network, which usually has the properties of a consortium or permissioned network and that corresponds to closed types of SMS organization. The authors thus justify the change of properties in trilemma by saying that the manufacturing world is more closed than the financial one, and there are already proven implementations of these mechanisms, such as Hyperledger. The blockchain structure solutions are mainly presented in concepts that use the specifically designed blockchain network IOTA, which targets the integration of IoT devices into the blockchain network, and there are many of them in the case of SMS.

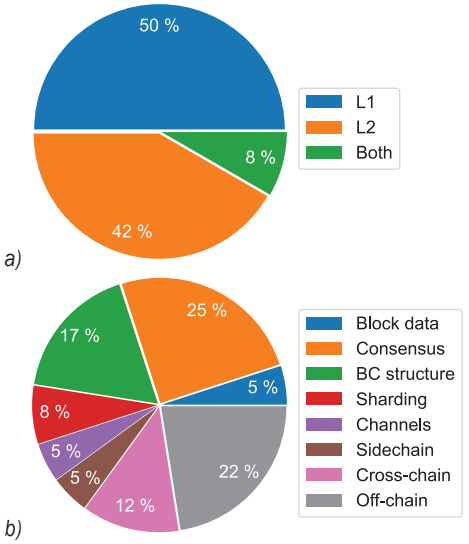

Fig. 12. *a) Proportions of proposed L1 and L2 solutions in literature; and b) proportions of specific scalability solutions proposed in the literature*

In the case of L2 solutions, a group of concepts stands out that suggests the use of off-chain solutions. As already described, most of these concepts want to transfer the data records generated by the manufacturing system from the blockchain to parallel storage infrastructure and consequently relieve the blockchain network. Given the amount of data generated by SMS, it seems reasonable that not all data is stored on such an "energy-intensive" network, but it should be noted that more scalable alternatives also mean less security of stored data. The reason for the highest number of concepts implementing off-chain solutions is that cryptography enables a simple connection between data written off-chain and on the blockchain (hash mappings) and that there already exist several data storage systems that can provide this kind of support (e.g. IPFS). Then, according to the number of solutions, the use of cross-chain solutions follows. Concepts employing cross-chain solutions are similar to the concepts that suggest the use of sidechain technology. The reason for a bigger number of concepts proposing cross-chain solutions instead of sidechain solutions is because cross-chain enables better modularity of the blockchain networks and additional opportunities to build blockchain infrastructure (e.g. existing blockchain networks can connect or disconnect from each other). The main

difference regarding user experience is where the identity of an individual system user is created. With sidechain solutions, this happens on the mainchain, and then with that identity, users access other sidechains. With cross-chain solutions, users can join the system on any chain.

In the selected literature, we observed whether the proposed concept is specific to any of the Smart Manufacturing paradigms. Different concepts of organizing manufacturing systems provide for a different number of interactions between entities in the system, which means that blockchain network scalability can be much more important for some concepts than for others. Fig. 13 shows how SMSs are defined in the reviewed literature. In most cases, the authors do not envisage a specific concept of organizing SMS. Only about a quarter of the posts deal with specific examples of SMS, these relate to CloudMfg, Smart Manufacturing supply chain, and other SMS (e.g. SharedMfg). Fig. 13 also shows a comparison between the choice of L1 or L2 solutions in the case of general SMS and specific SMS. In the case of any SMS system, the authors opt for L1 solutions, while for specific SMS the decision for L2 solutions prevails.

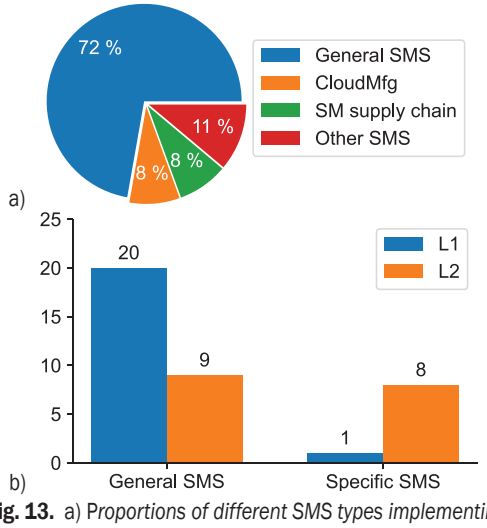

Fig. 13. a) *Proportions of different SMS types implementing scalability solutions in literature; and b) comparison between general and specific SMS concepts regarding the L1 and L2 solutions in the literature*

4 FUTURE DIRECTIONS AND OPEN ISSUES

The presented literature proposes different concepts and solutions however the authors acknowledge that studies have limitations and that there exists a research gap for future work. Based on the reviewed literature the following open research questions (RQ) are highlighted:

- **RQ1**: Do proposed solutions meet the performance requirements of the manufacturing systems?
- **RQ2**: What are the barriers to the real-world implementation and adoption of proposed solutions in a global manufacturing system?
- **RQ3**: How do scalability limitations of blockchain technology affect the performance of a manufacturing system?
- **RQ4**: How increased scalability of the system affect decentralization and security and how reduced trust affects the manufacturing systems?

RQ1 explanation: According to the reviewed literature on blockchain-supported manufacturing regarding the scalability of blockchain technology, most of the authors assume that the scalability of blockchain technology will be a problem when connecting to large manufacturing systems. All of the proposed solutions increase scalability of the blockchain-supported manufacturing, however, a few of the authors are trying to evaluate if such performance results are sufficient for the requirements of global manufacturing systems. The scalability and compatibility of the proposed platform should be further verified and evaluated in a real business environment with more nodes [70]. However, it is difficult to assess the number of nodes that are participating in the global manufacturing system. Furthermore, the capabilities of IIoT devices in manufacturing systems are improving. Evaluation of the concepts in the future should include additional devices with specialized hardware designed for blockchain-supported systems [82]. In the case of optimization of the consensus mechanism selection concept [75], the author proposes that in the future new consensus mechanism should be developed and that it should be adapted for different properties of manufacturing systems. Consequently, coordination with manufacturing companies is proposed to obtain more realistic performance requirements. Another challenge in answering this question is a representative assessment of different manufacturing systems' performance requirements. The diversity of existing systems seems to present a plethora of requirements. However, studies that would address this question could potentially define the necessary levels of blockchain scalability in relation to the type of manufacturing system. A benchmark would be beneficial for the comparison of different scalability solutions and manufacturing systems.

RQ2 explanation: Given the amount of published literature on blockchain-supported manufacturing, it is surprising that in reality none of the concepts has yet been implemented. Such a platform would make it possible to examine the real-world requirements of the global manufacturing system for scalability, decentralization, and security of blockchain technology [101]. In the case of the concept of blockchain-supported manufacturing industry supply chain management, the authors suggest that they would implement in the future a complete blockchain cross-chain platform based on the high-level model provided by this paper [90]. However, the authors acknowledge some of the barriers to the acceptance of such implementations by the existing manufacturing companies. As it is noted in the industrial implementation challenges, a coordinated effort of engagement must be initiated with manufacturing stakeholders across the industry – designers, job shop service providers, machine builders, regulators, certifiers, public policy, and corporate law [68]. In the future, a thorough study on the barriers to the adoption of proposed solutions in manufacturing would highlight the reasons why blockchain-supported manufacturing is not yet a viable concept in existing manufacturing systems.

RQ3 explanation: Currently, no existing research addresses how scalability limitations affect the performance of a manufacturing system. In the past, blockchain networks that have already implemented scalability solutions have encountered the same limitations. Questions arise as to what would happen if the blockchain network could not process all the transactions for manufacturing services and this would lead to congestion in manufacturing systems [30]. How would manufacturing systems react to this, or would parallel financial channels be established? In addition, there is an increase in the transaction fee in the congestion of the blockchain network, which could affect the price of the manufacturing service. Could transaction fees be higher than the price for manufacturing services? Blockchain represents the financial level that is appended to the manufacturing system in blockchain-supported manufacturing. Given that infrastructure needs to be maintained to operate, in addition to the usual manufacturing roles, financial roles will also emerge. How to ensure that the blockchain-supported manufacturing system emphasizes the role of the manufacturer and not other roles, such as the role of maintaining financial infrastructure. Research on this question would reveal what limitations in manufacturing emerges due to the scalability limitations of blockchain technology.

RQ4 explanation: Most of the concepts discussed in the literature largely neglect the role of the Scalability trilemma, which defines the properties of a blockchain network. Scalability solutions are understood as solutions that increase scalability while maintaining decentralization and security. However, these solutions only increase the scalability of the system at the expense of decentralization and security (they move the properties of the network to another point in the trilemma). The open question thus remains with all the proposed concepts of how increased scalability of the system affects decentralization and security [67]. Does this scalable solution change decentralization and security in such a way that such an approach would no longer guarantee trust in the system [76]? In the literature at the moment, no work has yet addressed how the Scalability trilemma of blockchain technology is reflected in the behavior of the users. Some of the presented solutions allow dynamic movement of the system along the trilemma following the requirements of users and this decision is in their hands. When and why users of the proposed systems will decide to move to the blockchain network with a different position in the trilemma? Which requirements of manufacturing systems dictate the different characteristics of blockchain technology and whether this technology can fulfill them? The analysis of human behavior could potentially answer the question, however, to provide statistically significant results a lot of participants and iterations of the experiment are necessary. Such studies would highlight the requirements of manufacturing systems regarding the trilemma properties of blockchain technology.

5 CONCLUSIONS

The key properties of blockchain technology, which highlight the security and trust issues in decentralized environments, have brought great attention to emerging smart manufacturing concepts. Blockchain technology enables the connection of manufacturing entities that otherwise compete with each other on a global scale in a trustful way. However, this technology also has limitations, namely, the main limitation is a trade-off between scalability, decentralization, and security of the network. Scalability solutions of blockchain technology aim to solve the scalability problem or to at least provide a variety of possible settings of the three main properties in the trade-off.

So far, 36 publications have been published on the topic of scalability solutions in blockchain-supported manufacturing. Different scalability

solutions have been used for different specific cases of smart manufacturing systems. L1 and L2 scalability solutions are employed evenly, with L1 solutions being more commonly used for general SMS, while L2 solutions are more commonly used in specific SMS concepts such as Cloud manufacturing. The extent of addressing scalability problems in literature and the number of proposed concepts that are extending general-purpose solutions with manufacturing-specific functionalities increases over time. However, there are still open issues on this topic, especially the lack of analysis of the impact of scalability limitations on the operation of blockchain-supported manufacturing systems. In addition, most of the literature ignores the scalability trilemma, which, despite the proposed scalability solutions, remains a constraint that large blockchain-supported manufacturing systems will encounter sooner or later. Furthermore, there is currently no implementation of the proposed concepts in the industry, which would confirm the need to comply with the limitations of the scalability of blockchain technology in manufacturing systems.

6 ACKNOWLEDGEMENTS

This research was funded by the Slovenian Research Agency under the funding "Young Researchers" and research program Grant P2-0270.

7 REFERENCES

[1] Kasten, J.E. (2020). Engineering and manufacturing on the blockchain: A systematic review. *IEEE Engineering Management Review*, vol. 48, no. 1, p. 31-47, **DOI:10.1109/EMR.2020.2964224**.

[2] Yang, H., Kumara, S., Bukkapatnam, S.T., Tsung, F. (2019). The internet of things for smart manufacturing: A review. IISE Transactions, vol. 51, no. 11, p. 1190-1210, **DOI:10.1080/24725854.2018.1555383**.

[3] Gao, J., Yao, Y., Zhu, V.C.Y., Sun, L., Lin, L. (2011). Service-oriented manufacturing: a new product pattern and manufacturing paradigm. *Journal of Intelligent Manufacturing*, vol. 22, p. 435-446, **DOI:10.1007/s10845-009-0301-y**.

[4] Hawlitschek, F., Notheisen, B., Teubner, T. (2018). The limits of trust-free systems: A literature review on blockchain technology and trust in the sharing economy. *Electronic Commerce Research and Applications*, vol. 29, p. 50-63, **DOI:10.1016/j.elerap.2018.03.005**.

[5] Wüst, K., Gervais, A. (2018). Do you need a blockchain?. *2018 Crypto Valley Conference on Blockchain Technology*, p. 45-54, **DOI:10.1109/CVCBT.2018.00011**.

[6] Leng, J., Ye, S., Zhou, M., Zhao, J.L., Liu, Q., Guo, W.,Cao, W., Fu, L. (2020). Blockchain-secured smart manufacturing in industry 4.0: A survey. *IEEE Transactions on Systems, Man, and Cybernetics: Systems*, vol. 51, no. 1, p. 237-252, **DOI:10.1109/TSMC.2020.3040789**.

[7] Buterin, V. (2017). On Sharding Blockchains from *https://vitalik.ca/general/2017/12/31/sharding_faq.html* accessed on 2022-06-02.

[8] Brewer, E.A. (2000). Towards robust distributed systems (abstract). *Proceedings of the 19th Annual ACM Symposium on Principles of Distributed Computing*, p. 7, **DOI:10.1145/343477.343502**.

[9] Chauhan, A., Malviya, O.P., Verma, M., Mor, T. S. (2018). Blockchain and scalability. *2018 IEEE International Conference on Software Quality, Reliability and Security Companion*, p. 122-128, **DOI:10.1109/QRS-C.2018.00034**.

[10] Alladi, T., Chamola, V., Parizi, R.M., Choo, K.-K. R. (2019). Blockchain applications for industry 4.0 and industrial IoT: A review. *IEEE Access*, vol. 7, p. 176935-176951, **DOI:10.1109/access.2019.2956748**.

[11] Leng, J. Ruan, G., Jiang, P., Xu, K., Liu, Q., Zhou, X., Liu, C. (2020). Blockchain-empowered sustainable manufacturing and product lifecycle management in industry 4.0: A survey. *Renewable and sustainable energy reviews*, vol. 132, art. ID 110112, **DOI:10.1016/j.rser.2020.110112**.

[12] Nofer, M., Gomber, P., Hinz, O., Schiereck, D. (2017). Blockchain. *Business & Information Systems Engineering*, vol. 59, p. 183-187, **DOI:10.1007/s12599-017-0467-3**.

[13] Iansiti, M., Lakhani, K.R. (2017). The Truth About Blockchain, *Harvard Bussiness Review*, p. 118-127.

[14] Gorkhali, A., Li, L., Shrestha, A., (2020). Blockchain: A literature review. *Journal of Management Analytics*, vol. 7, no. 3, p. 321-343, **DOI:10.1080/23270012.2020.1801529**.

[15] Lamport, L., Shostak, R., Pease, M. (2019). The byzantine generals problem. *Concurrency: the Works of Leslie Lamport*, p. 203-226, **DOI:10.1145/3335772.3335936**.

[16] Bamakan, S.M.H., Motavali, A., Bondarti, A.B. (2020). A survey of blockchain consensus algorithms performance evaluation criteria. *Expert Systems with Applications*, vol. 154, art. ID 113385, **DOI:10.1016/j.eswa.2020.113385**.

[17] Helliar, C.V., Crawford, L., Rocca, L., Teodori, C., Veneziani, M. (2020). Permissionless and permissioned blockchain diffusion. *International Journal of Information Management*, vol. 54, art. ID 102136, **DOI:10.1016/j.ijinfomgt.2020.102136**.

[18] Zheng, Z., Xie, S., Dai, H., Chen, X., Wang, H. (2017). An overview of blockchain technology: Architecture, consensus, and future trends. I*EEE, International Congress on Big Data*, p. 557-564, **DOI:10.1109/BigDataCongress.2017.85**.

[19] Buterin, V. (2015). On Public and private Blockchains, *https://blog.ethereum.org/2015/08/07/on-public-and-private-blockchains*, accessed on 2022-06-02.

[20] Hamilton, M. (2020). Blockchain distributed ledger technology: An introduction and focus on smart contracts. *Journal of Corporate Accounting & Finance*, vol. 31, no 2, p. 7-12, **DOI:10.1002/jcaf.22421**.

[21] Cong, L.W., He, Z. (2019). Blockchain disruption and smart contracts. *The Review of Financial Studies*, vol. 32, no. 5, p. 1754-1797, **DOI:10.1093/rfs/hhz007**.

[22] Swan, M. (2015). *Blockchain: Blueprint for a New Economy*, O'Reilly Media, Inc., Sebastopol.

[23] Croman, K., Decker, C., Eyal, I., Gencer, A.E., Juels, A., Kosba, A., Miller, A., Saxena, P., Shi, E., Sirer, E.G., Song, D., Wattenhofer, R. (2016). On scaling decentralized blockchains. *Lecture Notes in Computer Science*, vol. 9604. **DOI:10.1007/978-3-662-53357-4_8**.

[24] Slepak, G., Petrova, A. (2018). The DCS Theorem, *arXiv preprint*, arXiv:1801.04335, **DOI:10.48550/arXiv.1801.04335**.

[25] Abadi, J., Brunnermeier, M. (2018). *Blockchain Economics. Technical report*, National Bureau of Economic Research, Cambridge, **DOI:10.3386/w25407**.

[26] Gopalan, A., Sankararaman, A., Walid, A., Vishwanath, S. (2020). Stability and scalability of blockchain systems. *Proceedings of the ACM on Measurement and Analysis of Computing Systems*, vol. 4, no. 2, art. ID 35, **DOI:10.1145/3392153**.

[27] Chu, S., Wang, S. (2018). The Curses of Blockchain Decentralization, *arXiv preprint*, arXiv:1810.02937, **DOI:10.48550/arXiv.1810.02937**.

[28] Buterin, V. (2021). Why sharding is great: demystifying the technical properties, from: *https://vitalik.ca/general /2021/04/07/sharding.html*, accessed on 2022-09-02.

[29] Zhou, Q., Huang, H., Zheng, Z., Bian, J. (2020). Solutions to scalability of blockchain: A survey. *IEEE Access*, vol. 8 p. 16440-16455, **DOI:10.1109/ACCESS.2020.2967218**.

[30] Sanka, A.I., Cheung, R.C. (2021). A systematic review of blockchain scalability: Issues, solutions, analysis and future research. *Journal of Network and Computer Applications*, vol. 195, art. ID 103232, **DOI:10.1016/j.jnca.2021.103232**.

[31] Rousseau, D.M., Sitkin, S.B., Burt, R.S., Camerer, C. (1998). Not so different after all: A cross-discipline view of trust. *Academy of Management Review*, vol. 23, no. 3, 393-404, **DOI:10.5465/amr.1998.926617**.

[32] Seebacher, S., Schüritz, R. (2017). Blockchain technology as an enabler of service systems: A structured literature review. *Lecture Notes in Business Information Processing*, p. 12-23, vol. 279, **DOI:10.1007/978-3-319-56925-3_2**.

[33] Li, J., Maiti, A., Springer, M., Gray, T. (2020). Blockchain for supply chain quality management: challenges and opportunities in context of open manufacturing and industrial internet of things. *International Journal of Computer Integrated Manufacturing*, vol. 33, no. 12, p. 1321-1355, **DOI: 10.1080/0951192X.2020.1815853**.

[34] Leng, J., Yan, D., Liu, Q., Xu, K., Zhao, J.L., Shi, R., Wei, L., Zhang, D., Chen, X. (2019). Manuchain: Combining permissioned blockchain with a holistic optimization model as bi-level intelligence for smart manufacturing. *IEEE Transactions on Systems, Man, and Cybernetics: Systems*, vol. 50, no. 1, p. 182-192, **DOI:10.1109/TSMC.2019.2930418**.

[35] Ouyang, L., Yuan, Y., Wang, F.-Y. (2019). A blockchain-based framework for collaborative production in distributed and social manufacturing. *IEEE International Conference on Service Operations and Logistics, and Informatics*, p. 76-81, **DOI:10.1109/SOLI48380.2019.8955075**.

[36] Zuo, Y. (2021). Making smart manufacturing smarter-a survey on blockchain technology in industry 4.0, *Enterprise Information Systems*, vol. 15, no. 10, p. 1323-1353, **DOI:10.1080/17517575.2020.1856425**.

[37] Li, Z. Wang, W.M., Liu, G., Liu, L., He, J., Huang, G.Q. (2018). Industrial Management & Data Systems, Toward open manufacturing: A cross-enterprises knowledge and services exchange framework based on blockchain and edge computing. *Industrial Management & Data Systems*, vol. 118, no. 1, p. 303-320, **DOI:10.1108/IMDS-04-2017-0142**.

[38] Leng, J. Jiang, P., Xu, K., Liu, Q., Zhao, J.L., Bian, Y., Shi, R. (2019). Makerchain: A blockchain with chemical signature for self-organizing process in social manufacturing. *Journal of Cleaner Production*, vol. 234, p. 767-778, **DOI:10.1016/ j.jclepro.2019.06.265**.

[39] Lohmer, J. (2019). Applicability of blockchain technology in scheduling resources within distributed manufacturing. Logistics management. *Lecture Notes in Logistics*, p. 89-103, Springer, **DOI:10.1007/978-3-030-29821-0_7**.

[40] Li, Z., Barenji, A.V., Huang, G.Q. (2018). Toward a blockchain cloud manufacturing system as a peer to peer distributed network platform. *Robotics and Computer-Integrated Manufacturing*, vol. 54, p. 133-144, **DOI:10.1016/j.rcim. 2018.05.011**.

[41] Rožman, N., Diaci, J., Corn, M. (2021). Scalable framework for blockchain-based shared manufacturing. *Robotics and Computer-Integrated Manufacturing*, vol. 71, art. ID 102139, **DOI:10.1016/j.rcim.2021.102139**.

[42] Liu, J., Jiang, P. (2020). Consortium blockchain-driven decentralized organization and operation for manufacturing community in social manufacturing. *IEEE 16th International Conference on Automation Science and Engineering*, p. 576-581, **DOI:10.1109/CASE48305.2020.9216738**.

[43] Zheng, P., Zheng, Z., Luo, X., Chen, X., Liu, X. (2018). A detailed and real-time performance monitoring framework for blockchain systems. *IEEE/ACM 40th International Conference on Software Engineering: Software Engineering in Practice Track*, p. 134-143, **DOI:10.1145/3183519.3183546**.

[44] Decker, C., Wattenhofer, R. (2013). Information propagation in the bitcoin network. *IEEE P2P Proceedings*, p. 1-10, **DOI:10.1109/P2P.2013.6688704**.

[45] Weber, I., Gramoli, V., Ponomarev, A., Staples, M., Holz, R. (2017). On availability for blockchain-based systems. *IEEE 36th Symposium on Reliable Distributed Systems*, p. 64-73, **DOI:10.1109/SRDS.2017.15**.

[46] Goswami, S. (2017). *Scalability Analysis of Blockchains through Blockchain Simulation*, PhD thesis, University of Nevada, Reno.

[47] Chen, X., Lin, S., Yu, N. (2019). Bitcoin blockchain compression algorithm for blank node synchronization. *11th International Conference on Wireless Communications and Signal Processing*, p. 1-6, **DOI:10.1109/WCSP.2019.8928104**.

[48] Ehmke, C., Wessling, F., Friedrich, C.M. (2018). Proof-of-property: a lightweight and scalable blockchain protocol. *Proceedings of the 1st International Workshop on Emerging Trends in Software Engineering for Blockchain*, p. 48-51, **DOI:10.1145/3194113.3194122**.

[49] Palai, A., Vora, M., Shah, A. (2018). Empowering light nodes in blockchains with block summarization. *9th IFIP International Conference on New Technologies, Mobility and Security*, p. 1-5, **DOI:10.1109/NTMS.2018.8328735**.

[50] Rahmadika, S., Noh, S., Lee, K., Kweka, B.J., Rhee, K.-H. (2020). The dilemma of parameterizing propagation time in blockchain P2P network. *Journal of Information Processing Systems*, vol. 16, no. 3, p. 699-717, **DOI:10.3745/JIPS.03.0140**.

[51] Hafid, A., Hafid, A.S., Samih, M. (2020). Scaling blockchains: A comprehensive survey. *IEEE Access*, vol. 8, p. 125244-125262, **DOI:10.1109/ACCESS.2020.3007251**.

[52] Lombrozo, E., Lau, J., Wuille, P. (2015). Segregated witness (consensus layer), from: *https://github.com/bitcoin/bips/blob/master/bip-0141.mediawiki*, accessed on 2022-06-02.

[53] Ding, D., Jiang, X., Wang, J., Wang, H., Zhang, X., Sun, Y. (2019). Txilm: Lossy block compression with salted short hashing, *arXiv preprint*, arXiv:1906.06500, **DOI:10.48550/arXiv.1906.06500**.

[54] Nakamoto, S. (2008). *Bitcoin: A peer-to-peer electronic cash system*. Decentralized Business Review.

[55] Kiayias, A., Russell, A., David, B., Oliynykov, R., Ouroboros: A provably secure proof-of-stake blockchain protocol. *Annual International Cryptology Conference. Lecture Notes in Computer Science*, p. 357-388, **DOI:10.1007/978-3-319-63688-7_12**.

[56] Larimer, D. (2014). Delegated proof-of-stake (DPOS). *Bitshare Whitepaper*, from: *http://107.170.30.182/security/delegated-proof-of-stake.php*, accessed on 2022-06-02.

[57] Castro, M., Liskov, B. (1999). Practical byzantine fault tolerance. *Proceedings of the 3rd Symposium on Operating Systems Design and Implementation*, p. 1-14.

[58] Benčić, F.M., Žarko, I. (2018). Distributed ledger technology: Blockchain compared to directed acyclic graph. *2018 IEEE 38th International Conference on Distributed Computing Systems*, p. 1569-1570, **DOI:10.1109/ICDCS.2018.00171**.

[59] Zamani, M., Movahedi, M., Raykova, M. (2018). Rapidchain: Scaling blockchain via full sharding. *Proceedings of the ACM SIGSAC Conference on Computer and Communications Security*, p. 931-948, **DOI:10.1145/3243734.3243853**.

[60] Back, A., Corallo, M., Dashjr, L., Friedenbach, M., Maxwell, G., Miller. A., Poelstra, A., Timón, J., Wuille, P. (2014). Enabling blockchain innovations with pegged sidechains, from: *http://www.opensciencereview.com/papers/123/enablingblockchain-innovations-with-pegged-sidechains*, accessed on 2022-06-02.

[61] Poon, J., Buterin, V. (2017). Plasma: Scalable autonomous smart contracts, White paper, from *https://www.plasma.io/plasma.pdf*, accessed on 22-06-02.

[62] EthHub, Zk-rollups. (2020). from *https://docs.ethhub.io/ethereum-roadmap/layer-2-scaling/zk-rollups/* accessed on 2022-06-02.

[63] Wood, G. (2016.) Polkadot: Vision for a heterogeneous multi-chain framework, White Paper, from *https://polkadot.network/PolkaDotPaper.pdf?ref=hackernoon.com*, accessed on 2022-06-02 .

[64] Chen, Y., Li, H., Li, K., Zhang, J. (2017). An improved P2P file system scheme based on IPFS and blockchain. *IEEE International Conference on Big Data*, p. 2652-2657, **DOI:10.1109/BigData.2017.8258226**.

[65] Teutsch, J., Reitwießner, C. (2019). A scalable verification solution for blockchains, *arXiv preprint*, arXiv:1908.04756, **DOI:10.48550/arXiv.1908.04756**.

[66] Xu, J., Tian, Y., Ma, T., Al-Nabhan, N. (2020). Intelligent manufacturing security model based on improved blockchain. *Mathematical Biosciences and Engineering*, vol. 17, no. 5, 5633-5650, **DOI:10.3934/mbe.2020303**.

[67] Liu, M., Yu, F. R., Teng, Y., Leung, V. C., Song, M. (2019). Performance optimization for blockchain-enabled industrial internet of things (IIoT) systems: A deep reinforcement learning approach. *IEEE Transactions on Industrial Informatics*, vol. 15, no. 6, p. 3559-3570, **DOI:10.1109/TII.2019.2897805**.

[68] Angrish, A., Craver, B., Hasan, M., Starly, B. (2018). A case study for blockchain in manufacturing: "FabRec": A prototype for peer-to-peer network of manufacturing nodes. *Procedia Manufacturing*, vol. 26, p. 1180-1192, **DOI:10.1016/j.promfg.2018.07.154**.

[69] Yalcinkaya, E., Maffei, A., Onori, M. (2020). Blockchain reference system architecture description for the ISA95 compliant traditional and smart manufacturing systems. *Sensors*, vol. 20, no. 22, art. ID 6456, **DOI:10.3390/s20226456**.

[70] Liu, X., Wang, W.M., Guo, H., Barenji, A.V., Li, Z., Huang, G.Q. (2020). Industrial blockchain based framework for product lifecycle management in industry 4.0. *Robotics and Computer-Integrated Manufacturing*, vol. 63, art. ID 101897, **DOI:10.1016/j.rcim.2019.101897**.

[71] Pustišek, M., Chen, M., Kos, A., Kos, A. (2022). Decentralized machine autonomy for manufacturing servitization. *Sensors*, vol. 22, no. 1, art. ID 338, **DOI:10.3390/s22010338**.

[72] Javaid, U., Sikdar, B. (2021). A checkpoint enabled scalable blockchain architecture for industrial internetof things. *IEEE Transactions on Industrial Informatics*, vol. 17, no. 11, p. 7679-7687, **DOI:10.1109/TII.2020.3032607**.

[73] Shahbazi, Z., Byun, Y.-C. (2021). Smart manufacturing real-time analysis based on blockchain and machine learning approaches. *Applied Sciences*, vol. 11, no. 8, art. ID3535, **DOI:10.3390/app11083535**.

[74] Zhang, C., Zhou, G., Li, H., Cao, Y. (2020). Manufacturing blockchain of things for the configuration of a data-and knowledge-driven digital twin manufacturing cell. *IEEE Internet of Things Journal*, vol. 7, no. 12, p. 11884-11894, **DOI:10.1109/JIOT.2020.3005729**.

[75] Geng, T., Du, Y. (2022). Applying the blockchain-based deep reinforcement consensus algorithm to the intelligent manufacturing model under internet of things. *The Journal of Supercomputing*, vol 78, p. 15882-15904, **DOI:10.1007/s11227-022-04514-3**.

[76] Costa, D., Teixeira, M., Pinto, A.N., Santos, J., (2022). High-performance blockchain system for fast certification of manufacturing data. *SN Applied Sciences*, vol. 4, art. ID. 25, **DOI:10.1007/s42452-021-04909-6**.

[77] Zhang, Y., Xu., X., Liu, A., Lu, Q., Xu. L., Tao, F. (2019). Blockchain-based trust mechanism for iot-based smart manufacturing system. *IEEE Transactions on Computational Social Systems*, vol. 6, no. 5, p. 1386-1394, **DOI:10.1109/TCSS.2019.2918467**.

[78] Zheng, X., Lu, J., Sun, S., Kiritsis, D., (2020). Decentralized industrial IoT data management based on blockchain and IPFS. *IFIP International Conference on Advances in Production Management Systems*, vol. 592, p. 222-229, **DOI:10.1007/978-3-030-57997-5_26**.

[79] Suhail, S., Hussain, R., Jurdak, R., Hong, C.S. (2021). Trustworthy digital twins in the industrial internet of things with blockchain. *IEEE Internet Computing*, vol. 26, no. 3, p. 58-67, **DOI:10.1109/MIC.2021.3059320**.

[80] Shih, C.-S., Yang, K.-W. (2019). Design and implementation of distributed traceability system for smart factories based on blockchain technology. *Proceedings of the Conference on Research in Adaptive and Convergent Systems*, p. 181-188, **DOI:10.1145/3338840.3355646**.

[81] Ordieres-Meré, J., Villalba-Díez, J., Zheng, X. (2019). Challenges and opportunities for publishing IIoT data in manufacturing as a service business. *Procedia Manufacturing*, vol. 39, p. 185-193, **DOI:10.1016/j.promfg.2020.01.308**.

[82] Leivadaros, S., Kornaros, G., Coppola, M. (2021). Secure asset tracking in manufacturing through employing iota distributed ledger technology. *IEEE/ACM 21st International Symposium on Cluster, Cloud and Internet Computing*, p. 754-761, **DOI:10.1109/CCGrid51090.2021.00091**.

[83] Bhattacharjee, A., Badsha, S., Sengupta, S. (2020). Blockchain-based secure and reliable manufacturing system. *International Conferences on Internet of Things and IEEE Green Computing and Communications and IEEE Cyber, Physical and Social Computing and IEEE Smart Data and IEEE Congress on Cybermatics*, p. 228-233, **DOI:10.1109/iThings-GreenCom-CPSCom-SmartData-Cybermatics50389.2020.00052**.

[84] Cai, X., Geng, S., Zhang, J.,Wu., D., Cui, Z., Zhang, W., Chen, J. (2021). et al., A sharding scheme-based many-objective optimization algorithm for enhancing security in blockchain-enabled industrial internet of things. *IEEE Transactions on Industrial Informatics*, vol. 17, no. 11, p. 7650-7658, **DOI:10.1109/TII.2021.3051607**.

[85] Gao, N., Huo, R., Wang, S., Huang, T., Liu, Y. (2022). Sharding-hashgraph: A high performance blockchain-based framework for industrial internet of things with hashgraph mechanism. *IEEE Internet of Things Journal*, vol. 9, no. 18, p. 17070-17079, **DOI:10.1109/JIOT.2021.3126895**.

[86] Bose, S., Raikwar, M., Mukhopadhyay, D., Chattopadhyay, A., Lam, K.-Y. (2018). Blic: A blockchain protocol for manufacturing and supply chain management of ICS. *IEEE International Conference on Internet of Things and IEEE Green Computing and Communications and IEEE Cyber, Physical and Social Computing and IEEE Smart Data*, p. 1326-1335, **DOI:10.1109/Cybermatics_2018.2018.00229**.

[87] Ren, L., Zheng, S., Zhang, L. (2018). A blockchain model for industrial internet. *IEEE International Conference on Internet of Things and IEEE Green Computing and Communications and IEEE Cyber, Physical and Social Computing and IEEE Smart Data*, p. 791-794, **DOI:10.1109/Cybermatics_2018.2018.00155**.

[88] Chung, K., Yoo, H., Choe, D., Jung, H. (2019). Blockchain network based topic mining process for cognitive manufacturing. *Wireless Personal Communications*, vol. 105, p. 583-597, **DOI:10.1007/s11277-018-5979-8**.

[89] Westerkamp, M., Victor, F., Küpper, A. (2020). Tracing manufacturing processes using blockchain-based token compositions. *Digital Communications and Networks*, vol. 6, no. 2, p. 167-176, **DOI:10.1016/j.dcan.2019.01.007**.

[90] Xu, Z., Zhang, J., Song., Z., Zhou, J. (2021). A scheme for intelligent blockchain-based manufacturing industry supply chain management. *Computing*, vol. 103, p. 1771-1790, **DOI:10.1007/s00607-020-00880-z**.

[91] Li, S., Xiao, H., Qiao, J. (2021). Multi-chain and data-chains partitioning algorithm in intelligent manufacturing CPS. *Journal of Cloud Computing*, vol. 10, no. 9, **DOI:10.1186/s13677-021-00227-9**.

[92] Bellavista, P., Esposito, C., Foschini, L., Giannelli, C., Mazzocca, N., Montanari, R. (2021). Interoperable blockchains for highly-integrated supply chains in collaborative manufacturing. *Sensors*, vol. 21, art. ID 4955, **DOI:10.3390/s21154955**.

[93] Hofmann, A., Freichel, C., Winkelmann, A. (2021). A decentralized marketplace for collaborative manufacturing, Technical report. *ECIS 2021 Research Papers*, art. ID 135, from: *https://aisel.aisnet.org/ecis2021_rp/135*, accessed on 2022-06-02.

[94] Alkhader, W., Alkaabi, N., Salah, K., Jayaraman, R., Arshad, J., Omar, M. (2020). Blockchain-based traceability and management for additive manufacturing. *IEEE Access*, vol. 8 p. 188363-188377, **DOI:10.1109/access.2020.3031536**.

[95] Hewa, T. M., Braeken, A., Liyanage, M., Ylianttila, M. (2022). Fog computing and blockchain based security service architecture for 5G industrial IoT enabled cloud manufacturing. *IEEE Transactions on Industrial Informatics*, vol. 18, no. 10, p. 7174-7185, **DOI:10.1109/TII.2022.3140792**.

[96] Bai, L., Hu, M., Liu, M., Wang, J. (2019). BPIIoT: A light-weighted blockchain-based platform for industrial IoT. *IEEE Access*, vol. 7, p. 58381-58393, **DOI:10.1109/access.2019.2914223**.

[97] Adhikari, A., Winslett, M. (2019). A hybrid architecture for secure management of manufacturing data in industry 4.0. *IEEE International Conference on Pervasive Computing and Communications Workshops*, p. 973-978, **DOI:10.1109/PERCOMW.2019.8730717**.

[98] Hasan, M., Ogan, K., Starly, B. (2021). Hybrid blockchain architecture for cloud manufacturing-as-a-service (CMaaS) platforms with improved data storage and transaction efficiency. *Procedia Manufacturing*, vol. 53, p. 594-605, **DOI:10.1016/j.promfg.2021.06.060**.

[99] Qi, S., Lu, Y., Zheng, Y., Li, Y., Chen, X. (2020). Cpds: enabling compressed and private data sharing for industrial internet of things over blockchain. *IEEE Transactions on Industrial Informatics*, vol. 17, no. 4, p. 2376-2387, **DOI:10.1109/TII.2020.2998166**.

[100] Conti, M., Kumar, G., Nerurkar, P., Saha, R., Vigneri, L. (2022). A survey on security challenges and solutions in the IoTA. *Journal of Network and Computer Applications*, vol. 203, art. ID 103383, **DOI:10.1016/j.jnca.2022.103383**.

[101] Singh, A., Click, K., Parizi, R.M., Zhang, Q., Dehghantanha, A., Choo, K.K.R. (2020). Sidechain technologies in blockchain networks: An examination and state-of-the-art review. *Journal of Network and Computer Applications*, vol. 149, art. ID 102471, **DOI:10.1016/j.jnca.2019.102471**.

Strojniški vestnik - Journal of Mechanical Engineering 68(2022)10, 610-622
DOI:10.5545/sv-jme.2022.275
Original Scientific Paper
Received for review: 2022-07-08
Received revised form: 2022-08-28
Accepted for publication: 2022-09-30

A New Device Proposed for the Industrial Measurement of Rolling Bearing Friction Torque

Mateusz Wrzochal[1,*] – Stanisław Adamczak[1] – Ryszard Domagalski[1] – Grzegorz Piotrowicz[2] – Sylwester Wnuk[2]
[1] Kielce University of Technology, Poland
[2] Fabryka Lozysk Tocznych-Krasnik S.A., Poland

This article presents the general assumptions and the mechanical design of the new device for measuring the friction torque of rolling bearings, as well as a preliminary evaluation of the indications on the basis of which further detailed analyses and corrections of the prototype will be made. The device presented in the manuscript is dedicated to quality control as part of its support for rolling bearing plants.
Keywords: rolling bearings, friction torque, industrial measurement, quality control

Highlights
- *To support the rolling bearing quality control process, an industrial bearing friction torque measuring device was designed.*
- *A device was made on the basis of the proposed concept.*
- *The principle of operation and the role of the individual components of the innovative measuring device for rolling bearing testing are presented.*
- *The results of preliminary tests assessing the fulfilment of initial assumptions are presented.*

0 INTRODUCTION

Rolling bearings are a common component of machines and mechanical devices, which explains their great popularity among the interests of researchers throughout the world [1] to [3]. Often topics are taken up in relation to a specific bearing application [4] and [5]. Research from a typical production point of view is conducted less frequently [6] to [8]. It can be observed that problems related to bearing measurement under industrial conditions are generally solved by bearing producers individually; the information is confidential and, as such, it is not shared in the sector. It was thus very difficult for the researchers involved in the project to find any detailed descriptions of or patents for specialist measurement equipment to provide solutions to the specific problems encountered by Fabryka Lozysk Tocznych-Krasnik S.A., a leading Polish manufacturer of roller bearings. Since the main applications of roller bearings are in the mechanical equipment and automotive industries, the focus is on their quality. Credible measurement results obtained under laboratory conditions are required for reference by individual and industrial users all over the world to confirm the products they buy are of the best quality.

A rolling bearing can be assessed on the basis of a number of certain quantities. The friction torque, together with vibrations and durability, is one of the most important parameters determining the quality of bearings and their suitability for the intended applications. The friction torque contains a great deal of information about the bearing, whether in terms of its design, the quality of its mating parts, its cleanliness or certain lubricant properties [9] and [10]. Given the widespread use of bearings in the automotive, machinery or household appliance industries, a need is being generated to reduce friction in rolling bearings, which is a key measure in the quest to improve efficiency, reduce energy consumption, and protect the environment. Work in this direction focuses on isolating the factors that increase frictional resistance in a bearing and seeking to minimize their impact. At the same time, this creates the need to design devices that can accurately measure bearing friction torque and its subtle changes in relation to fluctuations in the factors that increase it [11].

The possibility of precise measurement of friction torque occurring in rolling bearings, as well as the knowledge of the dependence of their values on the conditions in which the bearings operate, including such factors as rotation and load, allows machine and equipment designers to optimize the selection of bearings in specific design nodes, while also enabling bearing manufacturers to assess their quality and choose the right directions for improving their designs [12] and [13].

Research on friction torque is especially important for nodes for which power losses are of high importance. Similar studies are undertaken by many research centres, as well as by leading bearing manufacturers [14] to [16]. They focus on isolating factors causing an increase in frictional resistance

*Corr. Author's Address: Kielce University of Technology, al. Tysiąclecia Państwa Polskiego 7, 25-314, Kielce, Poland, wrzochalm@gmail.com

in bearings and striving to reduce the influence of those factors [17]. All these efforts create the need to build devices that allow precisely measuring the tested bearings' friction torque and its subtle changes depending on the fluctuation of factors influencing its growth [18] to [20]. In the available sources, one can find both descriptions of test rigs measuring the friction torque of bearings intended for research purposes, as well as commercial offers of companies producing professional measuring equipment [21] to [23]. Industrial measuring devices at the disposal of companies producing rolling bearings are, however, an uncommon object of scientific research.

This article presents a new industrial device for testing the bearing friction torque of rolling bearings at the stage of their production. The device is characterized by an innovative design that allows for testing a wide range of bearing dimensions, applying significant axial loads, additional measurement of the mounting width of the bearings, and most importantly, testing the cone bearings.

1 FRICTION TORQUE OF ROLLING BEARINGS

Friction torque is defined as the resistance of the bearing when attempting to rotate one ring in relation to the other, and it depends to a greater or lesser extent on the following: type, variant and dimensions of the bearing, load values and its direction, rotational speed, type and properties of the lubricant and the method of lubrication. Friction losses in rolling bearings are caused, inter alia, by deformations at the contact between the rolling element and raceway, internal friction of the lubricant, slips and micro-slips, cage friction, as well as friction on seals [9] and [14].

The theoretical friction torque can be calculated from a well-established formula present in both older and more recent publications [3], [11], and [12]:

$$M = M_0 + M_1 , \tag{1}$$

where M_0 is a section of the equation independent of the load [N·mm]:

$$\begin{aligned} M_0 &= f_0 \cdot 10^{-7} \cdot (\nu \cdot n)^{2/3} \cdot d_m^3 \quad \text{for} \quad \nu \cdot n \geq 2000, \\ M_0 &= f_0 \cdot 10^{-7} \cdot 160 \cdot d_m^3 \qquad \text{for} \quad \nu \cdot n < 2000, \end{aligned} \tag{2}$$

where f_0 is the coefficient depending on the type of bearing and lubrication conditions, selected on the basis of tables; ν oil kinematic viscosity, [mm^2·s^{-1}]; n rotational speed, [min^{-1}]; d_m bearing pitch diameter [mm].

M_1 is the section of the equation dependent on the bearing load, [N·mm]:

$$M_1 = f_1 \cdot P \cdot d_m , \tag{3}$$

where P is equivalent load, [N]; and f_1 factor depending on the type and size of the bearing and the permissible static load coefficient.

It should be mentioned that Eq. (2), as it appeared in the publications, is simplified to some extent. For example, in Eq. (2) for $\nu \cdot n < 2000$ the component that is 160 has a unit corresponding to the expression $(\nu \cdot n)^{2/3}$. In addition, Eq. (2) assume that the density of the lubricant is equal to about 0.9 kg/dm^3. Therefore, the unit of density, which does not appear explicitly, compensates for the other units, which enables obtaining a unit that is identical to the friction torque.

There are other models proposed by industrial units, such as Timken FAG and SKF [24] to [26], which have extended the basic model with additional empirical components representing, for example, seal friction, friction resulting from the lubrication system,

Table 1. Table of values for the f_0 and f_1 factors

Bearing type	f_0			f_1
	Oil mist lubrication	Oil bath or plastic grease	Oil bath lubrication under pressure	Oil bath lubrication under pressure
Deep groove ball bearing	0.7 to 1	1.5 to 2	3 to 4	$0.0009 \cdot \left(\frac{P_0}{C_0}\right)^{0.55}$
Angular contact ball bearings	1	2	4	$0.0003 \cdot \left(\frac{P_0}{C_0}\right)^{0.4}$
Cylindrical roller bearings	1 to 1.5	2 to 3	4 to 6	0.00025 to 0.0003
Needle roller bearings	3 to 6	6 to 12	12 to 24	0.0004 to 0.0005
Spherical roller bearings	2 to 3	4 to 6	8 to 12	0.0001 to 0.0005
Tapered roller bearings	1.5 to 2	3 to 4	6 to 8	0.0004 to 0.0005

C_0 nominal static load capacity, and P_0 equivalent static load

grease compression or splash, or have formulated other relations for determining the friction torque, taking into account the structure and specific operating conditions of these bearings. However, none of these detailed proposed new models is universal; moreover, for the same bearing type and the same operating conditions, sometimes very divergent results are obtained using different models, as presented in [11]. In future it will be possible to attempt to establish a new mathematical model with the presented device, but it requires many test runs.

2 GENERAL DESIGN OF A SYSTEM FOR MEASURING THE FRICTION TORQUE OF ROLLING BEARINGS

The test rigs used to measure the friction torque, depending on the purpose of the objects tested, are suitable for tests with axial or transverse loads applied. Due to the technical difficulties related to the construction of devices used for torque measurement with simultaneous application of both axial or transverse loads, devices able to perform such tests are rare. All devices used to measure the friction torque in rolling bearings have components necessary to perform the testing procedures on the given test rig. Fig. 1 shows a general breakdown of the components (subassemblies) that make up an industrial friction torque measurement device.

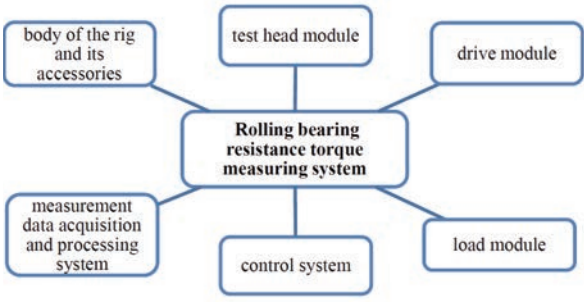

Fig. 1. *Design features of the measuring system used to test the friction torque of rolling bearings*

The test head must ensure repeatable testing conditions for the tested bearing. This is a precondition to ensure reliable comparison of results. The most dangerous situation for the node with the tested bearing is the introduction of interactions that go beyond the measurable load values in the directions controlled by the system supervising the testing process, especially the forces that may act in such a way that the bearing rings overlap each other. Solutions introduced by the testing equipment manufacturers are aimed at obtaining the best possible co-axiality and/or perpendicularity of the mated subassemblies and, where possible, to introduce a margin for connection flexibility to prevent excessive stiffness of the system. The key issue of the test head assembly design is the measuring method of the friction torque value generated by the tested bearing, especially that the measurement must be taken at different loads. The assembly transmitting the torque value to the measuring system must do so in a lossless manner or at least with a controlled loss included in the result obtained.

The spindle drive of the torque gauge should accurately reproduce the rotations set by the control system and keep them stable during the measurement. Manufacturers of torque-measuring devices typically use one of two spindle and test head power transmission systems. Some designs have the motor in line with the spindle, while other designs transmit the drive through a belt transmission. Each of the designs has its advantages and disadvantages. The advantage of placing the motor in line with the spindle is the possibility of reading the rotation of the tested bearing directly, especially if a servo drive is used as the drive unit. The introduction of a belt transmission, especially in applications requiring low revolutions and intended for measuring torques of high values, enables obtaining the required torque at lower engine power and significantly reduces the impact of its natural vibrations on the spindle and, consequently, on the test head. The selection of the motor depends on the implemented spindle speed control system.

The test load of the bearing during the test are generated, depending on its size, by gravity, a pneumatic system, or a hydraulic system. The design of the loading mechanism is to ensure that the axial (or radial) force at the value set by the test process control system is transferred to the tested bearing. Various designs of the loading systems are used, and their selection depends mainly on the value of applied force. When high value axial loads are required by the test procedure, the force is generally transmitted to the tested bearing via the spindle. When transverse loads are applied, the load is transferred to the bearing through its housing associated with the outer ring. Gravity systems can be used for a limited range of loads. Advantages of the systems based on gravity are the simple structure and high repeatability of the implementation of the set parameters. The disadvantage, however, is the problematic changing of load value and limited range of application. Systems based on pneumatic actuators are much more convenient to control but require more complex equipment and appropriate infrastructure.

Less frequently used hydraulic systems require a power station and are selected when high test loads are required.

The control and monitoring module is installed to ensure the safe operation of the device and to supervise the course of all processes carried out by the testing device. As far as the testing process carried out on the designed test rig is concerned, it is particularly important to maintain and record the parameters determining the conditions in which the measurements are taken. These include the rotational speed of the bearing and the magnitude of the applied load. The control system responsible for implementation of the testing process must effectively cooperate with the software and the driver's software by sending the information from monitoring and sensors. It must also properly react to commands resulting from procedures sent for execution. This control system is partially located directly on the test rig (sensors and amplifiers), and partially in the control cabinet equipped with an operation panel, together with the rig power supply equipment.

The test software is used to perform two basic functions. The first is transferring to the control and monitoring system the procedures necessary for the implementation of the test program, its execution and reacting to irregularities by correcting them or stopping the test rig. The second is collecting information about conducted measurements, their analysis, development, visualization of results, and preparing the test reports.

Like all measuring devices, the torque measuring device should be equipped with a stable body and anti-vibration feet. The body houses accessories such as media conditioning systems, power supply components, and control and measurement systems.

3 CONSTRUCTION OF A NEW DEVICE FOR MEASURING THE FRICTION TORQUE OF BEARINGS

The device that is the subject of this research, is one of the eight test systems built at Fabryka Lozysk Tocznych - Krasnik S.A. The new measuring practices that have been implemented allow for an improvement in the quality of the manufactured bearings and for the production of non-standard bearings, increasing the capacity of machines and mechanical devices. The new device allows controlling the friction torque: a parameter that has not been tested, as it has not been among the acceptance criteria for rolling bearings. The new device allows testing the friction torque of the bearings in any configuration of axial load and rotational speed.

For a more complete overview of the operational parameters of a tapered roller bearing, besides the knowledge of resistances that it generates at a certain axial load and rotational speed, it is important to know the changes of its mounting height. These changes are caused by the displacement of contact points of rolling elements with the ring raceways within the elastic limits of these elements under the influence of external loads imposed on the bearing. The mounting height of the tapered roller bearing, defined as the distance of the plane of the large section of the inner ring face from the plane of the large section of the outer ring face, is one of the basic parameters determining the correct mounting of a tapered roller bearing in a bearing node. It aids in determining and assuring the preload of the bearing, or possibly of the bearing unit when mounting them in a specific node, and also on the correct correction of these parameters when the node is in operation. The measurement of changes in the mounting height of tapered roller bearings as a function of load is an innovative concept for this class of industrial devices.

The design work performed allowed for the selection of 5 original design solutions. These solutions apply to both the entire test rig and its individual universal mechanisms, which can be used in other devices of a similar structure. The innovation of the presented test rig, which allows for:

- execution of cone bearing tests (similar devices are mainly used for ball bearings),
- increasing the number and range of test parameters,
- obtaining higher measurement accuracy.

The work on the bearing friction torque is important in terms of environmental protection, as striving to minimize frictional resistance increases the overall efficiency of the devices, thus reducing CO_2 emissions to the atmosphere.

It is not possible to identify a specific design principle. The starting point was the specific features and parameters that the device had to meet. The design process itself took several years. Many different solutions for individual nodes were considered, and the variant finally presented in the article was decided upon. The possibility to measure this parameter in the factory will result in significant technological progress, because the very appearance of the possibility of checking the friction torque is feedback for designers and technicians and a signal to increase the efficiency of rolling bearings.

The new device for measuring the friction torque of cone bearings is based on several plates, mounted on four columns. Some of these plates are fixed in

place with clamping blocks, while others move on linear bearings. A pneumatic actuator located on a fixed top plate drives the module that houses a spindle and a drive. This movement enables coupling and decoupling the drive with the test rig accessories. Under the movable plate with the pneumatic table, there is a force gauge measuring the load applied to the bearing. The central part of this device is a rotary table supported with an air bearing. This solution ensures the rotation of the tabletop with minimal losses. A measuring table is attached to the tabletop. The mechanism located next to the pneumatic table contains two opposing force sensors. A clamping bar moves between them, which is rigidly connected to the measuring table. The tested bearing is mounted in the special test fixture intended for a given type of bearing. The inner ring of the bearing is seated in the lower part of the fixture, which is connected to the measuring table, while the outer ring is seated in the upper part of the fixture, which is coupled with the spindle during the test.

The rotation of the outer ring (driven from the outside) causes the rolling elements to roll on the raceways, and the friction inside the bearing causes the inner ring to rotate freely, attempting to spin the entire measuring table. The pressure bar presses the sensor with a force proportional to the frictional resistance caused by the bearing operation. Higher resistance of the tested bearing (e.g., poor workmanship or a factory defect) causes the greater force to be indicated by the force sensors. The critical level of friction torque generated by a given bearing type is defined by internal company standards or requirements imposed by the customer.

3.1 Measuring Table Assembly

The measuring table assembly is the central part of the device where the actual measurement of the tested object is taken. The plate on which the measuring table assembly is placed is movable and is mounted on the columns by means of linear ball bearings, which enable it to move freely in the vertical direction. This is required to ensure the proper functioning of the device, because the pressure the plate generates allows the measurement of the force acting on the tested bearing. The pneumatic table on which the measuring table assembly with the tested bearing and the necessary accessories is mounted is designed not to resist the inner ring of the tested bearing during the test, thus allowing for a lossless measurement of the friction torque generated by the bearing loaded with high axial force, which is forced to rotate at the required rotational speed by means of the outer ring. A frame is mounted on the pneumatic table, allowing for the alignment and levelling of the measuring table assembly in relation to the loading-driving system. The lower part of the test fixture, having direct contact with the inner ring of the tested bearing, is connected to the frame by means of a steel pin. The outer ring of the bearing is located in the upper part of the fixture, which is coupled to the drive during the measurement. Due to this design, the rotation of the outer ring caused by the resistance created in the bearing causes the spontaneous rotation of the pneumatic table. The table has been adapted to test an extensive range of bearings. The measurement table assembly with the test accessories model is presented in Fig. 3. In addition to the measuring table assembly, a friction torque measurement subassembly is installed on the same plate, enabling the performance of the most important task for his device (Fig. 4). The friction torque is measured by means of two force gauges installed in opposite directions, which enables the measurements to be taken in both directions of rotation of the tested bearing. The pressure is transferred through the pressure bar attached to the base of the measuring table. It exerts pressure on one of the force gauges (depending on the rotation direction of the bearing) with a force proportional to the resistance of the tested bearing. The value of this force, multiplied by the arm length, which is the distance from the force gauge contact point with the measuring bar to the pneumatic table axis of rotation is the value that determines the friction torque of the tested bearing. The design of the subassembly protects the force gauges against overload, which could damage them if the tested object reaches a friction torque greater than the maximum assumed (e.g., as a result of bearing seizure). The protection is provided by a system of tilting arms on which force gauges and adjustable fenders are installed, limiting the possible movement of the pressure bar. The maximum pressure, and thus the load on the force gauges, controls the position of the overload protection spring.

An additional function of the device is the ability to measure the change in the width of the cone bearing caused by the applied load (displacement between the bearing rings in the axial direction). The displacement sensor positioning subassembly installed in the test zone allows monitoring changes in the height of the bearing as a function of the axial load during the test. The subassembly is fixed to the frame plate so as to be stationary in relation to its axis. Its cylindrical part is filled in the alignment hole and forms the basis for attaching the test accessories to the bearing. The

subassembly is shown in Fig. 5. The design of the subassembly is based on an eddy-current sensor and allows measurements to be made with an accuracy of 1 µm. The worm gear that drives the sensor support screw is responsible for the precise positioning of the sensor. A sensor is mounted in the head of the load-bearing screw. The axial plays in the worm wheel and plays in the screw thread are removed by springs. By one full turn of the worm wheel, the sensor moves approximately 0.2 mm vertically. This ratio allows for precise zero adjustment of the sensor position in relation to the bearing outer ring before starting the test. The assembly is rigidly fixed to the bottom of the test accessories and detects displacement of the shaft connected with the top of the test accessories. The measuring shaft, the displacement of which is formally measured, is shown in the cross-section in Fig. 3a.

3.2 Force Gauge Relieving Lever Assembly

The plate under the measuring system plate is permanently attached to the torque-measuring unit columns by means of clamping blocks, to which it is fixed by means of a sleeve with a flange. The sleeves must ensure the hole and the outer diameter are in line so as not to introduce errors in the spacing of the holes of all plates that constitute the structure of the device. A precise force gauge is installed on this plate to measure the test load during the test. A ball encapsulated in a sleeve with a conical bore presses the dynamometer. This sleeve is screwed to the underside of the movable plate with the entire measuring system.

Under the plate, there is a lever mechanism to relieve the force gauge during breaks between tests and when the device is not powered. This subassembly is constructed in such a way as to enable the lifting of the table above the pressure gauge by means of a set of springs, which exert pressure on it with appropriate force by means of a circular cam and two pins. When the device is being operated, the pneumatic actuator counteracts the pressure of the springs and lowers the spindles, freeing the measuring table and allowing measurement of the pressure. Due to the large gear ratio, the spring package and the actuator operate in the range of forces ten times smaller than the mass of the table with the test accessories. The use of such

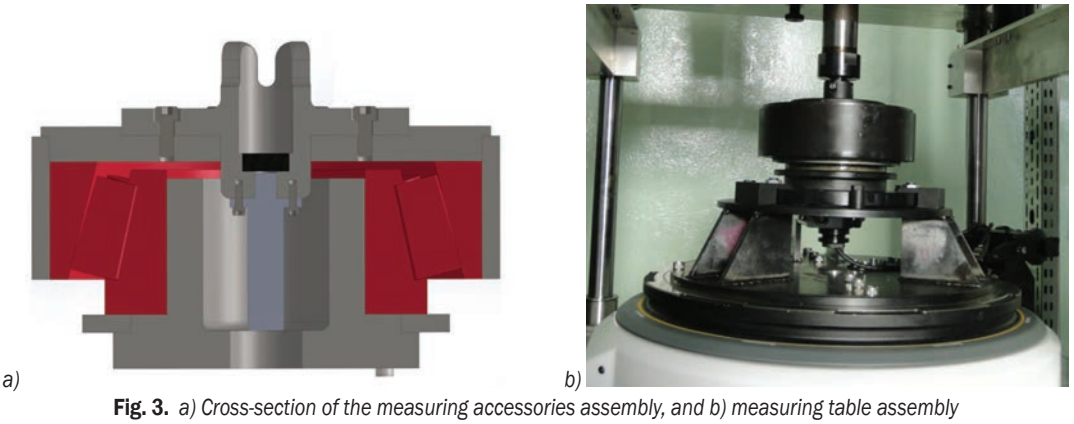

a) b)

Fig. 3. *a) Cross-section of the measuring accessories assembly, and b) measuring table assembly*

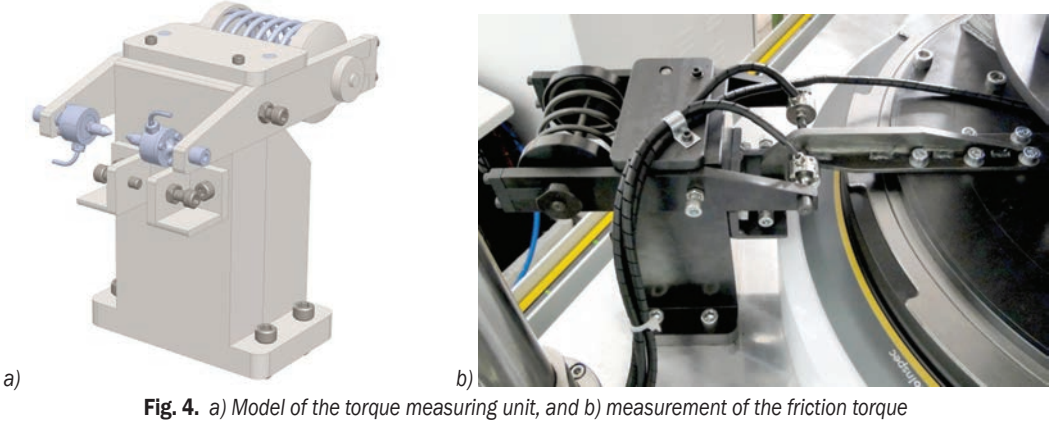

a) b)

Fig. 4. *a) Model of the torque measuring unit, and b) measurement of the friction torque*

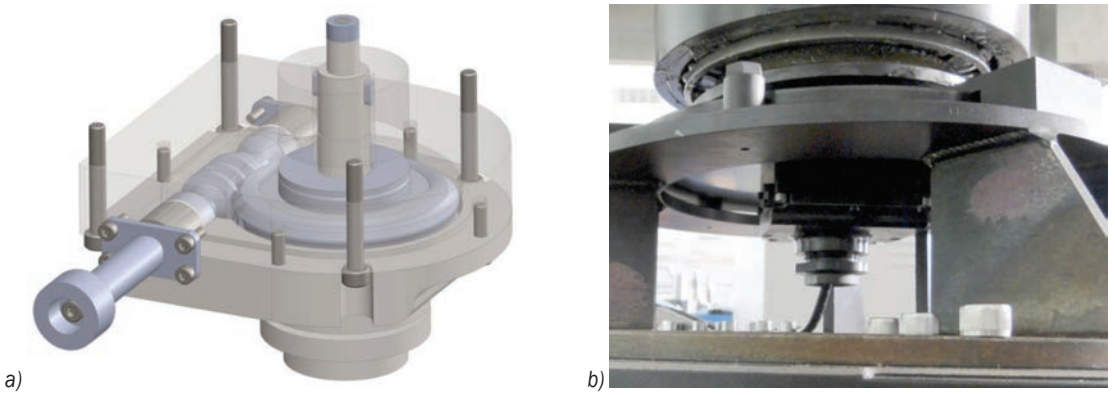

a) b)

Fig. 5. *a) Model of the assembly height measuring unit, and b) location of the assembly height measuring unit*

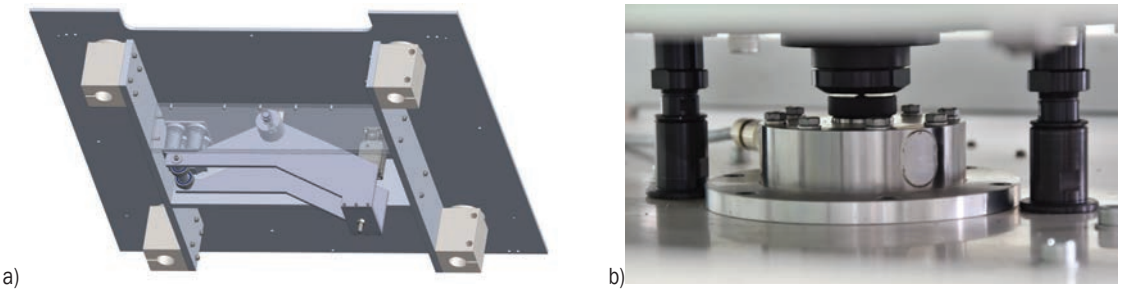

a) b)

Fig. 6. *a) Model of the lever relieving the force gauge, and b) measurement of the axial force*

a mechanism increases the durability and technical efficiency of the force gauge.

3.3 The Power and Load Transmission Unit

The power and load transmission unit plays a role of a complete power unit and an indirect load transmission unit from the pneumatic actuator. This unit has a form of a cage and includes a drive consisting of a spindle equipped with a motor and a belt transmission, which is simultaneously an intermediate element transmitting the load exerted by the pneumatic actuator to the tested bearing. Four tubes guide the assembly along the columns. They link three load-bearing posts with load-bearing plates, forming a compact integrated unit. The tube guides are supported by four pairs of linear ball bearings. Very important parameters determining the correct functioning of this unit are the equal length of the posts and the separation provided by the bearing tubes and, as in the case of all six supporting plates, the appropriate spacing of the holes leading to the columns. The power unit is fully assembled into the power and load transmission unit. The spindle, mounted in the centre of the bottom plate of the assembly, is inserted from the bottom and screwed with a ring attached from above.

The servomotor is suspended on a rotatable mounted support, which has a wide range of adjustment its position in relation to the spindle. The tensioner is mounted on a bearing tube with a block clamp. Fig. 7 shows the cage model and the spindle with the drive.

To ensure safety, the cage forming the power and load transmission unit is suspended on the relief assembly, which lifts it up and keeps it in a safe position in any emergency (power outage, compressed air outage, overload of the measuring system or emergency shutdown by the personnel). The general view of the assembly is shown in Fig. 8. The relief assembly consists of a set of four special spring shock absorbers.

The assembly is also suspended to a set of loads that is designed to apply the loads predetermined by the program to the tested bearing In addition to ensuring work safety, the relief assembly is designed to keep the spindle at a level that allows for the assembly and disassembly of bearing samples with the test accessories and to disengage the package of accessories with the sample when the test is finished or in emergency cases.

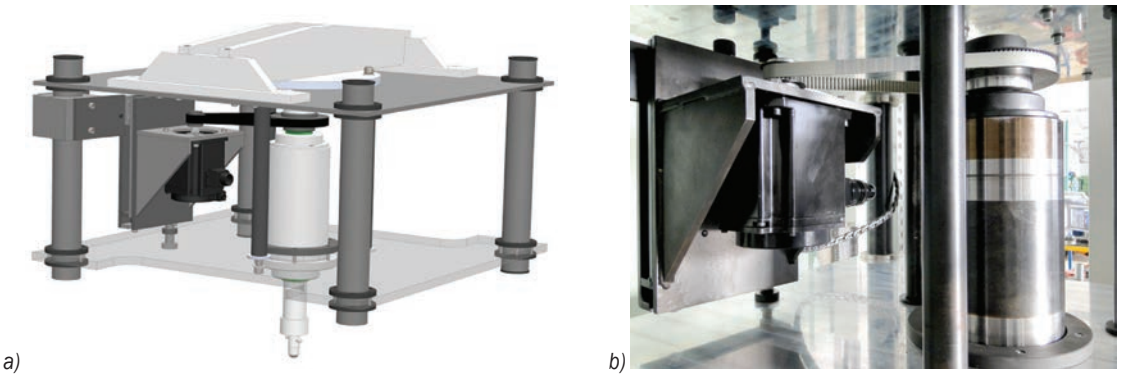

a) b)

Fig. 7. *a) Model of the power and load transmission unit, and b) drive unit with the spindle*

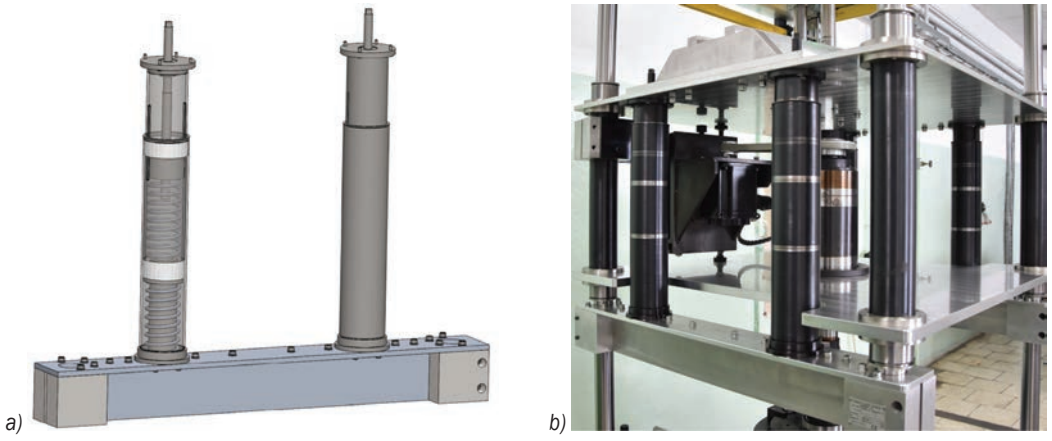

a) b)

Fig. 8. *a) Shock absorber model, and b) shock-absorbing suspension of the power and load transmission unit*

3.4 Load Assembly

The last, upper support plate is permanently connected to the columns by means of clamping blocks similarly to the two lower support plates, The plate encapsulates the entire structure of the device from above, and at the same time, serves as a platform for mounting the pneumatic actuator and creates a set of axial loads with the cylinder. This unit is coupled with the structure of the power transmission system, so as to ensure the pressure exactly along the axis of the unit. Fig. 9 shows design of the assembly. In order to couple the spindle with the measuring system and set the required force, the actuator on the top plate must first overcome the force exerted by the shock absorber springs.

Additionally, in Fig. 9b, one can see a chain of light curtain panels. Appropriate pairs of the panels are attached to the main plate of the force gauge relieving lever assembly. Interruption of the invisible light beam flowing between the pairs of the curtain panels results in the automatic stopping of the upper actuator and lifting the power and load transmission unit mechanically.

4 TESTS AND TEST PROGRAM PREPARATION

After the first launch of the test rig tests were carried out during which the following activities were performed:

- The mass, force and displacement sensors were calibrated.
- Adjustments were made to the height setting of the clamps blocking the plates in order to provide as much space as possible for the replacement of the test accessories while using the greatest possible displacement of the upper actuator.
- The degree of parallelism of the stationary plates and the degree of concentricity of the central holes (in plates, measuring table, spindle shaft, etc.) were checked using the coordinate measuring device (mobile measuring arm).
- The operation of the mechanical units of the device was checked.

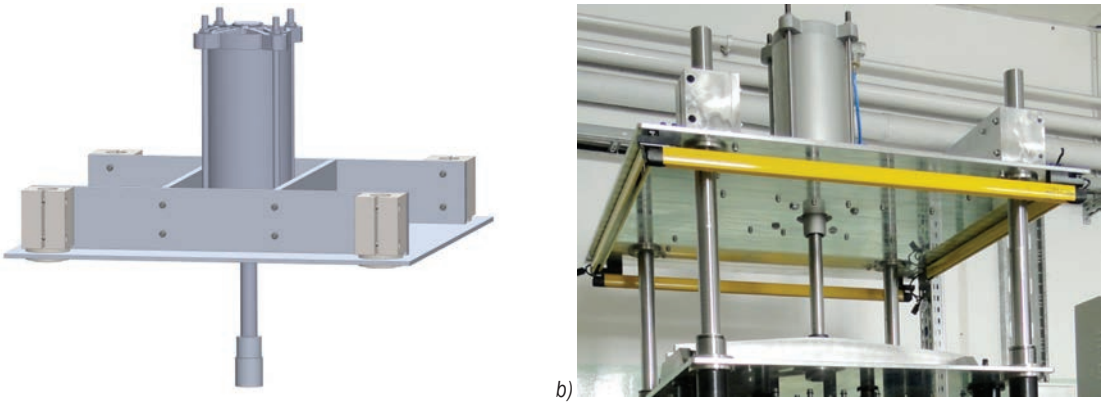

a) b)

Fig. 9. *a) Load assembly model, and b) location of the top plate with light curtains*

- The reaction of assemblies and executive subassemblies to commands of control systems sent by software and directly from the control panel was tested.
- The reaction of the safety systems to simulated threats was checked.
- The measurement sensors indications to the given loads were checked.

The activities performed above proved that the constructed test rig used for measuring the friction torque value in rolling bearings meets the initial assumptions and the general requirements for this device class. Fig. 10 show a direct screen view of the device software, which presents the measurement data on its panel in this manner. The graph is illustrative and is intended to enable the operator to quickly assess the repeatability of the results. However, the way the results shown in Fig. 10 is presented does not contribute much to their analysis in terms of evaluation of repeatability of the results obtained on a particular device. It only shows the behaviour of a specific bearing in response to changes to external parameters. In order to evaluate the repeatability of the test procedures, the results were compiled on Fig. 11 in such a way that the trend in their behaviour was visible as a function of subsequent measurements.

The task of the test program was to establish a forecast of the test results values. Therefore, the test program was prepared for a medium-sized bearing that can be tested for the maximum loads achieved on the rig. The obtained results were verified on the basis of friction torque measurement analysis for a cone roller bearing type 33213. The test program is presented below:

- The tests lasted one week; during one day two measurements of one bearing were taken, several hours apart. The tested bearing had a chance to return to the previous condition before the next test, which should help ensure the highest possible repeatability of the measurement conditions.
- Each measurement consisted of three stages, each of which had a different rotational speed: 50 rpm, 150 rpm, and 250 rpm. For each of these speeds, the axial force that loaded the bearing was changed four times: 200 daN, 500 daN, 800 daN, 1100 daN.
- Each measurement program was therefore executed as follows: after mounting the bearing in the housing and placing it on the device, the bearing was loaded with an initial force of 50 daN. The spindle then accelerated the bearing outer ring housing to 50 rpm. After reaching the set rotations, the bearing was loaded with a force of 200 daN. Once the torque value was stabilized, the measurement was taken. In the next step, the load was increased to 500 daN, and the measurement was taken again. The same steps were repeated for the load values of 800 daN and 1100 daN. An analogous sequence of measurements with different axial forces was executed after increasing the speed to 150 rpm, and then to 250 rpm. Once the test was completed, the bearing was removed from the housing.

5 THE RESULTS OF THE FRICTION TORQUE TEST

By using above methodology, a series of 10 friction torque measurement results were obtained for one cone roller bearing type 33213, at 12 different combinations of rotational speed and load. The example of obtained results presented in Fig. 10 refer to the one measurement while Fig. 11 refers to whole series of 10 measurements.

When analysing the results, it good to know the hypothetical value of the friction torque, which is calculated on the basis of Eqs. (1) to (3). By substituting the data on the 33213 bearing geometry, the viscosity of the lubricants used, the selected coefficients characteristic for the cone roller bearings, as well as the test parameters in the form of rotational speed and axial load, the theoretical values of the friction torque values presented in Table 2 were obtained. The calculated values are indicative, because the friction torque is very difficult to determine unambiguously by a theoretical calculation. This is mainly due to the fact that the coefficients f_0 and f_1 are determined empirically, and these are not unambiguous values but only a certain range of the very general three groups of lubricants. Secondly, the model described by Eqs. (1) to (3) is the basic model and one of the few models used for the calculations. As already mentioned, original formulas have been developed by SKF, FAG and Timken **[24]** to **[26]**, and the resulting predicted theoretical value of the resisting torque may differ significantly between the formulas. This is very well illustrated in **[11]**.

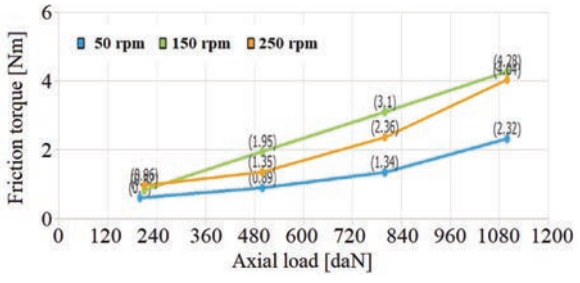

Fig. 10. *Example chart of the friction torque value changes as a function of load for various rotational speeds*

In addition to the measurement results, Table 2 shows the theoretical friction torque values for the bearing 33213. The viscosity of the oil used was assumed to be 220 mm²/s (based on the manufacturer's data). The analysis of the obtained data on the tested torque allows the following conclusions to be drawn:

Functions for a specified rotational speed value are corresponding (correlated). The only difference is the friction torque value, which always increases consistently when the load is increased. The exception is the function for the force of 1100 daN, which sometimes does not follow the trend set by the previous load values. Presumably, the bearing has inadequate operating conditions for such a high load if lubricated with a lubricant of relatively low viscosity. As a result, the friction torque behaviour is unstable.

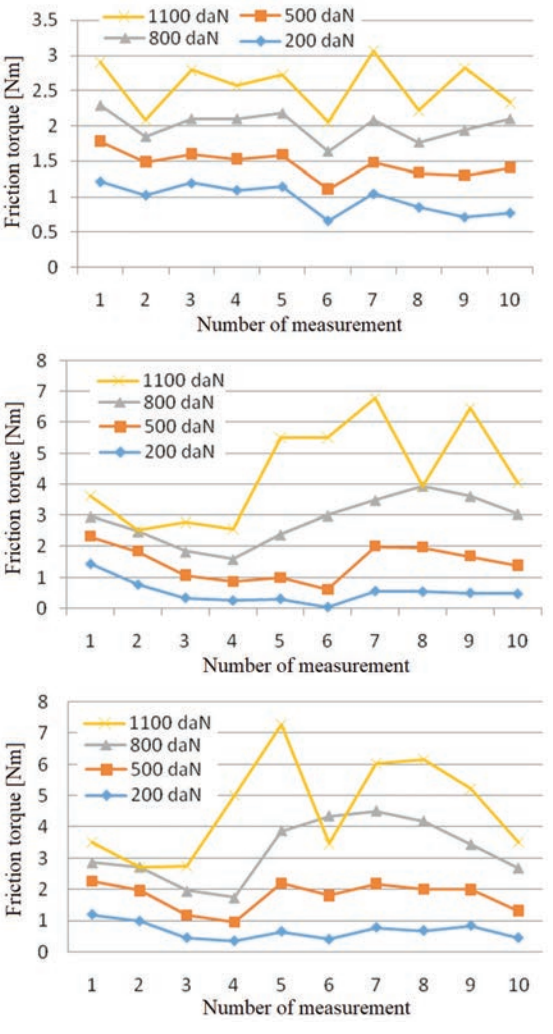

Fig. 11. *Bearing friction torque measurement series; a) rotational speed 50 rpm, b) rotational speed 150 rpm, and c) rotational speed 250 rpm*

The phenomenon of consistent duplication of the function curve when using the same rotational speed may also indicate the impact of the bearing fixture mounting method, incorrect zeroing of sensors or changes on of the bearing mating surface that occurred in previous tests (especially if the lubrication did not effectively fulfil its function).

The variabilities of the results are rising together with the rotational speed increase. The smallest variations were noticed for the rotational speed of 50 rpm. The measurement uncertainty depends mainly on the stability of the tested bearing, and not on the testing device itself. This is confirmed by the increase in the dispersion of the results along with the growing research parameters, creating more and more difficult conditions for maintaining the elasto-hydrodynamic

film. The curves obtained during the tests show that the most stable operation of the bearing is at 50 rpm, so it can be roughly assumed that the dispersion obtained for this speed is the dispersion closest to that dispersion caused by the testing device itself.

Table 2. *Results of 10 bearing 33213 measurements at different combinations of test parameters, together with a comparison with theoretical values*

Rotational speed [rpm]	Axial load, [daN]	Theoretical friction torque, [Nm]	Friction torque of bearing 33213 in the presence of 220 mm²/s viscosity oil, [Nm]		
			Arithmetic mean	Root-mean-square deviation	maximum/ minimum value
50	200	0.36	0.97	0.2	1.21/0.66
50	500	0.77	1.46	0.16	1.78/1.11
50	800	1.19	1.97	0.18	2.29/1.64
50	1100	1.6	2.56	0.36	3.06/2.05
150	200	0.44	0.54	0.21	1.46/0.06
150	500	0.86	1.49	0.52	2.33/0.62
150	800	1.27	2.83	0.8	3.93/1.6
150	1100	1.69	4.37	1.67	6.78/2.53
250	200	0.51	0.68	0.22	1.19/0.35
250	500	0.92	1.78	0.47	2.26/0.95
250	800	1.34	3.23	1.04	4.51/1.74
250	1100	1.76	4.57	1.65	7.28/2.72

In conclusion, the variability of the result of the rolling bearing friction torque measurement seems to be rational in a significant part of the obtained data. However, in order to finally decide on the reliability of the obtained results, the experiments should be repeated. This will be particularly important after adjustments have been made to the alignment or design corrections have been made.

6 CONCLUSIONS AND RECOMMENDATIONS

The performed tests showed that the obtained accuracy of the performed measurements meets the requirements of the assumptions adopted at the test rig designing stage.

The measures include:

- additional calibration of measuring sensors,
- conducting a cycle of tests aimed at optimizing the methodology of sensors zeroing before starting the measurement process,
- carrying out tests using various lubricants in order to optimize their selection for the bearing operating conditions assumed for the test,
- checking whether the function for specific rotational speeds is consistently reproduced at various loads (without dismantling of the bearing),
- performing tests on a series of bearings of different sizes and on a larger number of samples,
- checking the possibility of measuring the friction torque on a bearing with the outer ring slidably mounted.

Finally, it is worth paying attention to the level of values obtained in the test. The torque values obtained empirically are consistently greater than those obtained through calculation. This is obviously due to not taking into account all the factors affecting the bearing friction torque, such as cage friction, the geometric structure of the mating surfaces, the dimensional and shape accuracy of the bearing elements or even the lubricant purity.

Future experimental works should be aimed at determining as many factors as possible influencing the result of the friction torque measurement, simultaneously being aware that some of these factors will be caused by the measuring device itself, which is very often overlooked. Numerical simulations of the friction torque result of tapered roller bearings may also prove useful in further device evaluation studies **[27]**.

From an academic point of view, the most important thing is that the innovative solutions within the presented devices have been automatically implemented in industrial conditions as a prototype of a stand for inspecting newly manufactured bearings. The design work carried out has therefore contributed to increasing the base with new solutions for science and technology. In addition, many of the mechanisms are universal (lever, positioning mechanism, damper, pressure) and can be applied to other devices of this type.

It could also be important to investigate the influence of dynamics on the result of friction torque measurement. Eq. (2) cited in Chapter 2 suggests that as long as the quotient $v \cdot n$ is less than or equal to 2000, the friction torque does not depend on the rotational speed (no influence of dynamics on the measurement result). In other cases, the resisting torque is a function of the rotational speed (dynamics effects the measurement result).

However, measurement practice shows that the influence of dynamics can be greater even for low ranges of the product $v \cdot n$. In addition, the variability of the result over time under unchanging measurement conditions should also be investigated, as well as the reproducibility of the friction torque result.

The most difficult problem, however, is to assess the accuracy of the friction torque measuring device.

There are no standards with known friction torque. There are also no reference devices for measuring friction torque that can provide a reference for other devices. At the current level, the only possibility is to assess the accuracy of force sensors that directly measure the bearing's resistant force. From a metrological point of view, however, this is not a satisfactory solution, as the accuracy is affected by additional factors such as resistance or the rigidity of other components of the measuring system.

Further work should therefore focus on estimating uncertainty in the measurement of the friction torque, attempts to develop bearing standards with a known friction torque and comparative procedures of various devices and design solutions to select a reference stand.

7 ACKNOWLEDGMENTS

The publication was created as a result of research and development carried out by the Polish Bearing Factory, Kraśnik S.A. together with the Kielce University of Technology in the project entitled "The Establishment of R & D Centre in FŁT-Kraśnik S. A." under the Smart Growth Operational Programme 2014-2020, co-financed from the European Regional Development Fund No. CBR / 1 / 50-52 / 2017 from 07/04/2017.

8 REFERENCES

[1] Kydyrbekuly, A., Ibrayev, G., Ospan, T., & Nikonov, A. (2021). Multi-parametric dynamic analysis of a rolling bearings system. *Strojniški vestnik - Journal of Mechanical Engineering*, vol. 67, no. 9, 421-432, **DOI:10.5545/sv-jme.2021.7178**.

[2] Ying, J., Yang, Z., Chen, C., Yao, G., Hu, W., Tian, H. (2021). Lifetime analysis of motorized spindle bearings based ondynamic model. *International Journal of Advanced Manufacturing Technology*, **DOI:10.1007/s00170-021-07837-2**.

[3] Kalin, M., Vižintin, J. (1997). The influence of the lubrication type and the structure of friction torque on total friction in ball bearings. *Strojniški vestnik - Journal of Mechanical Engineering*, vol. 43, no. 5-6, p. 231-238.

[4] Liu, M., Zhou, W., Song, H., Wang, W., Zhou, S. (2018). Study of the temperature distribution of a machine tool spindle bearing based on FBG quasi-distributed sensing. *International Journal of Advanced Manufacturing Technology*, vol. 98, p. 263-274, **DOI:10.1007/s00170-018-2215-3**.

[5] Okorn, I., Nagode, M., Klemenc, J. (2018). Analysis on damage to rolling bearings at small turning angles. *Strojniški vestnik - Journal of Mechanical Engineering*, vol. 64, no. 4, p. 209-215, **DOI:10.5545/sv-jme.2017.5063**.

[6] Jiang, J., Ge, P., Sun, S., Wang, D. (2017). The theoretical and experimental research on the bearing inner ring raceway grinding process aiming to improve surface quality and process efficiency based on the integrated grinding process model. *International Journal of Advanced Manufacturing Technology*, vol. 93, p. 747-765, **DOI:10.1007/s00170-017-0462-3**.

[7] Jurko, J., Panda, A., Valíček, J., Harničárová, M., Pandová, I. (2016). Study on cone roller bearing surface roughness improvement and the effect of surface roughness on tapered roller bearing service life. *International Journal of Advanced Manufacturing Technology*, vol. 82, p. 1099-1106, **DOI:10.1007/s00170-015-7449-8**.

[8] Nosrati, A.S., Abrinia, K. (2020). A new method for bearing design in the metal extrusion of profiled sections. *International Journal of Advanced Manufacturing Technology*, vol. 106, p. 1069-1084, **DOI:10.1007/s00170-019-04681-3**.

[9] Sikorski, J., Pawlowski, W. (2020). Internal friction of ball bearings at very low temperatures. *Strojniški vestnik - Journal of Mechanical Engineering*, vol. 66, no. 4, p. 235-242, **DOI:10.5545/sv-jme.2019.639**8.

[10] Vale, J.L., Silva, C.H. (2020). Kinetic friction coefficient modeling and uncertainty measurement evaluation for a journal bearing test apparatus. *Measurement*, vol. 154, art. ID 107470, **DOI:10.1016/j.measurement. 2020.107470**.

[11] Adamczak, S., Domagalski, R., Sender, E. (2011). Friction torque in rolling bearings - methods and test facilities. *Tribology*, vol. 6, p. 19-28.

[12] Geonea, I., Dumitru, N., Dumitru, I. (2017). Experimental and theoretical study of friction torque from radial ball bearings. *Materials Science and Engineering*, vol. 252, **DOI:10.1088/1757-899X/252/1/ 012048**.

[13] Bălan, M.R.D., Houpert, L., Tufescu, A., Olaru, D.N. (2015). Rolling friction torque in ball-race contacts operating in mixed lubrication conditions. *Lubricants*, vol. 3, no. 2, p. 222-243, **DOI:10.3390/lubricants3020222**.

[14] Li, J., Chen, W., Zhang, L., Wang, T. (2016). An improved quasi-dynamic analytical method to predict skidding in roller bearings under conditions of extremely light loads and whirling. *Strojniški vestnik - Journal of Mechanical Engineering*, vol. 62, no. 2, p. 86-94, **DOI:10.5545/sv-jme.2015.2848**.

[15] Qiu, C., Wu, X., Xu, C., Qiu, X., Xue, Z. (2020). An approximate estimation approach of fault size for spalled ball bearing in induction motor by tracking multiple vibration frequencies in current. *Sensors*, vol. 20, no. 6, art. ID 1631, **DOI:10.3390/s20061631**.

[16] Li, S., Li, Y., Choi, S.W., Sarlioglu, B. (2016). High speed electric machines - challenges and design considerations. *IEEE Transactions on Transportation Electrification*, vol. 2, no. 1, p. 2-13, **DOI:10.1109/TTE.2016.2523879**.

[17] Rabréau, C., Kekula, J., Ritou, M., Sulitka, M., Shim, J., Loch, S., Furet, B. (2018). Influence of bearing kinematics hypotheses on ball bearing heat generation. *Procedia CIRP*, vol. 77, p. 622-625, **DOI:10.1016/j.procir.2018.08.192**.

[18] Dykas, B. (2006). *Factors Influencing the Performance of Foil Gas Thrust Bearings for Oil-Free Turbomachinery Applications*. PhD thesis, Department of Mechanical and Aerospace Engineering, Case Western Reserve University, Cleveland.

[19] Marques, P.M.T., Martins, R.C., Seabra, J.H.O. (2020). Experimental measurement of rolling bearing torque loss in a

modified Four-Ball machine: An improved setup. *Lubrication Science*, vol. 32, no. 5, p. 245-259, **DOI:10.1002/ls.1499**.

[20] Paleu, V., Cretu, S., Drăgan, B., Bălan, R. (2004). Test rig for friction torque measurement in rolling bearings. *The Durham University Journal. University of Durham*, vol. VIII, no. 1, p. 85-91.

[21] Fiedler, S., Kiekbusch, T., Sauer, B. (2011). Investigation of inner contact and friction conditions of a spherical roller bearing using multi-body simulation. *Periodica Polytechnica, Mechanical Engineering*, vol. 55, no. 2, p. 79-84, **DOI:10.3311/pp.me.2011-2.03**.

[22] Li, X., Liu, Y., Zhao, H., Deng, W., Sun, Y. (2017). A novel bearing fault diagnosis method based on LMD and wavelet packet energy entropy. *International Journal of Emerging Electric Power Systems*, vol. 18, no. 5, p. 1-16, **DOI:10.1515/ijeeps-2017-0091**.

[23] Dindar, A., Akkök, M., Caliskan, M. (2016). Experimental determination and analytical model of friction torque of a double row roller slewing bearing. *Journal of Tribology*, vol. 139, no. 2, art. ID 021503, **DOI:10.1115/1.4033364**.

[24] Radial Insert Ball Bearings and Housing Units. Catalogue of Schaeffler Technologies AG & Co. KG, from *https://www.bearingsandindustrialsupply.com/pdf/Schaeffler%20-%20FAG%20-%20Bearings.pdf*, accesed on 2022-10-12.

[25] The SKF model for calculating the frictional moment. SKF company materials, from *https://www.skf.com/binaries/pub12/Images/0901d1968065e9e7-The-SKF-model-for-calculating-the-frictional-moment_tcm_12-299767.pdf*, accesed on 2022-10-12.

[26] TIMKEN Engineering Manual. TIMKEN Company Handbook, from *https://www.timken.com/resources/timken-engineering-manual/*, accesed on 2022-10-12.

[27] Liebrecht, J., Si, X., Sauer, B., Schwarze, H. (2015). Investigation of drag and churning losses on tapered roller bearings. *Strojniški vestnik - Journal of Mechanical Engineering*, vol. 61, no. 6, p. 399-408, **DOI:10.5545/sv-jme.2015.2490**.

Strojniški vestnik - Journal of Mechanical Engineering 68(2022)10, 623-634
DOI:10.5545/sv-jme.2022.169
Original Scientific Paper
Received for review: 2022-04-19
Received revised form: 2022-06-23
Accepted for publication: 2022-07-11

The Nickel Aluminide Coatings Obtained on Small Holes Produced with the EDD Method

Marcin Trajer[1,*] – Łukasz Pyclik[2] _ Jerzy Robert Sobiecki[1]
[1] Warsaw University of Technology, Faculty of Material Science and Engineering, Poland
[2] Silesian University of Technology, Faculty of Materials Engineering, Poland

Recently, airplane travel has become more affordable and thus more common. This has required engineers and scientists to spend thousands of hours on the development of new material and production technologies. High-pressure turbine (HPT) components are the most heavily loaded parts from the thermal, mechanical, and corrosion points of view. Therefore, both the material from which blades and vanes are cast as well as protective coatings are being constantly developed. Better material translates into longer and safer engine operation. Coatings maintain material structures within aggressive environments. However, despite the wide scope of development, there are areas that have not been investigated, one of which is electro-discharge drilling (EDD) machined cooling holes surface and its influence on environmental coating durability. In this paper, the EDD process impact on coating durability is shown. Process residuals, such as redeposited material and recast layers, result in coating inclusions. Oxidation testing also shows the relationship between the cooling hole diameter and coating durability.
Keywords: EDD method, nickel aluminide, turbine blade, durability, jet engine

Highlights
- *Continuous performance growth pushes the exhaust gases of jet engines to higher temperatures exceeding superalloys' melting temperatures.*
- *The most common (and the only commercially utilized) design method of HPT utilizes a cooling system that consists of cooling holes creating an insulating layer of cold air.*
- *Cooling holes are machined by means of non-conventional machining methods, which result in material melting, redeposition or evaporation. EDD is one such method.*
- *Parts durability was significantly improved with the environmental coating application; the most common are those based on Al with some modifications.*
- *Aggressive HPT environments affect the whole part. Most surfaces are coating-covered; however, cooling holes' surfaces are different than the cast surface of the airfoil. The hole surface is modified due to tge manufacturing process, which impacts chemistry, phase structure and roughness.*

0 INTRODUCTION

The growth of jet engines started in early 1940s [1] with their first application. Since then, each engine element has undergone significant development. Modern trends and requirements push component manufacturing to the technological limits. Advanced statistical methods, modelling, data mining, and neural networks are in use in the race. The goal is continuous product improvement in terms of weight, cost, and durability. At the same time, the thermodynamic basis used by Frank Whittle has not changed and remains in effect for the newest engines, such as GE9X or RR Trent7000. A more efficient thermal cycle translates into higher operation temperatures, reaching up to 1350 ºC to 1550 ºC of thermal barrier coating (TBC) temperature for recent commercial engines [2]. Therefore, more durable materials as well as new cooling methods [2] are needed. Advanced film cooling through micro holes or double wall castings allowing near-wall cooling are being investigated in parallel with more resistant environmental coatings [3]. An example of a modern highly cooled and TBC-covered high-pressure turbine (HPT) blade is shown in Fig. 1. Fig. 2 shows the relationship between component heat load, cooling effectiveness and new materials application.

Fig. 1. *Recent film-cooled high-pressure turbine blade covered with ceramic TBC coating [4]*

*Corr. Author's Address: Warsaw University of Technology, Faculty of Material Science and Engineering, Wołoska 141, 02-507 Warsaw, Poland marcin.trajer.dokt@pw.edu.pl

Improvements in high temperature creep and rupture properties contrast the machinability of those materials. In parallel with requirement for more sophisticated cooling systems and tighter tolerances [5], production methods are being studied for their enhancement. There are methods that might be used for cooling hole manufacturing. Li et al. [6] provide a comprehensive summary of the following drilling methods: mechanical, laser, electro-discharge, and electrochemical. Each method has its own advantages but also difficulties. Each method differently influences manufactured material surface properties including chemical and physical changes. Electro-discharge machining (EDM), laser, and chemical are contactless methods, but EDM and laser use heat, which influences surface integrity. In contrast, electro-chemical machining (ECM) of small holes relates to significant technological and environmental challenges. Mechanical drilling is an unsuitable technique for current heat-resistant alloys mainly due to technical issues related to material hardness and hole sizes (less than 1 mm in diameter). With the above short summary, there are two main techniques currently used for drilling and shaping holes cooling: electro-discharge drill (EDD) and laser. What is common for them is surface modification resulting from local melting and evaporation of the material. Melting can drive local changes in material chemical composition and crystallographic structure. As discussed by Zielinska [7], that can influence the environmental coating applied on such surfaces.

Numerous papers describe generic aspects of the EDD process, either from a general perspective, such as Kunieda et al. [8], or from a process parameters point of view, as presented by Machno [9]. Scientists look for optimal relationships between the material removal rate (MRR), surface roughness (SR) and tool wear (TW), as well as the post EDD surface condition and its susceptibility for fracturing [10]. Such studies allow for a better understanding of the process. That allows for its optimization by means of statistical and neural network analysis (NNA). Such models enable defining certain process parameters, which result in optimal process factors, such as MRR, TW, or SR.

The influence of EDD parameters on holes surface topography was verified by Novovic [11]. The impact on surface quality was studied by Ekmekci [12]. It was verified when certain parameters influence part life (roughness, cracks). However, even outstanding progress in cooling design and manufacturing is not enough to ensure the sufficient durability of the components. Fig. 3 shows a blade fracture example. That is mainly due to coatings being a limiting chain. For that reason, new protection methods are developed.

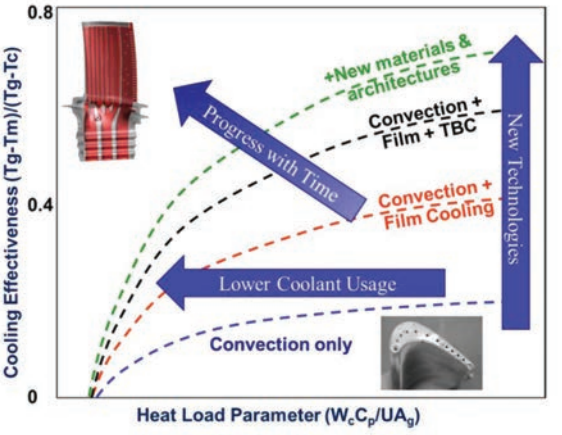

Fig. 2. *Notional component cooling technology curves* [2]

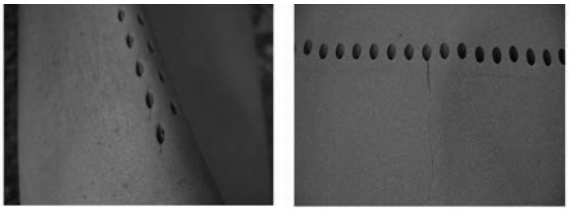

Fig. 3. *Examples of cracks initiated from EDD holes on rotating blades* [10]

Multiple studies have been performed regarding coating durability and methods for its improvement. Sun et al. showed the impact of cooling holes on part durability [13]. Accordingly, publications related to aluminide coating application, chemical composition and durability were reviewed, which revealed a lack of verification of whether the EDM manufacturing process had any impact on subsequently applied aluminide coating. This paper summarizes articles in which authors evaluated EDM cooling holes process as well as environmental aluminide coating durability. Additionally, initial tests verifying the interaction between aluminide coating and machined EDM surfaces is presented.

1 REVIEW OF EDD PROCESS AND ITS INFLUENCE ON SURFACE CONDITION

Within the electro-discharge drilling process, there is no tool material contact. No mechanical forces are applied by the tool. Material removal occurs due to energy transfer between the electrode and the part. Energy in the form of a spark causes local material melting and evaporation. Other models describe

that as a material disruption under thermal load. During operation, both the electrode and the part material are removed. Such process physics results in its complexity and specific surface conditions. The electro-discharge process has been under constant development and improvement since the 1940s when it was first developed. In 1943, Lazarenko and Lazarenko [14] investigated ways of preventing the erosion of tungsten electrical contacts due to sparking. They noticed that when the contacts were immersed in oil, sparking could result in controllable material removal. Simultaneously, a similar sparking tool for broken drill removal from aluminium castings was developed in the US. Over the years, several aspects of the EDM process have been evaluated.

One of the crucial factors of the EDD process is recast layer thickness and microcrack occurrence in the machined surfaces. Recast is a material that melted during sparking and then rapidly solidified see Fig. 4. Due to its cracking susceptibility, high hardness, and the number of microcracks, cracks and high tensile stress [15] recast layer thickness (RLT) reduction methods have been investigated. Li described with basic process parameters such as pulse width, pulse interval, voltage, current and flushing pressure within an experiment [16]. The study enabled an RLT reduction from 10.472 µm to 2.416 µm.

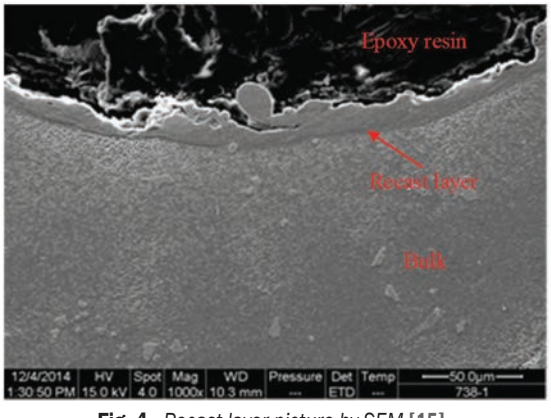

Fig. 4. *Recast layer picture by SEM* [15]

Swiercz et al. [17] shows key parameters impacting surface roughness as well as RLT. It was proved that key factor is pulse duration and current value. Similar, but not identical conclusions were shared by Lee [18]. The main factor responsible for RLT increase is pulse-on whereas current is listed as a second factor responsible for RLT thickness variation. Another key aspect of the EDM process used for small hole manufacturing is its accuracy. Process parameters influence not only surface roughness or its integrity but also manufacturing accuracy. Hole diameter and tapering are commonly evaluated parameters. Machno [9] shows that increases in pulse-on time reduces hole tapering. At the same time, the pulse current is indicated as the main contributor to increased hole taper [19].

However, even extremely durable turbine components equipped with advanced cooling systems are still exposed to exhaust gases in combustion products. Such an environment significantly influences material durability by oxidation and/ or corrosion. State-of-the art manufacturing itself is not capable of eliminating or even reducing that condition.

2 SURFACE PROTECTION

High operating temperature [20] negatively influences material mechanical properties, such as low cycle fatigue life, high cycle fatigue life, or creep. However, there are other factors with adverse effects. Corrosion and oxidation play significant roles in component degradation. Exhaust gases are rich in oxygen, and fuel combustion products have high sulphur context. Accompanied by high temperatures, these elements play a key role in material reduction [21].

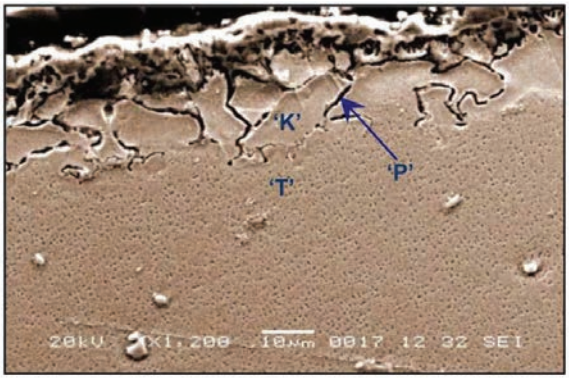

Fig. 5. *Corroded depleted zone (K)* [21]

Extensive research of protective coatings for nickel-based alloys started in the early 1960s [3]. Experiments proved that aluminide coatings provide the best environmental protection for nickel-based superalloys. Since then, aluminide coating technology has improved constantly. The most common verification method for new concepts is a cyclic oxidation test [22] and [23], which simulates engine-induced thermal and mechanical loads [3]. Such testing allows for material/coating oxidation resistance verification under transient thermal loads. Even verified as sufficient for the design, coating technology requires constant improvement. That

happens due to already mentioned situation: the technical race for more efficient jet engines and their longer flight times. As stated earlier, each new engine generation is designed for higher temperatures of its thermal cycle. That results in a larger spread of temperatures over turbine parts, especially nozzles. Improvements in coating system durability can be made in several ways. Historically, the first step was to improve the aluminide coating process to allow "self-healing" by alumina transfer. However, as the thermal gradient on the parts increases, coating brittleness becomes a significant issue. The search for improvement in that area led to different application methods **[24]** or specific dopants **[25]** to **[27]** such as rhodium, zirconium, hafnium, palladium, and yttrium. Another path is thermal gradient reduction, which reduces the spallation of the protective layer of alumina oxides. That is realized by the physical insulation of the metal surface from hot path gasses by ceramic coating. The application of those coatings, their properties and thermal loads resistance is another area of coatings, which is intensively investigated.

3 MATERIALS

Inconel 718 material samples were used; the plates had dimensions as follows: 50 mm × 25 mm × 3 mm. Table 1 shows material composition.

Table 1. *Inconel 718 composition*

	Ni	Cr	Nb	Mo	Ti
Inco 718	52.5	19	5.15	3.05	0.85
	Al	Co	Cu	C	Si/Mn
	0.5	1	0.3	0.08	0.35

Samples were cut from 3 mm thick sheet metal were delivered by TW Metals, Poland together with material certification.

Brass tube electrodes were used for EDD process. Material certification was not provided. SEM evaluation was performed to reveal material composition.

The SEM evaluation shows Cu/Zn composition at 70/30 rate (Fig. 6). This fits to ASTM B135 brass. This alloy is dedicated to extruded elements.

Within the EDD process, deionized water circulates in a closed system. Process debris are removed by two stage filtering system based on 5-micron paper filers. Constant 1 S/m water conductivity is maintained. If needed, ions are moved by resin source.

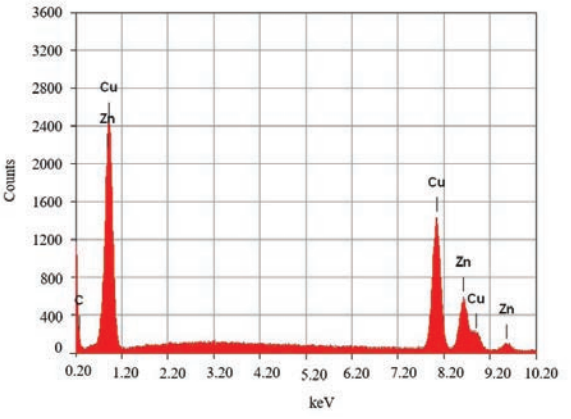

Element	keV	Mass [%]	Error [%]
Cu	8.04	68.67	1.53
Zn	8.63	31.33	1.96
Total		100	

Fig. 6. *Electrode material verification by means of EDS*

4 METHODS

4.1 Electro-Discharge Drilling

The drilled hole pattern is shown on Fig. 7. The smallest and medium holes were created by EDD, while the largest one was shaped by the electrode. Brass electrodes were used in all cases: 0.25 mm, 0.3 mm, and 0.3 mm milling, respectively. Holes are 30 deg inclined to the surface. Discharge parameters were identical between samples with the difference that largest holes were milled. That technique uses an electrode similarly to milling cutting tool. The electrode tip travels horizontally. All holes were drilled through and are open on both surfaces. Fig. 8 shows EDD system schematic.

Fig. 7. *Inconel 718 test samples*

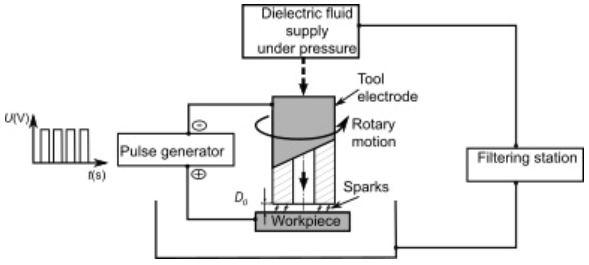

Fig. 8. *EDD system schematics*

4.2 Holes Geometrical Measurements

Pattern holes have been measured by means of an Alicona G5 optical system, which uses a variable focus method for surface scanning. A 10× lens dedicated for small holes inspection was used. After scanning, the data were transferred to the GOM Inspect software where measurements were done automatically with the macro-calculating best fit cylinder for each hole. Gaussian roughness distribution was used for inscribed cylinder fitting.

4.3 Out-of-pack Coating Process

Protective coating is frequently used in the aeronautics industry, especially on the blades of the high-pressure turbine, which run at very high temperatures and in a highly oxidizing atmosphere.

The out-of-pack or over-pack process operates in a manner like pack cementation except that the components to be coated are suspended either above the pack or below from the pack (vapour generator) retort.

The transfer of aluminium species from the vapour phase to the substrate occurs by gas-phase diffusion and by solid-phase diffusion of aluminium into the substrate to form the aluminide phases. The former increases the surface concentration of aluminium in the coating while the latter decreases it. The surface composition of the coating tends to reach a steady state value in a short time after the commencement of the process. In the vapour phase aluminizing, the rate of transport of aluminium to the substrate is much faster than the solid phase diffusion of aluminium into the substrate. Thus, the composition of aluminide coating is decided by the kinetics of the solid phase diffusion. The coating process is divided into several steps:

a) Formation of the aluminium subchlorides by the reaction of the aluminium metal or alloy and the aluminium chloride vapor;
b) Transport of the subchlorides to the substrate by gas-phase diffusion;
c) Reaction leading to the deposition of aluminium at the substrate surface;
d) Diffusion of aluminium into substrate with the formation of the coating consisting of different intermetallic phases;
e) Diffusion of the reaction products from the substrate back to the reactor.

Steps a) and c) are very fast at the operating temperature; therefore, the thickness of the coating process is controlled by step b) the vapor transport and d) the solid-phase diffusion. Step e) determines the purity of the coating [28].

The schematic diagram of the out-of-pack process is given in Fig. 9. The coating vapours are transported to the components by an inert carrier gas. The plumbing is designed so that the vapours can access both external and internal surfaces of the components. The retort is inserted into a furnace and held at the desired temperature for the selected duration.

This approach results in a much cleaner and uniform coating for very complicated geometry components, with no entrapped pack particles [28].

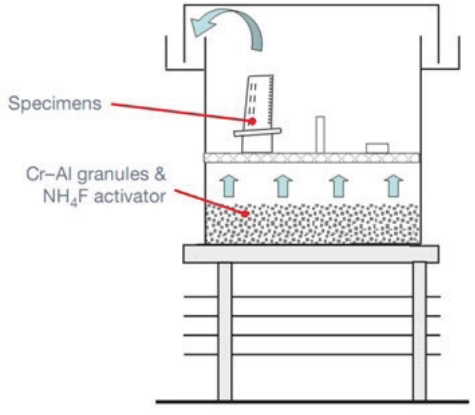

Fig. 9. *Schematic of the out-of-pack vapor phase aluminizing process*

4.4 Metallography and Coating Characterization

Analysis of the morphology, surface topography, and chemical composition of the coating was carried out by optical microscope. as well as by SEM equipped XRD evaluation and material composition. For visual observation, a Keyence VHX-7000 device was used. SEM evaluation was performed with a JEOL JSM-6490LA device equipped with an XRD extension.

The XRD phase composition of the obtained layers was determined with Brucker AXS D8

Discover diffractometer using CuK_α radiation with a wavelength of $\lambda = 0.154$ nm. In order to provide the opportunity to probe the structural evolution of solid near the surface, the grazing incidence X-ray diffraction (GIXRD) was used. A monochromatic X-ray beam with a wavelength of 0.15 nm was used. The GIXRD setup is equipped with a parabolic Göbel mirror and a conventional line focus Cu radiation tube (40 kV / 40 mA). The incidence angle was fixed at 2º with 2θ range 20º to 120º with step of 0.025º.

Adhesion of the coating to the Inconel substrate was verified using a CMS Instruments RST scratch tester with a diamond stylus with a 200 µm spherical tip radius. The indenter load was set to several values: 5 N, 20 N, 40 N, 60 N, 80 N, 100 N, and 200 N. All tests were performed over a 4 mm length. The adhesion of the coatings was evaluated based on an LC_3 curve. The LC_3 critical load occurs with the coating delamination force and was determined based on acoustic emission measured and post-test scratch images evaluation.

5 OXIDATION TESTING

Testing was performed in air atmosphere with a MAB FE37 furnace (Forno Mab, Italy) for oxidation testing. Samples were placed on ceramic support, heated in air up to 1100 ºC and treated for 23 hours. After that time, heating was turned off. Samples cooled down in the furnace.

5.1 Metallographic Evaluation

Metallurgical evaluation was performed with a Keyence VX7000 microscope. Keyence software was used.

6 EXPERIMENTAL PROCEDURE

6.1 Hole Manufacturing

Hole drilling was performed automatically using a CNC-coded procedure. All holes were drilled with same parameters. Moreover, each new electrode was checked for minimum water flow. If the flow rate was below a certain level, the electrode was assumed to be not acceptable and replaced with a new one. Samples were hold by dedicated fixture ensuring position repeatability. Manual assistance was limited to electrodes and sample change. Each hole was verified if drilled through. Once drilled, each sample was vibropeen marked.

6.2 Aluminide-coating Process

Machined samples were cleaned in isopropyl alcohol. The next step was the vapor phase aluminizing "above pack" process.

The vapor phase aluminizing (VPA) installation is a full industrial-scale furnace equipped with carbon boxes and plates shown Fig. 10. The donor in the form of a pellet and activator were distributed on the box bottom evenly. Then, a carbon perforated plate was installed as a base for positioning of components to coat.

Fig. 10. *Bell-cover with boxes before loading to VPA furnace*

The sample was installed on a hanger and placed in a box, and then moved under a sealed bell-cover in the aluminizing process. The hangers were previously qualified to ensure coating results like the components.

The protective gas is sent to the boxes and the bell-cover with the appropriate flow rate after whole air evacuation by reaching a high vacuum level. Load temperature and argon flows (primary and secondary) are key controlled parameters. The bell-cover was removed after cooling below 300 ºC. After reaching ambient temperature, carbon boxes were disassembled. The sample was dedicated to lab preparation without further post coating heat treatment in "as coated" condition.

The consumable materials are collected in Table 2 and heat treatment process shown in Table 3 were matched to obtain aluminide coating within aviation industry requirements.

Table 2. *Consumables used in standard aluminization process*

Material	Function	Chemical composition	Quantity
Al-Cr alloy (granulates)	Donor	30/70	50 kg
Ammonium fluoride (powder)	Activator	NH4F	40 kg
Protective gas	Protection	Technical Ar	as needed

Coating is done following dedicated cycle.

Table 3. *Coating heating testament process cycle*

Phase	Set point [ºC]	Main argon flow [l/h]	Secondary argon flow [l/h]	Time /ramp [h]
Heating	800	2500		2.0
Soak	800	2500		0.5
Heating	1050	2500		2.0
Heating	1080	2500		0.5
Soak	1080	2500		6.0
Cooling	300	3600	300	Until set temperature reached

6.3 Oxidation Test

Next, the sample was placed in a high temperature furnace, heated up to 1100 ºC and held in air atmosphere for 23 hours and then cooled down in the furnace. An oxidized plate was cut following the cut-up plan and subsequently a mount was processed. Several grades of sandpaper were used for sample preparation. Final polishing was done with diamond paste.

7 RESULTS

7.1 Diameter and Surface Roughness of Drilled Holes

The first measurement was geometrical holes verification. Each hole was 3D scanned using the Alicona system. Figure 11 shows a scan example. A dedicated macro was used for scanning and geometry extraction automation. That also reduced the operator influence on the measurement. The average diameter for largest holes (A) was: 1.085 mm with standard deviation 0.02 mm, for medium holes (B): 0.639 mm with standard deviation 0.016 mm and the smallest (C): 0.394 mm with standard deviation of 0.009 mm.

One plate was cut, and a hole was opened through polishing to allow hole wall roughness measurement (Fig. 12). The hole internal surface roughness is about 3.2 Ra. This was also done with the Alicona system. At this point, roughness was not a subject of further evaluation.

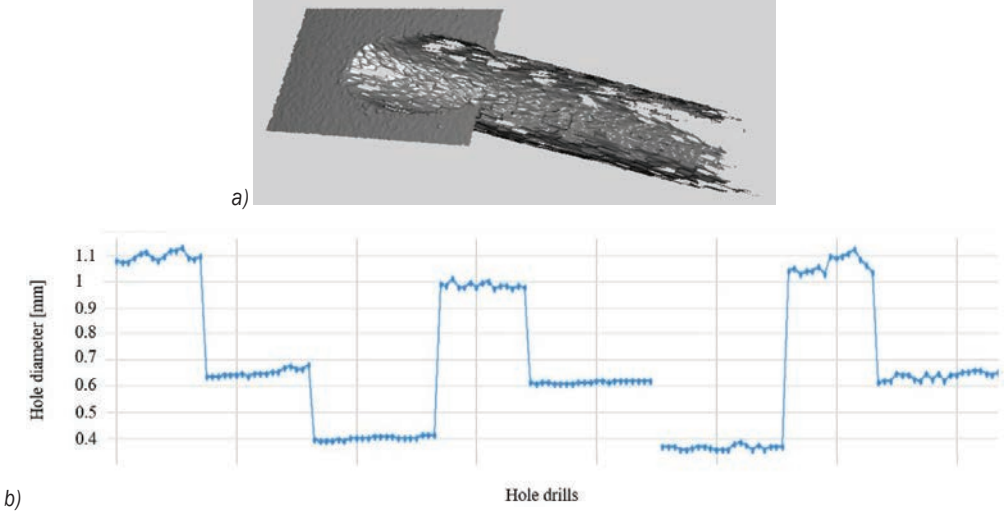

Fig. 11. *a) Scan of the hole, and b) measurements of the pattern*

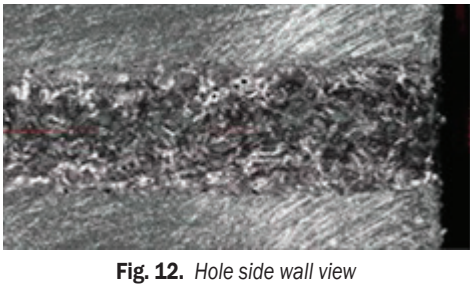

Fig. 12. *Hole side wall view*

7.2 As Drilled Surface Characterization

Prior coating of the "as drilled" sample was evaluated for surface condition. Fig. 13 shows the hole surface. Remelted material is visible. The performed material compositing analysis did not reveal any significant deviation from INCO 718. Moreover, no electrode material was recorded. Composition is shown on Fig. 14.

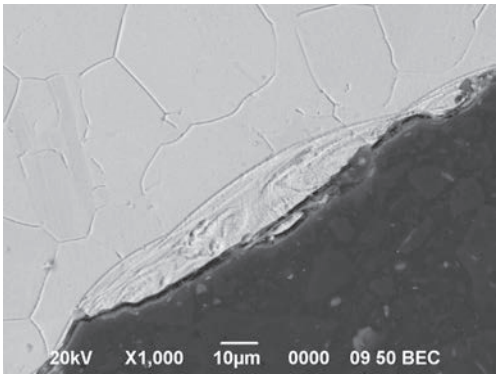

Fig. 13. *View of remelted material (recast)*

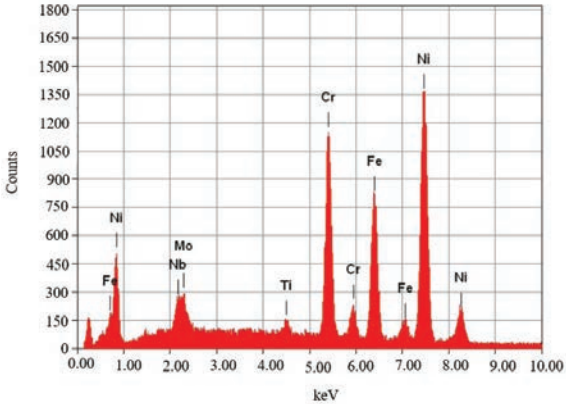

Fig. 14. *Recast composition*

7.3 Coating Characterization

Post-coating metallographic evaluation was performed on one half of the sample. Coating was evaluated for thickness (Fig. 16), inclusions (Fig. 17), and aluminium content. Visual observation of all holes was performed. It was noticed that smaller hole additive coating layer contains more contaminants (dark areas) comparing to other two-hole sizes.

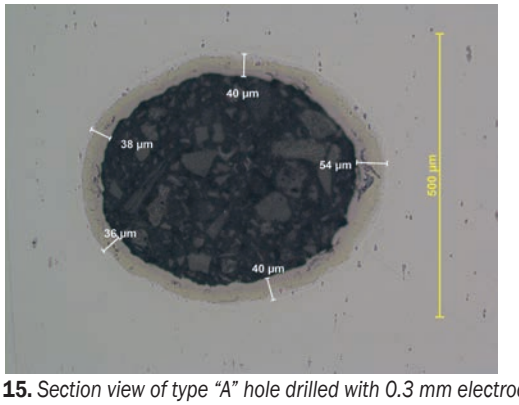

Fig. 15. *Section view of type "A" hole drilled with 0.3 mm electrode*

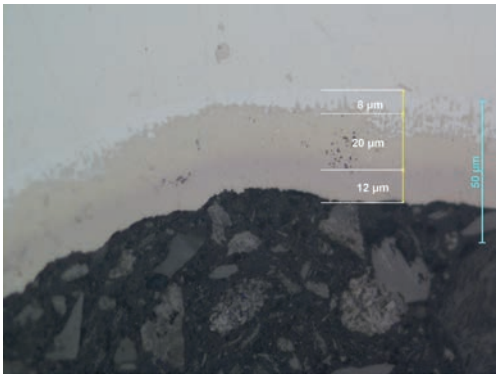

Fig. 16. *Coating thickness for "A" hole. Three layer visible: diffusion, build-up, build-up blue zone*

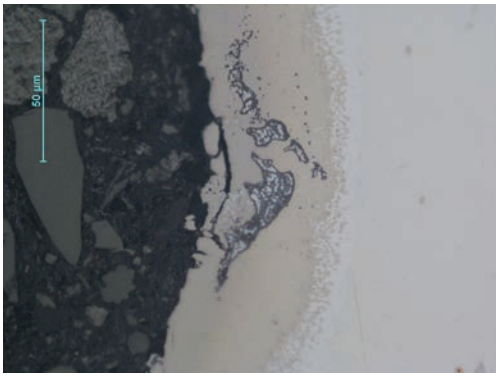

Fig. 17. *Coating inclusion for type "A" hole*

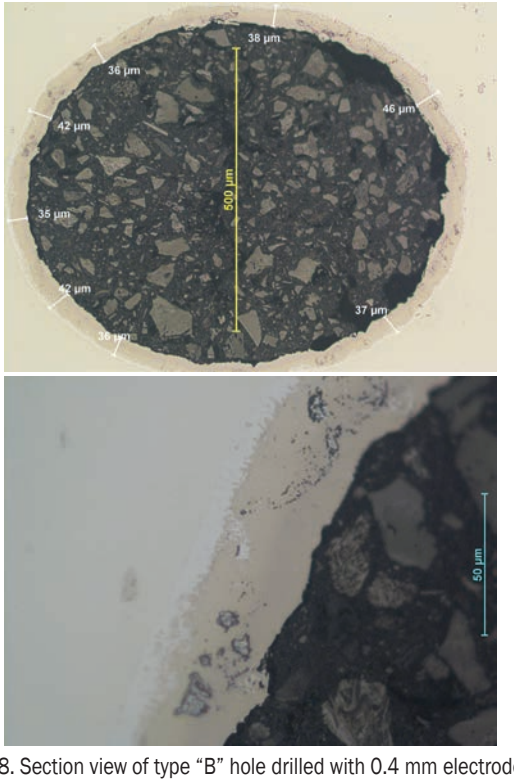

Fig. 18. Section view of type "B" hole drilled with 0.4 mm electrode; a) complete hole view, and b) coating debris

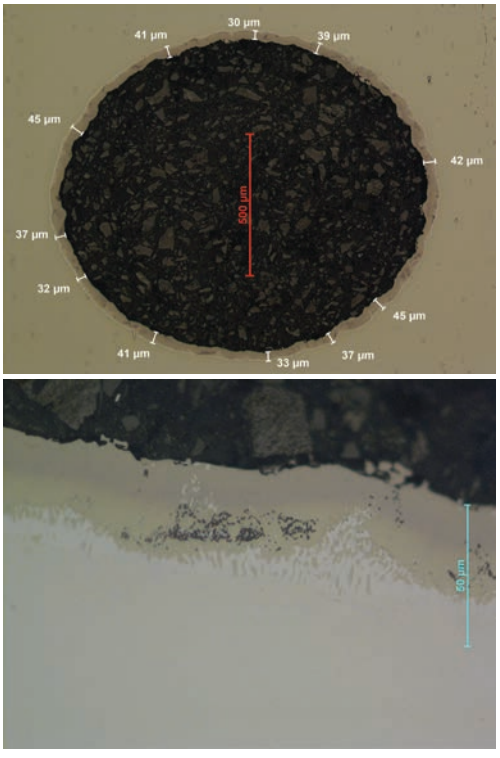

Fig. 19. *a) Section view of the type "C" hole milled with 0.4 electrode, and b) coating inclusions*

During the evaluation, the authors had no apparatus or software to perform quantitative measurements on inclusion quantity or their total area. If studies are continued, such equipment could allow for more precise evaluation. Coating thickness was measured (Figs. 18 and 19). Measurements were made with a Keyence VHX7000 microscope. Fig. 22 shows box plot graph summarizing thickness measurements.

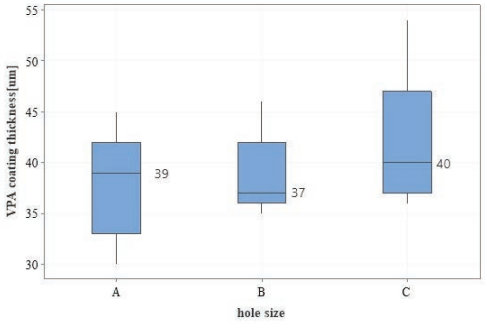

Fig. 20. *Example of coating thickness (overall) measurements for smallest hole and summary box plot*

SEM evaluation revealed that the coating consists of two layers: additive and diffusion. The JEOL JSM-6490LA device was used for measurements. As mentioned, dark areas have also been observed during this evaluation. Similarly, as for visual examination, the smallest hole section is used to show results (Fig. 21a and c).

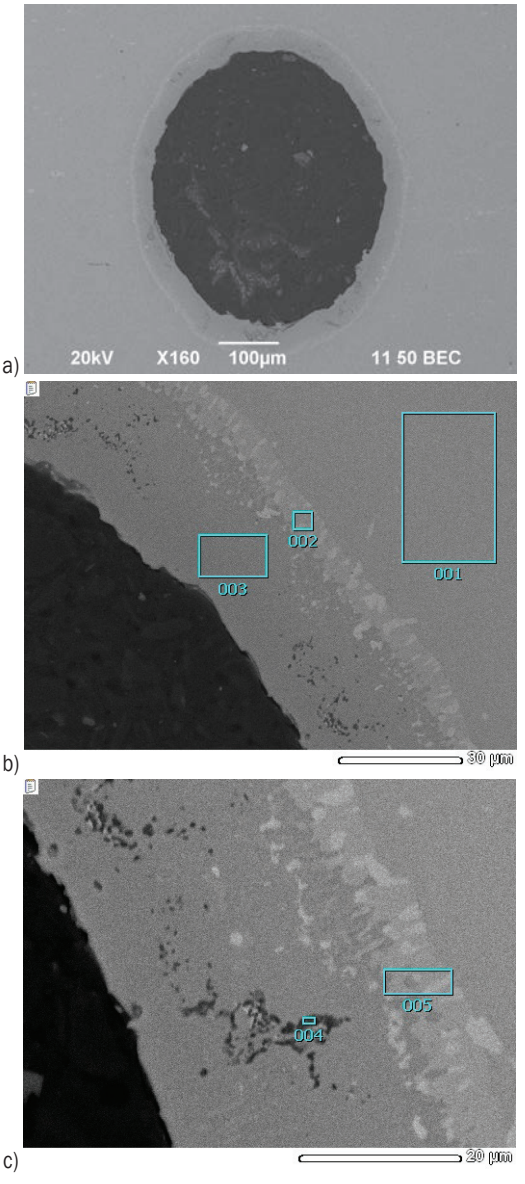

Fig. 21. *a) hole section, and b) and c) EDS zones*

EDS analysis confirmed aluminium content; however, in case of dark spots, oxygen was also detected. It might be assumed that dark spots are alumina oxides. For zones 2 (Fig. 21b) and 5 (Fig. 21c) examination of hole C coating, as well as EDS results show higher aluminium content than alloy composition. Zone 1 (Fig. 21b) shows composition corresponding to Inconel, except for carbon which might come from the resin used for mount preparation.

Table 4. *EDS results for zones 1 to 5*

	EDS zone [mass %]				
Element	1	2	3	4	5
C	1.99	4.38	3.14	10.23	1.6
O				10.79	1.91
Al	0.32	1.7	15.14	29.85	3.39
Ti	0.85	0.56		0.46	0.66
V		0.58			
Cr	17.65	35.69	2.64	5.47	31.43
Mn		1.48			0.88
Fe	19.6	27.9	9.5	7.06	24.76
Ni	54.73	24.63	69.59	30.68	27.35
Nb	3.59				5.39
Mo	1.27	3.09			2.64

7.4 XRD Testing

The sample's external surface was examined for phase composition. X-ray diffractometry was used. Graphs for two angles (1 and 2 degrees) were made. Both showed the same spectra. Therefore, detailed evaluation was performed only for the 2 degrees angle shown on Figs. 22 and 23.

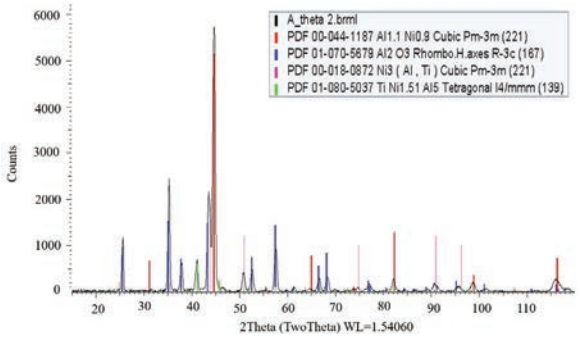

Fig. 22. *Phase analysis for 2deg theta angle*

Surface layer evaluation revealed the presence of aluminide oxide (Al_2O_3) and nickel aluminide (NiAl). This composition was expected and confirmed aluminide type coating existence on the surface.

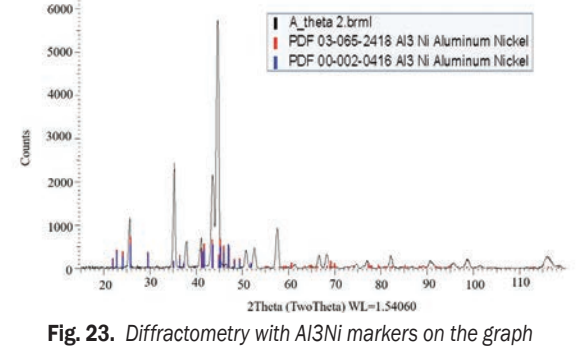

Fig. 23. *Diffractometry with Al3Ni markers on the graph*

Analysis confirmed presence of Al_3Ni, which confirmed the existence of key coating compounds including oxidized aluminium layer.

7.5 Oxidation Testing

Second half of the sample was placed into the air furnace and heated up to 1100 ºC. Atmospheric oxidation test was held for 23 hours. Next, the sample mount was prepared. Visual examination conducted with the Keyence 7000 device revealed a coating thickness reduction, as well as surface degradation. Fig. 24a shows post oxidation SEM examination of hole outline. The zoomed area in Fig. 24b contains alumina rich dark spots.

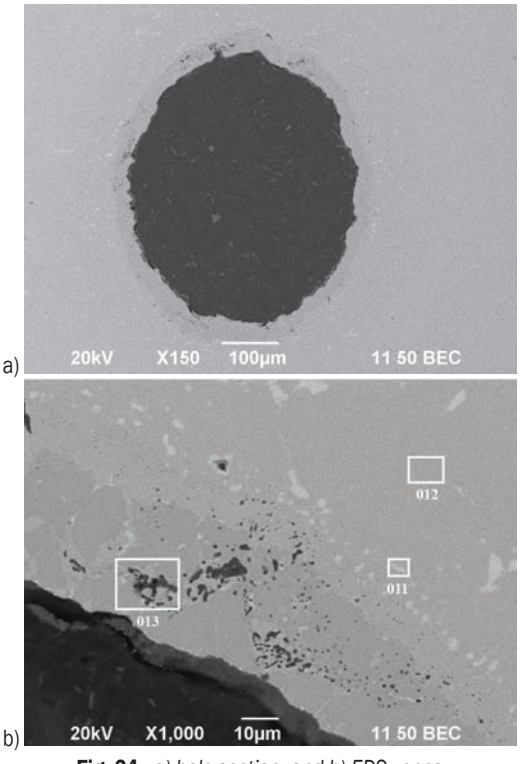

Fig. 24. *a) hole section, and b) EDS zones*

Zone 13 shown on Fig. 24b shows almost 40 % weight of aluminium together with oxygen. Zone 11 is dominated by Nb. Such Nb rich spots were not observed before oxidation testing. It is suspected that heat treatment drove topologically closed pack segregation.

Oxidation testing reduced coating thickness for all hole diameters. However, the most significant reduction was observed for 0.35 mm diameter holes. Coating was reduced by one thirds of its initial thickness. The results shown on Fig. 25 seem to

confirm the hypothesis that EDM process residuals (remelts, oxides) contaminate coating process and by that reduce its durability.

Table 5. *Coating thickness before and after oxidation*

Hole type	Coating thickness after HT [mm]	Coating thickness after oxidation [mm]	Thickness change [%]
A	38	32	18
B	39	30	23
C	42	28	32

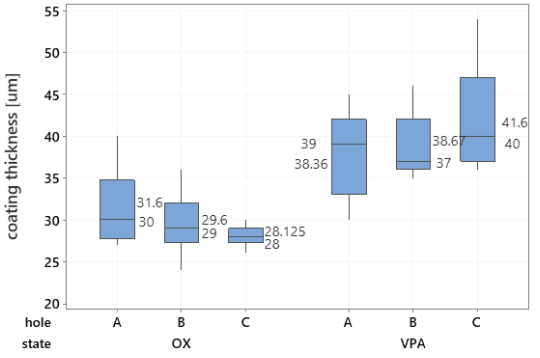

Fig. 25. *Comparison of coating thickness for as coated holes VPA and after oxidation test*

7.6 Scratch Test

The scratch test did not reveal loss of adhesion. Initial results of the test with 100 N final load and 4 mm scratch length, were questioned, and procedure was repeated for several loads (20 N, 40 N, 60 N, 80 N, and 200 N). However, all tests gave same results. A lack of clear coating damage during scratch test. Fig. 26 shows scratch as well as its end close view. The same observation was made by Kukla et al. **[29]**.

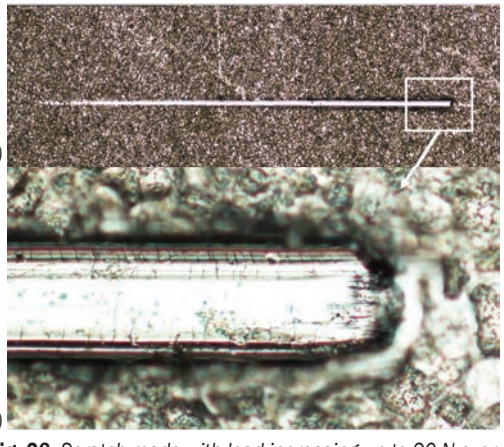

Fig. 26. *Scratch made with load increasing up to 20 N over 4 mm; a) complete scratch, b) zoomed end of scratch visible parent material with cracks introduced by the indenter*

8 CONCLUSIONS

The manufacturing of cooling holes by means of EDM is widely researched. Process parameters, electrode materials, and dielectrics used for the process are being verified by means of advanced statistical tools. More often, traditional mathematical models are replaced by machine learning.

It is shown within this paper that:

a) VPA aluminide coating may be deposited within holes 0.4 mm in diameter;
b) XRD testing proved coating consist of NiAl and Ni_3Al, and Al_2O_3. The last compound provides component corrosion resistance;
c) 1100 ºC 23 h oxidation test resulted in coating thinning from 18 % up to 32 % for smallest holes.

The available literature does not investigate the influence of EDD-modified surfaces on aluminide coating durability. As the test results show, manufacturing process such as EDD has an influence on coating composition and by that on its durability. That hypothesis requires further deeper investigation.

9 FUTURE WORK

The performed evaluation revealed influence of EDD on aluminide coating durability. Future work will focus on:

a) coating durability in deep holes (l/d>> 30),
b) oxidation testing of the VPA and CVD coated holes,
c) improvements in both hole manufacturing methods (improved flushing, di-water additives, electrode modifications) as well as coatings (dopants, thermal cycle changes).

10 ACKNOWLEDGEMENT

Project co-financed by the European Union within the European Regional Development Fund Smart Growth Operation Programme 2014-2020 – Grant Agreement No. POIR.01.01.01-00-D007/16 “Development of cooling technology for hot section components in rotating machines with particular reference to high-pressure turbine blades and vanes.

11 REFERENCES

[1] The Jet Engine (1988). *Rolls-Royce*, London.
[2] Bunker, R.S. (2017). Evolution of turbine cooling. *Proceedings of the ASME Turbo Expo 2017: Turbomachinery Technical Conference and Exposition, vol 1: Aircraft Engine; Fans and Blowers; Marine*, **DOI:10.1115/GT2017-63205**

[3] Tamarin, Y. (2002). *Protective Coatings for Turbine Blades*. ASM International, Materials Park.

[4] Winbro Group Technologies (2022). From: *https://www.winbrogroup.com*, accessed on 2022-04-19.

[5] Bunker, R.S. (2009). The effects of manufacturing tolerances on gas turbine cooling. *ASME Journal of Turbomachinerry*, vol. 131, no. 4, art. ID 041018, **DOI:10.1115/1.3072494**.

[6] Li, Z.Y., Wei, X. T., Guo, Y. B., Sealy, M.P. (2015). State-of-art challenges, and outlook on manufacturing of cooling holes for turbine blades. *Machining Science and Technology*, vol. 19, no. 3, p. 361-399, **DOI:10.1080/10910344.2015.1051543**.

[7] Zielinska, M., Sieniawski, J., Yavorska, M., & Motyka, M. (2011). Influence of chemical composition of nickel based superalloy on the formation of aluminide coating. *Archives of Metallurgy and Materials*, vol. 56, no. 1, art. ID 193, **DOI:10.2478/v10172-011-0023-y**.

[8] Kunieda, M. Lauwers B., Rajurkar K.P., Schumacher, B.M. (2005). Advancing EDM through fundamental insight into the process. *CIRP Annals*, vol. 54, no.2, p. 64-87, **DOI:10.1016/S0007-8506(07)60020-1**.

[9] Machno, M. (2019). Impact of process parameters on the quality of deep holes drilled in inconel 718 using EDD. *Materials*, vol. 12, no. 14, art. ID 2298, **DOI:10.3390/ma12142298**.

[10] Kang, S.H., Kim, D.E. (2006). Fatigue crack susceptibility of electrical discharge drilled holes in nickel based heat resistant alloy. *Materials Science and Technology*, vol. 22, no. 1, p. 21-28, **DOI 10.1179/174328406X78389**.

[11] Novovic, D., Dewes, R.C., Aspinwall, D.K,. Voice, W., Bowen, P. (2004). The effect of machined topography and integrity on fatigue life. *International Journal of Machine Tools & Manufacture*, vol. 44, no. 2-3, p. 125-134, **DOI:10.1016/j.ijmachtools.2003.10.018**.

[12] Ekmekci, B., Sayar, A., Öpöz, T.T., Erden, A. (2009) Geometry and surface damage in micro electrical discharge machining of micro-holes. *Journal of Micromechanics and Microengineering*, vol. 19, no. 10, art. ID 105030, **DOI:10.1088/0960-1317/19/10/105030**.

[13] Sun, W., Xu, Y., Hu, C., Liu, X. (2017) Effect of film-hole configuration on creep rupture behavior of a second generation nickel-based single crystal superalloys. *Materials Characterization*, vol. 130, p. 298-310, **DOI:10.1016/j.matchar.2017.06.019**.

[14] Lazarenko, B.R. (1943). *To Invert the Effect of Wear on Electric Power Contacts*. PhD thesis. The All-Union Institute for Electro Technique, Moscow. (in Russian)

[15] Ramasawmya, H., Blunt, L. (2004). Effect of EDM process parameters on 3D surface topography. *Journal of Materials Processing Technology*, vol. 148, no. 2, p. 155-164, **DOI:10.1016/S0924-0136(03)00652-6**.

[16] Li, C., Li, Y., Tong, H., Zhao, L. (2016). Thinning process of recast layer in hole drilling and trimming by EDM. *Procedia CIRP*, vol. 42, p. 575-579, **DOI:10.1016/j.procir.2016.02.262**.

[17] Świercz, R., Oniszczuk-Świercz, D., Chmielewski, T. (2019). Multi-response optimization of electrical discharge machining using the desirability function. *Micromachines*, vol. 10, no. 1, art. ID 72, **DOI:10.3390/mi10010072**.

[18] Lee, H.T., Tai, T.Y. (2003). Relationship between EDM parameters and surface crack formation. *Journal of Materials Processing Technology*, vol. 142, no. 3, p. 676-683, **DOI:10.1016/S0924-0136(03)00688-5**.

[19] Sarıkaya, M., Yılmaz, V. (2018). Optimization and predictive modeling using S/N, RSM, RA and ANNs for micro-electrical discharge drilling of AISI 304 stainless steel. *Neural Computing & Application*, vol. 30, p. 1503-1517, **DOI:10.1007/s00521-016-2775-9**.

[20] Reed, R.C. (2006). *The Superalloys Fundamentals and Applications*. Cambridge University Press, New York, **DOI:10.1017/CBO9780511541285**.

[21] Ejaz, N., Tauqir, A. (2006). Failure due to structural degradation in turbine blades. *Engineering Failure Analysis*, vol. 13, no. 3, p. 452-463, **DOI:10.1016/j.engfailanal.2004.12.041**.

[22] Zielinska, M., Zagula-Yavorska, M., Sieniawski, J., Filip, R. (2013). Microstructure and oxidation resistance of an aliminide coating on the nickel based supperalloy MAR M247 deposited by the CVD alumionizing process. *Archives of Metallurgy and Materials*, vol. 58, no. 3, p. 697-701, **DOI:10.2478/amm-2013-0057**.

[23] He, J.L., Yu, C.H., Leyland, A., Wilson A.D., Matthews, A. (2002). A comparative study of the cyclic thermal oxidation of PVD nickel aluminide coatings. *Surface and Coatings Technology*, vol. 155, no. 1, p. 67-79, **DOI:10.1016/S0257-8972(02)00025-7**.

[24] Zagula-Yavorska, M., Kocurek, P., Pytel, M., Sieniawski, J. (2016). Oxidation resistance of turbine blades made of ZS6K superalloy after aluminizing by low-activity CVD and VPA methods. *Journal of Materials Engineering and Performance*, vol. 25. p. 1964-1973, **DOI:10.1007/s11665-016-2032-5**.

[25] Zagula-Yavorska, M., Romanowska, J., Pytel, M., Sieniawski, J. (2015). The microstructure and oxidation resistance of the aluminide coatings deposited by the CVD method on pure nickel and hafnium-doped nickel superalloys. *Archives of Civil and Mechanical Engineering*, vol. 15, no. 4, p. 862-872, **DOI:10.1016/j.acme.2015.03.006**.

[26] Zagula-Yavorska, M., Sieniawski, J. (2018). Cyclic oxidation of palladium modified and nonmodified aluminide coatings deposited on nickel base superalloys. *Archives of Civil and Mechanical Engineering*, vol. 18, no. 1, p. 130-139, **DOI:10.1016/j.acme.2017.05.004**.

[27] Wu, Q., Yang, R., Wu, Y., Li, S., Ma, Y., Gong, S. (2011). A comparative study of four modified Al coatings on Ni3Al-based single crystal superalloy. *Progress in Natural Science: Materials International*, vol. 21, no. 6, p. 496-505, **DOI:10.1016/S1002-0071(12)60089-6**.

[28] Cigada, P.A. (2011). *Diffusion Coatings for High- Temperature Applications on Ni-based Superalloys*. Politechnico di Milano, Milan.

[29] Kukla, D., Kopec, D., Kowalewski, Z.L., Politis, D.J., Jozwiak, S., Senderowski, C. (2020) Thermal Barrier Stability and Wear Behavior of CVD Deposited Aluminide Coatings for MAR 247 Nickel Superalloy. *Materials*, vol. 13, no. 17, art. ID 3863, **DOI:10.3390/ma13173863**.

Strojniški vestnik - Journal of Mechanical Engineering 68(2022)10, 635-641
DOI:10.5545/sv-jme.2022.222
Short Scientific Paper
Received for review: 2022-06-20
Received revised form: 2022-09-08
Accepted for publication: 2022-09-09

Thermal Evaluation of Multilayer Wall with a Hat-Stringer in Aircraft Design

Volodymyr Brazhenko[1,2] – Yibo Qiu[1] – Jiancheng Cai[1,2,*] – Dongyun Wang[1,2]

[1] Zhejiang Normal University, College of Engineering, China
[2] Zhejiang Normal University, Key Laboratory of Urban Rail Transit Intelligent Operation and Maintenance Technology & Equipment of Zhejiang Province, China

In the present paper, we investigate the heat transfer through the multilayer wall of aircraft cabins, as this process influences the comfortable conditions created for most passengers and crew members. The numerical modelling results and calculation of a multilayer wall with a hat-stringer in aircraft design are presented. The thermal characteristics evaluation and their relationship with the design parameters were made. The effect of the air layer size on the overall thermal resistance of the multilayer wall, taking into account the geometrical dimensions and properties of the surfaces, was studied. The relative temperature field in the insulation layer, which crosses the hat-stringer elements of the fuselage frame, is calculated. It is shown that the insufficient thickness of the layer of thermal insulation material in the zone of the hat-stringer at low temperatures leads to a significant deterioration in the multilayer wall characteristics, which can worsen the microclimatic conditions inside the aircraft cabin.

Keywords: numerical modelling, heat transfer, aircraft design, multilayer wall, hat-stringer

Highlights

- *The air layer thickness, up to which the thermal resistance of the multilayer wall increases, was determined.*
- *The relationship between the size of the insulating material and the heat transfer coefficient was obtained.*
- *The effect of a hat-stringer on the thermal characteristics of a multilayer wall of an aircraft cabin was evaluated.*

0 INTRODUCTION

Nowadays, the civil aircraft industry faces a variety of challenges and demands, including ensuring a comfortable environment for passengers on board aircraft. In the rational design of present-day passenger aircraft, a heightened level of attention is focused on creating a comfortable condition for travellers and crew members in the aircraft cabin, chiefly by improving the quality of indoor climate conditions [1] to [5]. The core part of an aircraft is the cabin, which provides the necessary environmental conditions for travellers and crew members. The first priority of the cabin is to protect people on board from the harmful effects of the external atmosphere. The second is to ensure that the required pressure, temperature, and air composition are maintained on board the aircraft. To shield passengers from aggressive environmental conditions outside the cabin, in particular, from low temperatures outside and to ensure comfortable thermal conditions for humans inside, a specific insulation material and air layer are provided in the construction of the multilayer wall of the aircraft cabin (Fig. 1a). When designing an aircraft, the most significant heat characteristic of the cabin is thermal protection, which can be determined based on the cabin heat exchange with the environment. Insulation material with a very small value of thermal conductivity coefficient is typically utilized in multilayer walls to insulate the aircraft cabin.

Several recent articles on this topic have considered the challenges of providing thermal comfort [6] to [9] and heat transfer in the cabin [10] to [14]. However, the construction of the multilayer cabin wall in the design of aircraft and its influence on the comfortable environment for passengers play a significant role, which is not considered in these papers.

The multilayer wall of an aircraft cabin consists of the outer shell of the fuselage, the insulation layer, and the inner edging. There is an air layer between the edging and the insulation that houses the equipment wires and other hardware (Fig. 1b).

Of particular interest is the intersection of the thermal insulation layer with the stringers of the fuselage frame since the thermal conductivity of the stringers is several orders higher than the thermal conductivity of the insulation [15]. At sufficiently low ambient temperatures outside the aircraft, stringers are good conductors, through which there is significant heat loss that can cause deterioration of the microclimate in the cabin and the appearance of condensation.

The key question that this paper will address is the thermal evaluation of cabin multilayer walls with a hat-stringer, which crosses the insulation layer. It

*Corr. Author's Address: Zhejiang Normal University, 688 Yingbin Road, Jinhua, Zhejiang Province, China, cai_jiancheng@foxmail.com

should be noted that this study can be useful for the comprehensive development of lightweight insulation materials [16] and [17], to study the reduction of moisture accumulation in insulation materials [18], as well as to find new ways to protect the insulation layer from moisture penetration [19] to [21].

1 NUMERICAL MODEL AND SETTINGS

The heat transfer process through a wall consisting of several layers with different thermophysical characteristics and homogeneous properties was analysed. Heat flux through the layer is directed along the normal to external and internal surfaces and contingent only on the temperature difference. Heat transfer through the edging and insulation layer is carried out as a result of the material thermal conductivity, as for the air layer due to thermal conductivity, natural convection, and heat emission. The principle of independent accounting of heat transfer was applied to the air layer. Also, the area with the insulation layer was considered, inside which the hat-stringer is positioned (Fig 1c).

The heat flux density due to heat conduction through the multilayer cabin wall with flat homogeneous layers without internal heat sources: $\partial T/\partial n = dT/dx$, is determined with the Fourier equation:

$$\bar{q} = -\lambda \frac{dT}{dx} = -\frac{\lambda}{\delta}\Delta T, \tag{1}$$

where $\bar{q}$ is the heat flux density vector, λ is the layer thermal conductivity and equals to constant, ΔT is the temperature difference on boundaries of the layer, and δ is the layer thickness. For edging and insulation layers, λ is the thermal conductivity of solid material. In this model, we investigated the thermal resistance of the cabin multilayer wall, which involves an air layer with its specific dimensions and emissivity factor of boundaries. For the air layer, λ_{AL} is the equivalent coefficient of heat transfer by heat conduction and is defined as specified in Eq. (2):

$$\lambda_{AL} = \varepsilon_{AL}\lambda_a + \alpha_{AL}\delta_{AL}, \tag{2}$$

where ε_{AL} is the convection factor to take into account the effect of natural convection on boundaries of air layer (Eq. (3)); λ_a is the thermal conductivity coefficient of air; δ_{AL} is the thickness of an air layer; α_{AL} is the radiation heat transfer coefficient. The coefficient ε_{AL} depends on the temperature difference at the surfaces of the air layer. The value of the coefficient can be determined using Eq. (3):

$$\varepsilon_{AL} = 0.105 \cdot \left(\frac{g\delta_{AL}{}^3 \left(\frac{(T_e - T_i)}{0.5 \cdot (T_e + T_i) + 273} \right)}{\nu^2} \mathrm{Pr} \right)^{0.3}, \tag{3}$$

where g is the acceleration of gravity, ν is coefficient of kinematic viscosity of air, δ_{AL} is air layer thickness, T_e, T_i are temperatures on the boundaries of air layer, and Pr is Prandtl numbers (taken up as Pr = 0.7). The radiation heat transfer coefficient is determined according to the following expression:

$$\alpha_{AL} = \frac{C_0 \left[\left(\frac{T_e + 273}{100} \right)^4 - \left(\frac{T_i + 273}{100} \right)^4 \right]}{\left(\frac{1}{\varepsilon_e} + \frac{1}{\varepsilon_i} - 1 \right) (T_e - T_i)} \tag{4}$$

where ε_e and ε_i are the emissivity coefficients of the air layer surfaces; C_0 is the blackbody coefficient.

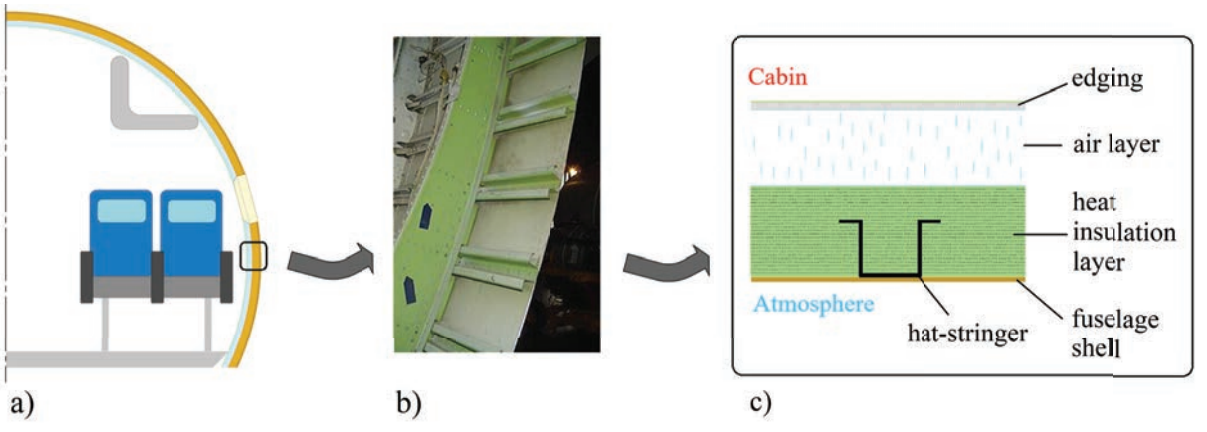

Fig. 1. *Placement of stringers; a) cabin cross-section, b) original fuselage [22], c) fuselage design scheme*

It is necessary to solve a system of equations with unknown temperatures T_i, T_e and total heat flux q to obtain the equation of heat transfer through the multilayer wall of the considered aircraft cabin.

$$\begin{cases} q = \dfrac{\lambda_i}{\delta_i}\left(T_i - T_a\right) \\ q = q_\lambda + q_\alpha + q_\varepsilon = \dfrac{\lambda_{AL}}{\delta_{AL}}\left(T_e - T_i\right), \\ q = \dfrac{\lambda_e}{\delta_e}\left(T_c - T_e\right) \end{cases} \tag{5}$$

where in this system q_λ, q_α, and q_ε are heat fluxes, caused by thermal conductivity, natural convection and heat radiation; δ_i and δ_e are thicknesses of insulation and edging layers; λ_i and λ_e are thermal conductivities of insulation and edging layers; T_a and T_c are temperatures on outside aircraft cabin and air in-cab environment. The change in the amount of heat that passes through a multilayer wall is related to the thermal resistance of each layer. The wall resistance is specified by the geometry configurations and heat properties of the layer material: $r_{full} = \delta_i/\lambda_i + \delta_{AL}/\lambda_{AL} + \delta_e/\lambda_e$; the temperatures T_i and T_e are determined by a solving system of Eq. (5) and taking into account values of Eq. (2) to (4). These temperatures enable determining the equivalent heat transfer coefficient λ_{AL}, and values λ_i and λ_e were taken as constant heat transfer coefficients of corresponding layers.

The thermal emissivity on the fuselage shell of a multilayer wall is mainly determined according to the ambient conditions outside the aircraft cabin. Since the thickness of the layer shell is relatively small and the thermal conductivity of its material has a sufficiently high value, we did not take into account the influence of the thermal resistance of the outer shell on the total resistance in the model. Thus, on the outer surface of the insulation layer, we set the temperature determined from outside of the aircraft cabin. The temperature on the internal surface of the edging can be set according to comfortable thermal conditions for people inside the cabin.

The system of equations in Eq. (5) consists of nonlinear algebraic equations. The exact solution to this system is impossible. Therefore, an approximate iterative method with the control of heat balance in mesh cells was proposed for solutions [22] and [23]. The temperature distribution in all layers and on internal surfaces of the multilayer wall was calculated numerically. The changing of heat transfer characteristics of insulation was estimated in the presence of a hat-stringer inside (Fig. 2). The influence of the air layer parameters on the change in multilayer wall thermal characteristics was investigated.

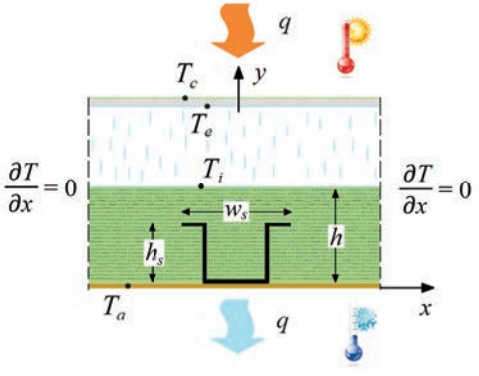

Fig. 2. *Schematic diagram of multilayer wall with hat-stringer in thermal insulation*

The steady-state differential equation of heat conduction in a two-dimensional xy coordinate system has the form:

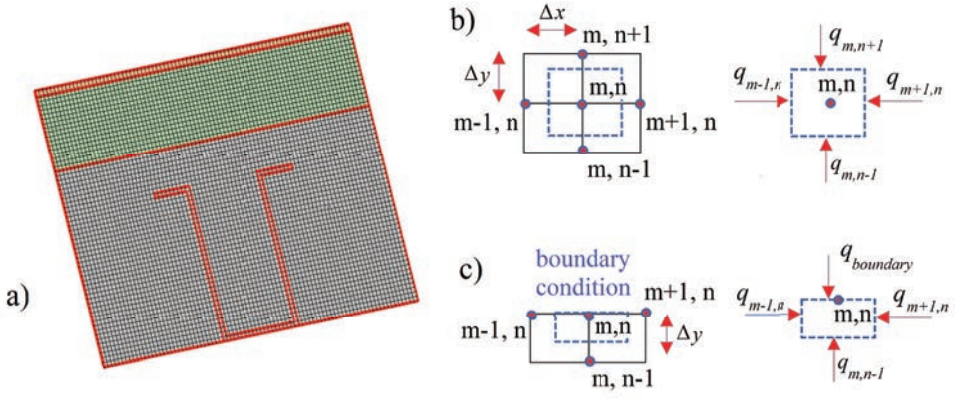

Fig. 3. *Calculation mesh and control cells: a) computational mesh view, b) internal control cell, c) control cell near boundary*

$$\frac{\partial}{\partial x}\left(\lambda \frac{\partial T}{\partial x}\right)+\frac{\partial}{\partial y}\left(\lambda \frac{\partial T}{\partial x}\right)=0. \qquad (6)$$

The temperature on the external surface of the insulation is set by the temperature outside the aircraft, as noted earlier. Adiabatic conditions $\partial T / \partial x = 0$ are fulfilled at the free boundaries. The boundary condition for the internal surface (e.g., for insulation) is written as:

$$\lambda_i \frac{\partial T}{\partial y} = -\alpha \left(T_{AL} - T_c\right). \qquad (7)$$

To solve Eq. (6) with given boundary conditions, we used a numerical method with mesh (Fig. 3a) based on the heat balance equation with the finite-difference approach over the control cell (Fig. 3b):

$$q_{m-1,n} + q_{m+1,n} + q_{m,n-1} + q_{m,n+1} = 0. \qquad (8)$$

The heat flux through the multilayer wall of the cabin can be written by substituting Fourier's Law and the definition of heat rate per unit area for each heat flux node:

$$A_1\left(-\lambda \frac{T_{m,n} - T_{m-1,n}}{\Delta x}\right) + A_2\left(-\lambda \frac{T_{m,n} - T_{m+1,n}}{\Delta x}\right) + A_3\left(-\lambda \frac{T_{m,n} - T_{m-1,n}}{\Delta y}\right) + A_4\left(-\lambda \frac{T_{m,n} - T_{m+1,n}}{\Delta y}\right) = 0, \qquad (9)$$

where A_1, A_2, A_3 and A_4 are the unit areas; T is the temperature in the corresponding node. Since in computation mesh $\Delta x = \Delta y$ previous equation can be rewritten as with rearranging:

$$4T_{m,n} - T_{m,n+1} - T_{m,n-1} - T_{m+1,n} - T_{m,n-1} = 0. \qquad (10)$$

For mesh cell with boundary case (Fig. 3c):

$$4T_{m,n} - 2T_{m,n-1} - T_{m+1,n} - T_{m-1,n} = 0. \qquad (11)$$

In the last step, an augmented matrix $[A|b]$ consisting of temperatures at each node was compiled. The solution of the matrix equation $[A]x = b$, was expressed as $x = [A]^{-1}b$.

2 THERMAL EVALUATION OF MULTILAYER WALL

For the thermal evaluation of the multilayer wall with a hat-stringer, the next modelling constants were adopted: air temperature of atmosphere outside and inside cabin: T_a = –25 °C, T_e = 20 °C; thermal conductivity and thickness of edging and thermal insulation, respectively: λ_e = 0,5 W/(m·°C), λ_i = 0.05 W/(m·°C), $\delta_e = 3 \cdot 10^{-3}$ m, $\delta_i = 9 \cdot 10^{-2}$ m. The thermal conductivity in the air layer λ_a was calculated by the average temperature T_{AL} in the air layer. Air layer characteristics were varied for investigation: thickness δ_{AL} in a range from 0 m to $7.5 \cdot 10^{-2}$ m and emissivity factor of air layer boundaries $\varepsilon_e = \varepsilon_i$ from 0.1 to 0.9. As noted earlier, the aircraft cabin shell can be neglected because of its physical and geometric properties.

Fig. 4 demonstrates a relative thermal resistance of insulation layer $r_i' = r_i / r_{full} \cdot 100$ % and air layer $r_{AL}' = r_{AL} / r_{full} \cdot 100$ %, Fig. 5 shows $\kappa_{full} = 1 / r_{full}$ is the heat transfer coefficient; in Fig. 6, $\lambda_{full} = (\delta_i + \delta_{AL} + \delta_e) / r_{full}$ is the equivalent coefficient of thermal conductivity of cabin multilayer wall.

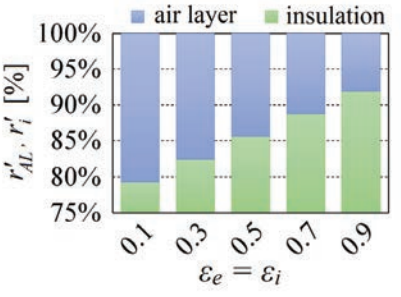

Fig. 4. *Contributions of air layers and insulation in full thermal resistance of multilayer wall ($\delta_{AL} = 2.9 \cdot 10^{-2}$ m), for different $\varepsilon_e = \varepsilon_i$*

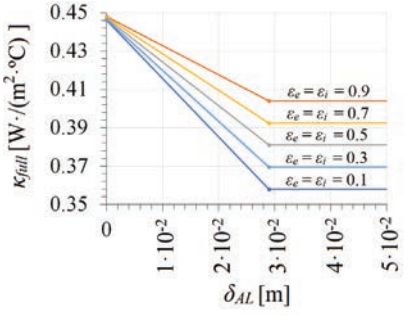

Fig. 5. *Heat transfer coefficient of multilayer wall for different values $\varepsilon_e = \varepsilon_i$*

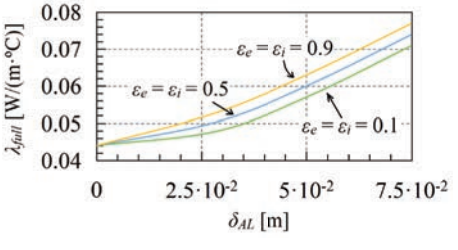

Fig. 6. *Thermal conductivity coefficient of cabin multilayer wall*

The contribution of air layer thermal resistance for different values $\varepsilon_e = \varepsilon_i$ is changing from 20.7 % for $\varepsilon_e = \varepsilon_i$ = 0.1 to 8.1 % for $\varepsilon_e = \varepsilon_i$ = 0.9 from the

total resistance of multilayer wall. According to results in Fig. 5, we may conclude that increasing the thickness of the air layer by more than $2.9 \cdot 10^{-2}$ m does not provide an increase in multilayer wall thermal resistance.

Fig. 7 shows the changing of relative temperature in the insulation of the cabin multilayer wall, in which the hat-stringer is placed. For this, according to Earth's atmosphere conditions, we considered temperature $T_a = -55$ ºC (the atmospheric temperature at an altitude of 11 kilometres), $T_a = -65$ ºC and $T_a = -75$ ºC (minimum temperature, depending on the season). The temperature inside the cabin was taken as $T_c = 20$ ºC; the difference between cabin temperature and internal surfaces $\Delta T_w = T_c - T_w = 5$ ºC; the heat-transfer coefficient of internal surfaces was 8 W/(m²·ºC). The thermal conductivity ratio between of hat-stringer and the thermal insulation was 5500. The relative height of the insulation layer was determined according to the expression: $\overline{h} = w_s/(h - h_s)$ and equals 2.5, 3, or 3.5, respectively. The evaluation of the thermal field for $t_a = -55$ ºC, $\overline{h} = 3.5$ are shown in Fig. 6 in the curves form of constant relative temperature changing $\psi_i = (T_i - T_a)/(T_c - T_a)$, where T_i is the temperature field in the insulation layer.

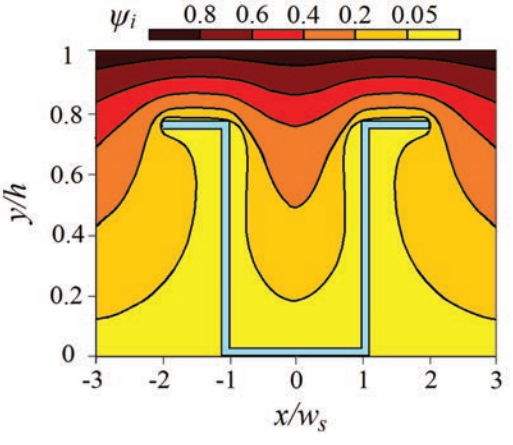

Fig. 7. *Relative temperature changing in thermal insulation layer with hat-stringer inside*

Based on the numerical modelling data, the dependences of the temperature drop on the inner surface of the thermal insulation layer with a hat-stringer inside for different insulation thicknesses and the temperature outside the cabin are plotted (Fig. 8):

$$\psi_w = \frac{(T_w - T_{wn}) - (T_{w0} - T_{wn})}{\Delta T_{wn}}, \qquad (12)$$

where T_{wn} is the scaled temperature of internal layer surfaces; T_{w0} is the surface temperature without the effect of a hat-stringer; $\Delta T_{wn} = T_c - T_{wn}$ is the scaled temperature difference.

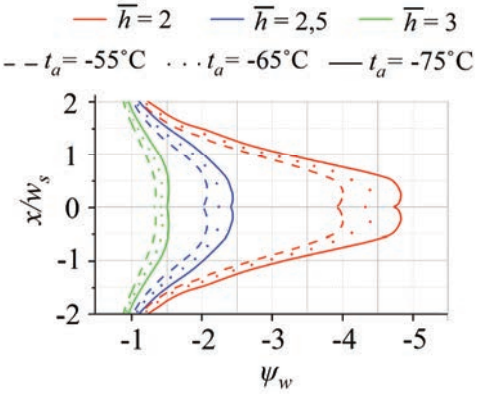

Fig. 8. *Temperature decreasing on internal wall within the area of hat-stringer*

An estimation of the heat properties deterioration of the multilayer wall, associated with the location of a hat-stringer in the thermal insulation layer, was conducted. For this purpose, the effect of the ratio of the thermal insulation size to the size of the stringer, the change in the thermal conductivity coefficient of the thermal insulation was evaluated:

$$\Delta\kappa_i = \frac{(\kappa_i - \kappa_{i0})}{\kappa_{i0}} \cdot 100\ \%, \qquad (13)$$

where κ_{i0} and κ_i are the heat transfer coefficient of the insulation layer without and with a hat-stringer inside. Changing of the heat-transfer coefficient of thermal insulation, conditioned by the hat-stringer, are shown in Fig. 9.

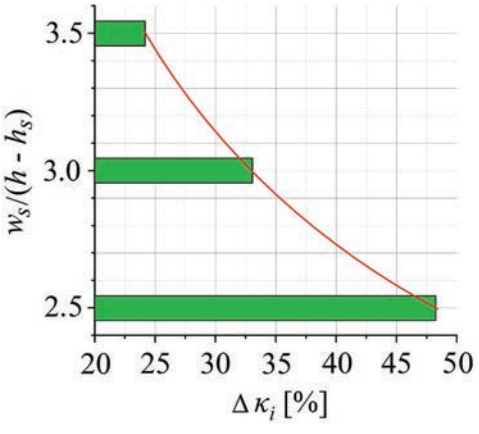

Fig. 9. *Changing of heat transfer coefficient of thermal insulation, conditioned by hat-stringer*

3 CONCLUSIONS

In this article, the results of numerical modelling and evaluation of thermal characteristics of multilayer wall of aircraft cabin with hat-stringer inside are presented. Summarizing the results, it can be concluded that:

1. According to heat transfer modelling through an aircraft cabin wall with an air layer and hat-stringer inside, the evaluation and prediction of thermal characteristics were obtained. As the results of the numerical modelling demonstrate, the thermal resistance of a cabin's multilayer wall does not change with the increase of air layer thickness for more than $2.9 \cdot 10^{-2}$ m.
2. The contribution of the air layer to the overall thermal resistance of the multilayer wall of the aircraft cabin decreases with the increasing emissivity factor of the layer surfaces and equals 20.7 % for $\varepsilon_e = \varepsilon_i = 0.1$ and 8.1% for $\varepsilon_e = \varepsilon_i = 0.9$.
3. The heat changing in the insulation layer with a hat-stringer inside is presented on the grounds of numerical modelling. The modelling results prove that the small thickness of the insulation layer in the area of the hat-stringer in possible minimum temperature contributes to a significant deterioration of thermal resistance in the aircraft multilayer wall, including the rise of the heat transfer coefficient of insulation by more than 47 % and a weighty change in the temperature drop between the internal walls within the area of the insulation layer.

The presented results make it possible to evaluate the thermal characteristics of cabin multilayer walls depending on the material parameters of layers during the rational design creation for the aerial vehicle.

4 ACKNOWLEDGEMENTS

The research described in this paper was financially supported by the National Natural Science Foundation of China (51976201) and the Natural Science Foundation of Zhejiang Province (LY22E06006)

5 REFERENCES

[1] Qu, J., Wang, D., Wang, W., Dang, S. (2022). Study on bidirectional coupling of human thermal comfort parameters and cabin thermal environment. *Journal of System Simulation*, vol. 34, no. 1, p. 20-35, DOI:**10.16182/j.issn1004731x.joss.21-0558**.

[2] Sanchez, F., Liscouet-Hanke, S., Boutin, Y., Beaulac, S., Dufresne, S. (2018). Multi-level modeling methodology for aircraft thermal architecture design. *SAE Technical Paper Series*, 2018-01-1910, **DOI:10.4271/2018-01-1910**.

[3] Duan, X., Yu, S., Chu, J., Chen, D., Su, Z. (2021). CFD-based evaluation of flow and temperature characteristics of airflow in an aircraft cockpit. *Computer Modeling in Engineering & Sciences*, vol. 130, no. 2, p. 701-721, **DOI:10.32604/cmes.2022.016779**.

[4] Wang, J., Xiang, Z. R., Zhi, J. Y., Chen, J. P., He, S. J., Du, Y. (2021). Assessment method for civil aircraft cabin comfort: contributing factors, dissatisfaction indicators, and degrees of influence. *International Journal of Industrial Ergonomics*, vol. 81, p. 103045, **DOI:10.1016/j.ergon.2020.103045**.

[5] Fan, J., Zhou, Q. (2019). A review about thermal comfort in aircraft. *Journal of Thermal Science*, vol. 28, no. 2, p. 169-183, **DOI:10.1007/s11630-018-1073-5**.

[6] Yu, N., Zhang, Y., Zhang, M., Li, H. (2021). Thermal condition and air quality investigation in commercial airliner cabins. *Sustainability*, vol. 13 no. 13, p. 7047, **DOI:10.3390/su13137047**.

[7] Jia, S., Lai, D., Kang, J., Li, J., Liu, J. (2018). Evaluation of relative weights for temperature, CO_2, and noise in the aircraft cabin environment. *Building and Environment*, vol. 131, p. 108-116, **DOI:10.1016/j.buildenv.2018.01.009**.

[8] Cui, W., Wu, T., Ouyang, Q., Zhu, Y. (2017). Passenger thermal comfort and behavior: a field investigation in commercial aircraft cabins. *Indoor Air*, vol. 27, no. 1, p. 94-103, **DOI:10.1111/ina.12294**.

[9] Winzen, J., Marggraf-Micheel, C. (2013). Climate preferences and expectations and their influence on comfort evaluations in an aircraft cabin. *Building and Environment*, vol. 64, p. 146-151, **DOI:10.1016/j.buildenv.2013.03.002**.

[10] Lei, L., Zheng, H., Xue, Y., & Liu, W. (2022). Inverse modeling of thermal boundary conditions in commercial aircrafts based on Green's function and regularization method. *Building and Environment*, vol. 217, p. 109062, **DOI:10.1016/j.buildenv.2022.109062**.

[11] Çiçek, O., & Baytaş, A. C. (2021). Local thermal non-equilibrium conjugate forced convection and entropy generation in an aircraft cabin with air channel partially filled porous insulation. *Aircraft Engineering and Aerospace Technology*, vol. 94, no. 2, p. 210-225, **DOI:10.1108/AEAT-02-2021-0039**.

[12] Dong, L., Chen, X., Wang, Z., & Zhang, Z. (2018). Factors affecting overall and local temperature distribution in aircraft cabins. *Journal of Building Engineering*, vol.18, p. 125-129, **DOI:10.1016/j.jobe.2018.03.013**.

[13] Geron, M., Butler, C., Stafford, J. Newport, D. (2013). Development and validation of a compact thermal model for an aircraft compartment. *Applied Thermal Engineering*, vol. 61, no. 2, p. 65-74, **DOI:10.1016/j.applthermaleng.2013.07.012**.

[14] Butler, C., Newport, D. (2014). Experimental and numerical analysis of thermally dissipating equipment in an aircraft confined compartment. *Applied Thermal Engineering*, vol. 73, no. 1, p. 869-878, **DOI:10.1016/j.applthermaleng.2014.08.035**.

[15] Wanhill, R., Barter, S., Molent, L. (2019). Fokker 100 fuselage test: Lap joints exponential FCG analysis. Fatigue crack growth failure and lifing analyses for metallic aircraft structures and components. *Springer Briefs in Applied Sciences and Technology*, Springer, Dordrecht, **DOI:10.1007/978-94-024-1675-6_9**.

[16] Wu, D., Wang, Y., Gao, Z., Yang, J. (2015). Insulation performance of heat-resistant material for high-speed aircraft under thermal environments. *Journal of Materials Engineering and Performance*, vol. 24, p. 3373-3385, **DOI:10.1007/s11665-015-1626-7**.

[17] Çiçek, O., Baytaş, A.C. (2021). Local thermal non-equilibrium conjugate forced convection and entropy generation in an aircraft cabin with air channel partially filled porous insulation. *Aircraft Engineering and Aerospace Technology*, vol. 94, no. 2, p. 210-225, **DOI:10.1108/AEAT-02-2021-0039**.

[18] Chen, L., Wang, S., Li, G., Lin, C.-H., Zhang, T. T. (2016). CFD modeling of moisture accumulation in the insulation layers of an aircraft. *Applied Thermal Engineering*, vol. 102, p. 1141-1156, **DOI:10.1016/j.applthermaleng.2016.04.048**.

[19] Zhang, T.T., Tian, L., Lin, C.-H., Wang, S. (2012). Insulation of commercial aircraft with an air stream barrier along fuselage. *Building and Environment*, vol. 57, p. 97-109, **DOI:10.1016/j.buildenv.2012.04.013**.

[20] Zhang, Y., Liu, J., Pei, J., Li, J. Wang, C. (2017). Performance evaluation of different air distribution systems in an aircraft cabin mockup. *Aerospace Science and Technology*, vol. 70, p. 359-366, **DOI:10.1016/J.AST.2017.08.009**.

[21] Liu, M., Chang, D., Liu, J., Ji, S., Lin, C.H., Wei, D., Long, Z., Zhang, T., Shen, X., Cao, Q., Li, X. (2021). Experimental investigation of air distribution in an airliner cabin mockup with displacement ventilation. *Building and Environment*, vol. 191, art. ID. 107577, **DOI:10.1016/j.buildenv.2020.107577**.

[22] Minkowycz, W. J., Sparrow, E. M., & Murthy, J. Y. (2006). *Handbook of Numerical Heat Transfer*, John Willey & Sons. Inc., New York.

[23] Patankar, S.V. (2018). Numerical Heat Transfer And Fluid Flow. CRC Press, Boca Raton, **DOI:10.1201/9781482234213.**

Strojniški vestnik - Journal of Mechanical Engineering 68(2022)10, 642-653
DOI:10.5545/sv-jme.2022.298
Short Scientific Paper
Received for review: 2022-07-23
Received revised form: 2022-09-16
Accepted for publication: 2022-09-28

Development of a New Expert System for Diagnosing Marine Diesel Engines Based on Real-Time Diagnostic Parameters

Hla Gharib – György Kovács*
University of Miskolc, Faculty of Mechanical Engineering and Informatics, Institute of Manufacturing Science, Hungary

Implementing adequate diagnostic strategies for marine engines offers a good possibility to focus on the early recognition of potential problems and prevent catastrophic and costly consequences. The successful and increasing application of diagnostic systems and devices for machines depends significantly on the precision of the diagnostic approaches. This research aims to develop an improved diagnosis expert system for determining the real-time technical condition of marine diesel engines. The adequate selection of the diagnostic parameters is crucial in detecting early-stage defects and failures since each parameter responds to the changes in structural parameters of the engine in different modes and degrees. This result provides valuable information on the accurate location of the fault and describes the relationship between operational and structural parameters. Firstly, this article introduces the relevant literature relating to the selection of the diagnostic parameters for marine engines and their subsystems through different statistical methods. The next part contains the description of marine diesel engine subsystems and the selected marine diesel engine's diagnostic parameters. After that, a newly developed expert system for diagnosing marine diesel engines' technical conditions is introduced. Finally, a case study of the operation of the developed diagnostic system is presented. The main contribution of the article is the introduction of the newly developed diagnosis expert system, which can be offered to inexperienced users on ships to effectively manage abnormal situations. Furthermore, this diagnostic tool can be applied to the engines' subsystems to improve the reliability and efficiency of the marine diesel engines' operation and maintenance.
Keywords: marine engines, diagnostic parameters, maintenance, newly developed diagnosis expert system, case study

Highlights

- *The selection of the most effective diagnostic parameters related to the subsystem of the marine diesel engines (fuel, lubrication, cooling, and air and exhaust systems) based on statistical studies and research experiments were studied.*
- *A knowledge-based diagnostic system, based on the selected diagnostic parameters, was developed for the whole engine system to determine the technical condition of the engine.*
- *The newly developed diagnosis expert system can be applied to every four-stroke marine diesel engine to increase their operational efficiency and reliability.*
- *The new diagnostic system can be used to manage abnormal situations on ships effectively and promptly.*
- *A case study for marine diesel engines' technical diagnosis is also introduced to show the operation of the developed expert system.*

0 INTRODUCTION

Marine diesel engines are complex systems; due to the relatively high costs of fuels and lubricating oils, their operational expenses are quite high. This cost may reach 70 % of the ship's machinery operational expenses [1]. The increased operating expenditures are related to the ship engine's technical condition. Application of an adequate maintenance strategy depends on the continuous technical diagnosis with minimal intervention, considering a long process with important multiple steps affecting the system efficiency. The diagnostic system provides a high-quality output (i.e., describes the most possible causes and provides maintenance advice) that helps the decision-making process, which saves time and reduces costly unnecessary maintenance actions.

A proper selection of diagnostic parameters depends on valuable information relating to the current technical condition. Therefore, many relevant articles were reviewed for this paper. Several statistical studies researched the proper diagnostic parameters for each engine's functional subsystem and component, starting with the fuel feeding and injection systems. Witkowski has demonstrated that damage in the injection system can be detected by the heat release characteristic, which enables the use of it in a diagnostic procedure; he focused on the course of heat release reacting to the fuel intensity per cycle [1]. In another paper, Witkowski studied the importance of the selection and minimization of the number of diagnostic parameters. This study aims to simplify the diagnostic process with effective fault recognition; he used the trivalent residue method for injection systems in marine diesel engines. Even though it is a time-consuming and expensive method, it could provide a good diagnostic result [2]. Yu et al. studied the possibility of using a Long Short-Term Memory (LSTM) neural network to study thermal faults. They used seven thermal parameters in their database and

*Corr. Author's Address: University of Miskolc, Faculty of Mechanical Engineering and Informatics, Institute of Manufacturing Science, Hungary altkovac@uni-miskolc.hu

applied these to the Simulink software platform to simulate the thermal failure of marine diesel engines. The study confirmed that LSTM could complete the work with better accuracy than a backpropagation neural network [3].

Radica thermodynamically analyzed a marine engine working cycle using Expert System. The obtained results were compared using the Vibe and Watson-Piley Marzouk correlations. A good match exists between measured and numerically simulated values [4]. Rubio et al. described a failure simulator for marine diesel engines based on a one-dimensional thermodynamic model. This model made it possible to know the symptoms of one failure before it becomes dangerous for the engine and to build a reliable failure database for diagnosis purposes [5].

Monieta planned and performed an experiment on the injection subsystem; he dealt with theoretical research and diagnostic tests to select adequate diagnostic parameters. The results show a good correlation between the selected parameters and the changes in the properties of the injection subsystem [6]. Zadrag and Kniaziewicz studied diagnostic parameters' sensitivity during dynamic processes of fuel supply systems and their normalization for use in diagnostic applications [7]. Lu et al. used stochastic analysis in corporate decision-making models and proved the feasibility of increasing efficiency and reducing costs for managing processes [8]. Dragan addressed a two-stage model for fault detection of an industrial heat exchanger. He applied prior knowledge and collected data; furthermore, he used the least squares method to indicate the presence of initial faults accurately and thus support timely condition maintenance [9]. The same approach led the research for lubrication systems by analysing some sensor parameters in the subsystem; it can quickly and efficiently identify the failure occurrences of complicated marine diesel engine lubricating systems [10] and [11].

For cooling system research, the goals were to identify the diagnostic relationships between coolant parameters (temperature and pressure) and their effect on other structural parameters [12]. Nahim et al. [13] developed a model for the lubrication and cooling systems considering other engines' subsystem interactions. These depend on different fluids' thermal and pressure characteristics.

Relating to the air supply and turbocharger condition diagnosis, some studies assess the relationship between the cause and symptoms of all potential problems that may occur during the operation [14]. Other researchers took experiments on real marine diesel engines and proposed measurements on the sensitivity of signals and the characteristics of exhaust emission parameters [15] to [17]. Zadrag and Bogdanowicz [15] focus on the relationships between output and engine structural parameters, considering output parameters as symptoms of the engine's technical condition. When reliable statistical data is not available or evidence independence cannot be assumed, the certainty factors (CF) theory offers an alternative to Bayesian reasoning (an application of probability theory to inductive reasoning). This theory relies on probability interpretation as expressions of parameter uncertainty, meaning that inductive reasoning is a conception of deductive reasoning, where knowledge of the truth or falsity of a hypothesis corresponds to an extreme probability 1 and 0. The CF represents the degree of confidence in a fact or rule. The CF theory approach has been widely applied in uncertain rule-based inference due to its simplicity and lack of assumptions [18] and [19].

The first aim of this study is to select the most useful diagnostic parameters for each subsystem of marine diesel engines based on other authors' statistical studies and research experiments. The main aim is to develop a knowledge-based diagnostic system (based on the selected diagnostic parameters) for the whole engine system, which can determine the technical condition.

This system is the first specially developed prototype diagnostic expert system. At the same time, this system can be applied to every four-stroke diesel marine engine, which increases operational efficiency and reliability; furthermore, it is a specific diagnostic system for marine engines during operation.

Our newly developed expert system can be added to the ship's planned maintenance system (PMS) (which includes a condition- or preventive-based maintenance strategy) to be able to modify and provide specific maintenance tasks by the maintenance team instead of regularly scheduled activities. The new expert system helps to diagnose and provide supportive advice relating to optimal working conditions. Our system also allows the operator to change and modify the ideal diagnostic parameters' values on one simple screen, depending on the operation conditions, adding the different diagnostic scenarios to the knowledge base. These advantageous options can improve the expert system's efficiency during the operation, as well as the PMS software's efficiency.

This article introduces an overview of marine diesel engine subsystems and their possible failures and effects on the engine operation and condition in

Section 2. Then, in Section 3, parameter correlation analysis methods are introduced to find the direct and indirect relationship between the diagnostic signal and different faults and conditions. After that, a newly developed diagnostic expert system and a case study for the marine diesel engines' technical diagnosis are described in Section 4.

The main added value of the article is the introduction of the newly developed diagnostic expert system, which can be offered to inexperienced users on ships to effectively manage abnormal situations. Furthermore, this diagnostic tool can be applied to the engines' subsystems to improve the reliability and efficiency of the marine diesel engines' operation and maintenance.

1 MATERIALS AND METHODS

1.1 Marine Diesel Engines' Subsystems

Dividing the marine diesel engine into multiple functional subsystems is necessary for diagnosing tasks. Many researchers confirmed the correctness and usefulness of this approach [12] and [17].

1.1.1 Fuel System

The fuel system contains two parts: the fuel injection and the fuel supply system. Fuel supply deals with providing fuel suitable to use in the injection system. The main combustion engines, the fuel feed system, and injection valves in the injection are the most unreliable parts of ship engines [6]. According to statistics, almost 50 % of all possible problems in marine engines are the fault of this system, and it can be classified as shown in Fig. 1.

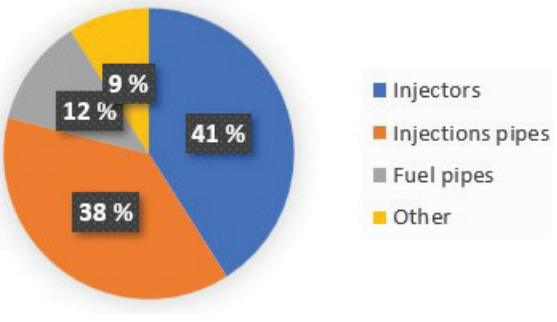

Fig. 1. *Failure statistic in fuel injection components* [1]

Indicator diagrams are the charts used to measure the thermal and cylinder performance of internal combustion engines on ships. Analysing these indicator diagrams' parameters, these parameters have limited value in marine engine technical diagnosis, even though this is a popular technique in actual operations. One of the important problems with injection systems' parameters is that their measurement is complicated due to the limited options for installing sensors [1] and [6].

1.1.2 Lubrication System

The lubrication system of a marine diesel engine distributes oil to engine bearings and as cooling oil to pistons. Oil is pumped from the lubrication oil circulation tank by an oil pump. It is then pumped directly to the main engine's lubrication oil cooler, thermostatic valve, full-flow filter, and eventually to the engine. The lubricating oil is collected in an oil pump before being drained and reused in the lubricating oil-circulating tank [10]. Operation practice shows that the lubrication system is one of the most frequently malfunctioning parts in marine diesel engines [12]. These malfunctions could be divided into four types: abnormal temperature, abnormal pressure, oil failure, and excessive oil consumption. However, the methods used currently to assess lubrication systems can only detect whether the lubrication system is defective or not, and do not provide the specific location, in addition to the major issue in obtaining data on lubrication malfunctions [11].

1.1.3 Cooling System

The cooling system's operation is essential since it is responsible for achieving and maintaining the engine's appropriate operating temperature. A fast increase of the temperature of the engine's critical components occurs when the cooling system is damaged. This change in temperature causes lubrication to degrade (the oil loses its lubricating characteristics and its combustion) and the occurrence of early ignition (self-ignition) of the fuel-air combination. In addition, excessive thermal expansion of the piston in the cylinder may occur, resulting in engine damage [12]. Moreover, low temperature is also inconvenient because the evaporation of the fuel occurs under less suitable conditions, causing the combustion process to be distorted and perhaps resulting in higher emissions of toxic substances. Finally, working at low temperatures can eject oil from the cylinder lining, which is very undesirable for lubrication [12].

1.1.4 Air Supply System

The adequate amount and quality of air needed for efficient combustion processes are determined according to the compressor wheel's efficiency and optimal operating conditions. The main failures of a scavenge air system include air filter blockage, compressor wheel pollution, turbine wheel pollution, cooler tube blockage, and cooler air side blockage [14]. The damage detection issue is critical in this system since the blade wears off 90 % of the time and may occur and lead to catastrophic failure. According to statistics, blades are involved in 65 % of centrifugal compressor unfitness conditions [20].

1.1.5 Exhaust System

The emission of toxic compounds in an engine's exhaust is affected by changes in the engine's structural parameters. This damage includes the charge exchange system, the fuel system, and the engine supercharging system. These changes are substantially greater during dynamic states and time-transient processes [15] and [21]. Generally, it can also be assumed that the increase in exhaust gas temperature decreases the maximum exhaust gas pressure, and the decrease in it causes an increase in the maximum exhaust gas pressure [1].

1.2 Correlation Methods for Diesel Engines' Diagnostic Parameters

One of the primary weaknesses of present marine diesel engine fault diagnostic systems is the inability to perform real-time fault diagnosis of diesel engines [16]. Each diagnostic parameter gives a certain diagnostic signal (depending on its sensitivity) to change and sometimes to the rate of this change. The direct and indirect relationship between the diagnostic signal and different faults determines the value of this parameter as a diagnostic parameter [22] and [23]. Unfortunately, the availability and measuring of the diagnostic parameter might sometimes be a reason for ignoring a good, diagnostically reasonable parameter in the diagnostic system.

One of the statistical analysis methods of data is the so-called correlation, which is a statistical concept explaining the relationship between two or more variables. Given the variety of data types, variables, and even units of measurement in scientific research, correlation coefficients can be calculated using several methods. The purpose of using these coefficients is to evaluate the existence of a relationship between two variables and check whether it is proportional or inversely proportional, strong or weak [24].

Due to the many parameters and sensors on diesel engines, correlation analysis will reduce diagnosis time as much as possible while ensuring the validity and accuracy of the results. In the next sub-sections, we introduce the most common correlation analysis methods used for numerical variables.

1.2.1 Pearson Correlation Coefficient Method

The Pearson correlation coefficient calculates the correlation between the dependent variable (output) Y and the diagnostic variable (input) X [6, 7]. The correlation coefficient values are in the range [−1; 1]; the sign indicates the correlation direction, while the absolute value presents the relation strength [7]. This formula takes the following form:

$$r_{yxk} = \frac{\sum_{i=1}^{N}\left(x_{ik} - \overline{x}_k\right)\left(y_i - \overline{y}\right)}{\sqrt{\sum_{i=1}^{N}\left(x_{ik} - \overline{x}_k\right)^2 \sum_{i=1}^{N}\left(y_i - \overline{y}\right)^2}}, \quad (1)$$

where r_{yxk} is the correlation coefficient, x_{ik}, y_i input and output variables, i the i^{th} values of variables, $\overline{x}_k$, $\overline{y}$ the mean values of variables, and N the number of observations.

1.2.2 Hellwig Method

This method's concern is selecting a set of variables with the largest information capacity and using all potential variables as an information storage unit [7] and [25]. The method requires "Test": an appropriate number of potential combinations of all $L = 2^k - 1$ combinations of k potential independent variables. For each combination, the individual index of information capacity (h_{mxk}) is defined for the variable xk in the m combination of variables:

$$h_{mxk} = \frac{r_{yxk}^2}{1 + \sum_{\substack{k,s \in km \\ k \neq m}} \left| r_{x_k x_s} \right|}, \quad (2)$$

where r_{yxk} is the correlation coefficient, $r_{x_k x_s}$ the coefficient of correlation between the explanatory variables, m the number of combinations, and k the number of variables for the index of individual capacity information.

The Hellwig analysis continues with the calculation of the H_m information for each combination of the integral capacity indicators:

$$H_m = \sum_{k \in K} h_{mxk}. \quad (3)$$

The criterion for determining the optimum combination of explanatory variables is the highest value of this indicator.

Other types of correlation analysis methods are used according to the type and number of variables or the type of the study. For example, the Spearman correlation coefficient **[26]** fits many types of relationships but also requires that the data must meet (monotonic relationship or ordinal data). The other variable must tend to increase or decrease, but not necessarily a linear function. This aspect of the Spearman correlation allows the fit of non-linear relationships. However, there must be a tendency to change in a particular direction.

Many studies used the aforementioned methods for the different subsystems' parameters of marine engines, such as fuel oil systems and lubrication systems. In our study, we will focus on the most sensitive diagnostic parameters selected based on the previous studies' statistical results, on other experimental studies on the real marine diesel engine, or on experts' knowledge. After the selection of these diagnostic parameters, we will develop a new diagnostic system for the whole engine subsystems.

We can classify the previous studies' results as shown in Table 1, which shows the diagnostic parameters for diesel engine subsystems and the methods used in the references to select them. The selection methods can be the following: experts' opinions; statistical data analyses (correlation analysis); experimental validation (on real ships and engines); marine diesel engine failure simulator (engines simulation models).

During our research (beside the application of the previous methods) we had long discussions with six marine experts (chief engineers) about the possibility of using their practical experience and knowledge to develop our new technical condition diagnosis expert system. We applied the selected most important diagnostic parameters and built the six marine chief engineers' opinions into the expert system relating to the specific rules for each condition.

2 RESULTS AND DISCUSSION

2.1 Introduction of the Newly Developed Diagnosis Expert System

The primary aim of our research was to develop a new diagnosis expert system to increase the reliability and efficiency of the engines' maintenance and repair strategies. During the research, we utilized previous statistical and experimental results and used the practical experiences of six expert chief engineers. Ship chief engineers are the head of the technical department of the ship; they should have many years of experience in different ranks and positions before they are qualified to become chief engineers. Our experts have at least five years of experience as chief engineers. In our future work, we are planning to add more expertise from other marine engineers with different practical backgrounds to improve our newly developed diagnosis expert system to determine and improve the marine diesel engine's technical condition more precisely.

Table 1. *Diagnostic parameters and their selection methods*

Subsystem	Parameters	Method	References
Fuel System	Pressure after feeding pump	Experts' opinion. Statistical data analyses. Experimental validation. Marine diesel engine failure simulator.	**[1], [2], [5], [6]**
	Injection pressure		
	Combustion pressure		
Lubrication System	Oil pump pressure	Experimental Validation. Marine diesel engine failure simulator.	**[5], [8], [12], [10]**
	Oil temperature		
	Oil pressure		
	Oil level		
Cooling System	Water pressure	Experimental Validation. Marine diesel engine failure simulator.	**[5], [11], [12]**
Air Supply System	Pressure after turbocharger	Experts' opinion. Statistical Data Analyses. Marine diesel engine failure simulator	**[2], [5], [13], [17]**
	Temperature after cooler		
Exhaust System	Exhaust gas temperature	Experts' opinion. Statistical data analyses. Thermal failure simulation of diesel engine.	**[2], [3], [7], [14], [15], [16]**
	Exhaust gas colour		

2.1.1 Conception of the New Expert System for the Diagnosis of Marine Engines

The conception and the evaluation process are demonstrated in Fig. 2. The newly developed software includes 12 diagnostic parameters and 44 most commonly occurring faults and abnormal cases. The operator (the user) inputs the normal ranges relating to the 12 diagnostic parameters (these data are depending on the type of the marine engine) in the main screen (Fig. 3). Then these data will be exported into MATLAB file to import them to CLIPS software. CLIPS is a public domain software tool for implementing expert systems, developed at NASA. CLIPS was written in C programming language. After the diagnosis process is finished, the results will be imported again into a second screen (Fig. 4).

Tables 2 to 6 describe the possible results for each case related to the abnormal conditions of the marine engine's subsystems according to the experts' opinions. The abnormality belongs to the two situations: the value of the diagnostic parameter is 1) higher than the normal ideal range or 2) lower than the ideal normal range.

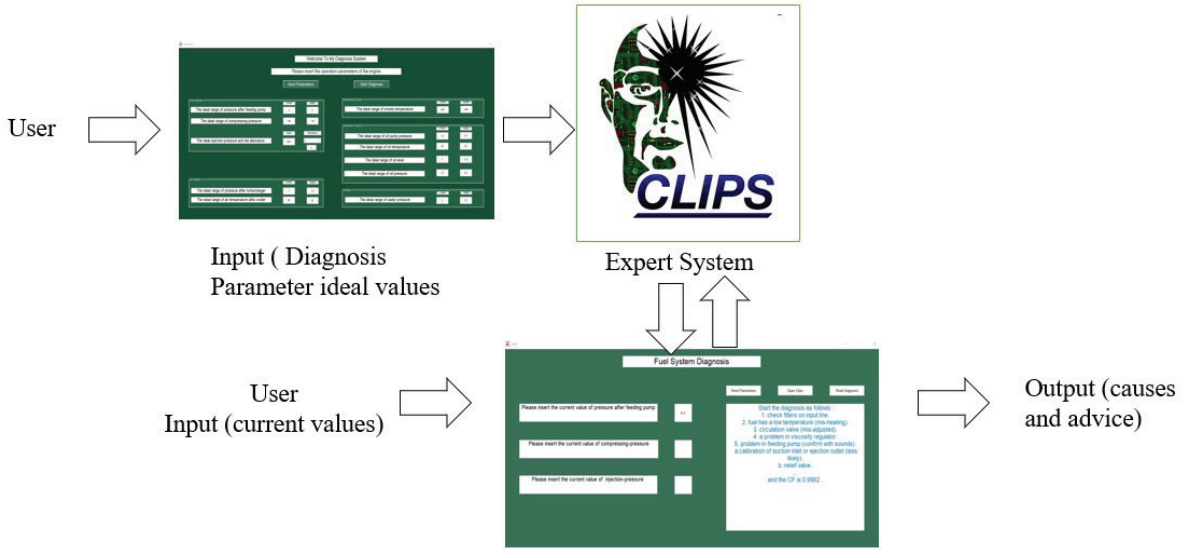

Fig. 2. *Conception of the new diagnosis expert system*

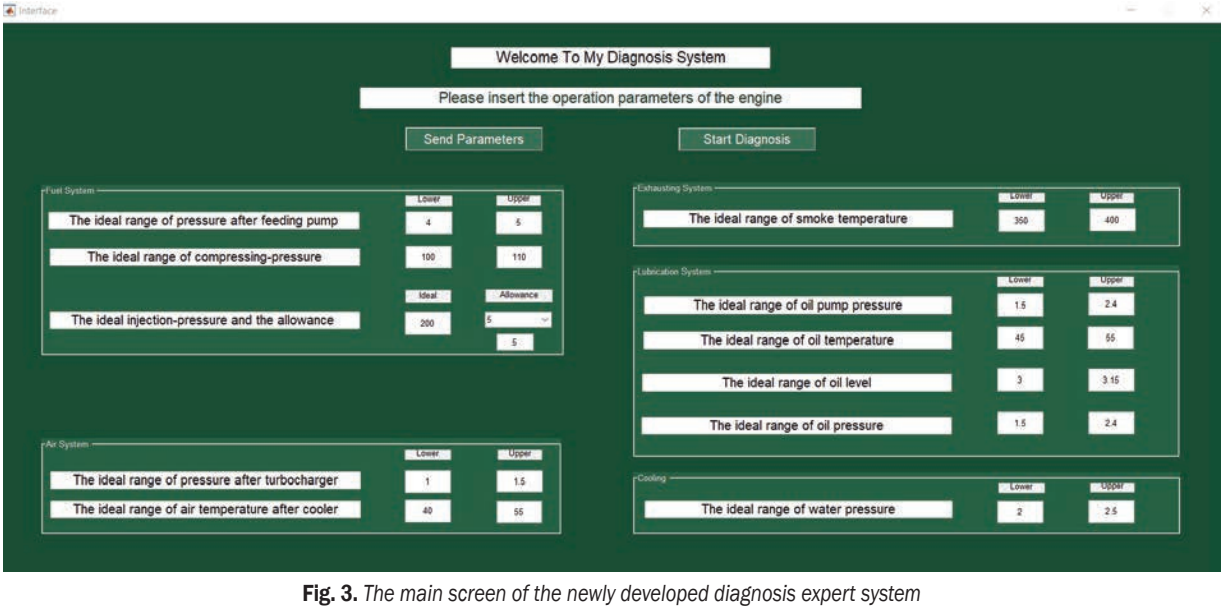

Fig. 3. *The main screen of the newly developed diagnosis expert system*

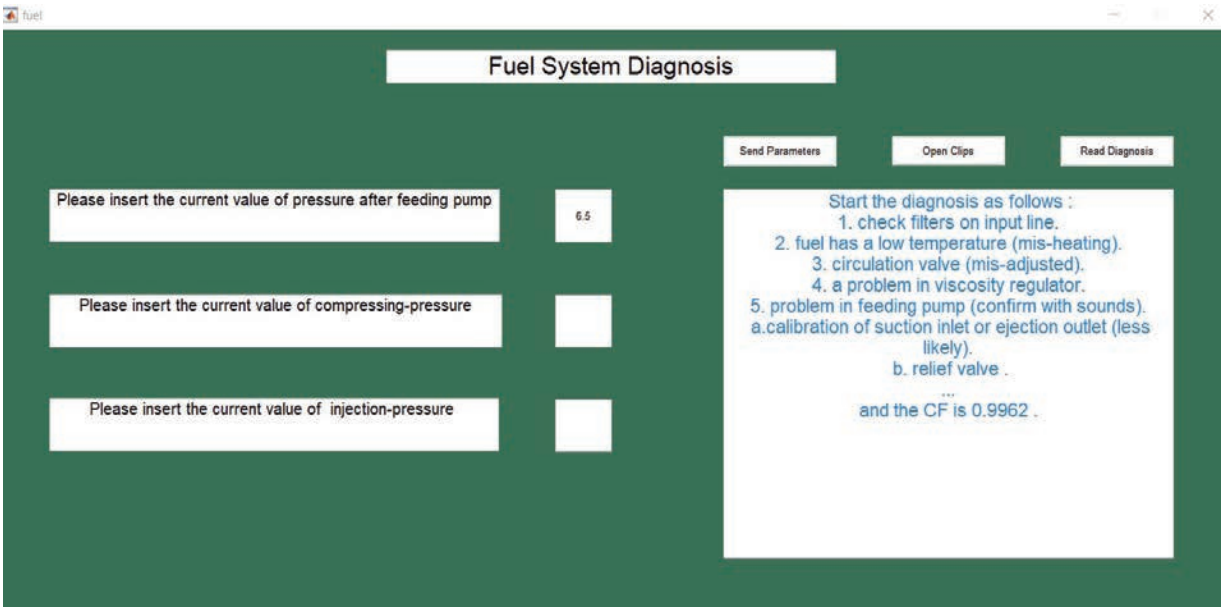

Fig. 4. *Diagnosis results (action plan) relating to the fuel system*

Table 2. *Diagnostic parameters, conditions, and experts' opinions (fuel system)*

Parameter	Condition	Diagnosis, Action
Pressure after feeding pump	Higher than normal range	1. Filters on the input line (check). 2. Fuel has a low temperature (mis-heating). 3. Circulation valve (wrong modification). 4. Problem in viscosity regulator. 5. Problem in feeding pump (confirm with sounds): a. calibration of suction inlet or ejection outlet (less likely); b. relief valve.
	Lower than normal range	1. Fuel has a high temperature. 2. Fuel level at daily service tank. 3. Polluted service tank\Blockage in the inlet pipe. 4. Check filters on the input line. 5. Leak from input line\ pressure sensors. 6. Problem in feeding pump (confirm with sounds). 7. Relief valve. 8. Check circulation line. 9. Measurement error (check with sight).
Injection pressure	Higher than normal value + tolerance	1. First, you must listen to injection sounds on high-pressure pipes (injector failure). 2. Wrong modification (late injecting), it should accompany low compressing pressure and an increase in temperature of exhaust gases.
	Lower than normal value – tolerance	1. Expansion in injection nozzle (chemical ingredients in fuel), check treatment process. 2. Spring elasticity. Both lead to early injection, accompanied by the decrease in the temperature of exhaust gases.
Combustion pressure	Higher than normal range	1. Problem in high-pressure pump (confirm with sounds). 2. Injector (confirm with sounds). 3. Feeding pump (confirm with sounds and pump temperature). 4. Delivery valve (after the high-pressure pump).
	Lower than normal range	1. Delivery valve (after the high-pressure pump). 2. Excessive clearance in the high-pressure pump. 3. Injector (confirm with sounds). 4. Feeding pump (confirm with sounds). 5. Problem in high-pressure pump (confirm with sounds). 6. Air valves (confirm with sounds).

Table 3. *Diagnosis parameters, conditions, and experts' opinions (Lubrication System)*

Parameter	Condition	Diagnosis, Action
Oil pump pressure	Higher than normal range	1. Cold oil (check oil temperature). 2. Pressure regulating valve on the oil pump. 3. Plugged pipes (less likely to happen).
	Lower than normal range	The possible problem is unsealed (or increasing in clearances).
Oil temperature	Higher than normal range	1. Oil cooler. 2. Solid bearing (check heat sensor).
	Lower than normal range	1. Cold engine. 2. Mis-cooling. 3. Polluted oil. 4. Leak from heat regulator. 5. Oil filters problem.
Oil pressure	Higher than normal range	The possible problem is a blockage in oil holes (accompanied by an increase in temperature).
	Lower than normal range	External: leak in the oil lines (diagnosed with sight and excessive heat). Internal leakage: 1. it may appear in exhaust gas colour; 2. oil-consuming detector; 3. it may appear in other systems.
Oil level	Higher than normal range	1. Water leak (confirm from the oil-mist detector). 2. Fuel leak (viscosity test).
	Lower than normal range	The possible problem is oil leakage (check for blue smoke) (in case of an external leak, check with sight).

Table 4. *Diagnosis parameters, conditions, and experts' opinions (Cooling System)*

Parameter	Condition	Diagnosis, Action
Water pressure	Higher than normal range	1. Blockage in water lines (problem in water treatment or calcareous sediments), less likely to happen. 2. Problem in regulator valve (accompanies with temperature change).
	Lower than normal range	Before the engine: 1. If it is not accompanied by an abnormal decrease in water level at the expansion tank, then it is pump problem (confirm with sounds). 2. If it is accompanied by a slow and gradual decrease in water level then it is an increase in wear at pump body (water mistreatment). 3. If it is accompanied by a fast and sudden water level decrease, then it is pump collapses.
		After the engine: the possible problem is accompanied by an abnormal decrease in the expansion tank and may be: 1. Leakage problem: Internal: check exhaust gases' colour and temperature. External: check pipes and joint points. 2. Measurement device error.

In the recent stage of our research, we selected and implemented the most important and most frequently used parameters applied in the practical diagnostic systems and mentioned in the literature. Many further parameters could be suitable for advanced future analysis to cover more abnormal and normal conditions. For example, additional data relating to the noise, the vibration and the engine's total running hours can be implemented in the expert system in the near future. Furthermore, in some specific subsystems like the air supply system, we will study the possibility of adding the air intake and airflow values to achieve more precise monitoring and more reliable decision-supporting output. We can add waterflow and potential of hydrogen (PH) values to the cooling system to check the coolant's acidity. These newly suggested parameters will help to reduce the risk of damaging seals and metal components. Selecting the adequate diagnostic parameters and sub-parameters can help to improve maintenance activities and engines' operation performance.

The main screen of the newly developed diagnosis expert system is shown in Fig. 3. The developed expert system provides the possibility for the end-user to set the ideal operation values of the diagnostic parameters relating to the five subsystems before the system starts running. The software also provides the possibility of changing these operation values after a long operation time because (after a certain amount of time) the ideal range may be changed due to some parts replacements, compulsory changes in the engines' fluids specifications, or increased abrasion.

Table 5. *Diagnosis parameters, conditions, and experts' opinions (Air Supply System)*

Parameter	Condition	Diagnosis, Action
Pressure after turbocharger	Higher than normal range	1. High backpressure. 2. Air valves problem. 3. Partial blockage in air pass (rarely happen). Immediate action: reduce speed, then start diagnosing
	Lower than normal range	Turbocharger surge: 1. Air filter plugging (remove and clean). 2. Polluted turbo (check if the compressor and the turbine had cleaned regularly). 3. Unsteady shaft\Wear damage. 4. Air cooler fouling (accompanied by high temperature). Immediate action: reduce speed to load at which surging stops; If necessary open the air cooler inspection hole to stop surging.
		The turbocharger does not surge: 1. Unsealed joints before engine (check). 2. Turbocharger calibration (check). 3. Excessive clearance (maintenance).
Temperature after cooler	Higher than normal range	1. Blockage in water tubes (sediments). 2. Blockage in air tubes (accompanied by surging in turbocharger).
	Lower than normal range	Overcooling (modify).

Table 6. *Diagnosis parameters, conditions, and experts' opinions (Exhaust System)*

Parameter	Condition	Diagnosis, Action
Exhaust gas temperature	Higher than normal range	One unit: 1. Injector (wrong modification), 75 % probability and accompanied with black smoke. 2. Loose valves. 3. High-pressure pump problem (less likely to happen and accompanied by a change in compressing- pressure).
		All units: 1. Over-loaded turbocharger (check air temperature and indicator card). 2. Fuel problem (check viscosity regulator).
	Lower than normal range	One unit: 1. Unsealed cylinder jacket. 2. Unsealed valves.
		All units: The possible problem is in air temperature.
Exhaust gas colour	Black	1. Small air amount (wrong modification\ leakage). 2. Unsealed cylinder jacket (accompanied by temperature drooping). 3. Fuel components (appear in first use). 4. Fuel parameter (temperature-viscosity); check viscosity regulator. 5. Injectors (wrong modification); check indicator card. 6. Pumps (wrong modification); check indicator card.
	White	1. Economizer (check by reducing load or conversing mechanism). 2. Check the temperature after all units (define the leaking unit) and (confirm from the water expansion tank) most likely: leak from piston cooling tubes (if it is water-cooled). less likely: leak from cylinder jacket. 3. Steam in the air
	Blue	The possible problem is that excess oil burning could be caused by: 1. Oil specifications (if the oil is being used for the first time). 2. Piston oil rings corrosion 3. Collapse in the fire valve lubrication system (wrong modification). 4. Increasing cylinder jacket lubrication (wrong modification). immediate action: Reducing oil amount to minimize leakage
	Yellow	The possible problem is a fuel problem (first use) has increase in sulphur amount.

Initially, the system operator estimates the parameters' ideal operating ranges based on the service instructions book and the engine's total running hours (the engine's operation age), the type of the engine, and its manufacturing year.

However, after unforeseen operational circumstances, like the usage of a not-recommended fuel or replacing of some parts, the ship's chief engineer can make a decision that the ideal intervals of the diagnostic parameters' range have to be smaller. Our expert system provides the possibility for the operator to modify the ideal ranges of the analysed diagnostic parameters. In addition, during the software's development, it is possible to transform the afore-mentioned decision-making of the chief engineer into a fully automated process in our expert system by correlating the values of the ideal diagnostic parameters to the engine's effectiveness. In the next phase of our software development, we will define the engine type specifications in greater detail, and the manufacturing year in the knowledge-base to obtain more precise and reliable diagnostic and maintenance procedures.

2.1.2 Advantages of the Newly Developed Diagnosis Expert System

The newly developed diagnosis expert system provides a high-quality and reliable diagnosis describing the engines' current condition and all the possible reasons and required actions to improve the maintenance and repair procedure, which will save time and eliminate unnecessary actions. Furthermore, this expert system has many advantages compared to other diagnostic systems mentioned in the literature and recently applied in the practice. These advantages are the following:

- The newly developed diagnosis expert system can be applied at the same time for all engine subsystems (fuel, lubrication, cooling, air, and exhaust systems).
- The software absolutely meets companies' demands and is customizable.
- The new expert system can be applied to every 4-stroke marine diesel engine. The user can flexibly set the normal ranges of the selected 12 diagnostic parameters according to the type of marine engine to be diagnosed.
- The application of the expert system does not require any new sensors or measuring devices on the engine; therefore, further investment is not needed.
- The new software is easy to use and very cost-effective.
- The new expert system can be used anytime and anywhere, both in on-line and off-line modes.

2.1.3 Case Study for the Validation of the New Diagnosis Expert System

We selected a multi-purpose ship to perform a test on the final diagnostic system with the following specifications:

- Ship name: LAODICEA; Build: in China in 2005;
- Purchase and operation date: 2009; IMO number: 9274343;
- Length of the ship: 138 m; Breadth of the ship: 21 m;
- Dead weight of the ship: 12744 tons;
- Engine type: MaK 6 M 43 C5700HP@500.

The values relating to the diagnostic parameters of the investigated marine engine are shown in Table 7.

Table 7. *Ideal ranges for the parameters to be diagnosed in the case of the examined marine engine*

Feeding pump pressure [bar]	[4; 5]
Combustion pressure [bar]	[100; 110]
Injection pressure [bar]	200 ± 5 %
Air pressure after turbocharger [bar]	[1; 1.5]
Air temperature after cooler [°C]	[40; 55]
Exhaust gas temperature [°C]	[350; 400]
Oil pump pressure [bar]	[1.5; 2.4]
Oil temperature [°C]	[45; 55]
Oil level [m]	[1.5; 2.4]
Oil pressure [bar]	[1.5; 2.4]
Water pressure [bar]	[2; 2.5]

In the case study, we simulated an abnormal situation when the feeding pump pressure increases up to 5.5 [bar], which means that this pressure becomes higher than the normal range [4; 5]. The operator must set this abnormal feeding pump pressure in the main screen of the expert system as can be seen in Fig. 4.

After running the diagnosis expert system, the operator received the action plan as a result of the diagnosis. It can be seen in Fig. 4 that the operator must take the following actions in the given preference order to remove the abnormally high pressure to prevent an accidental catastrophe and costly consequences.

The results of the diagnosis are the following as can be seen in Fig. 4:

1. Check the filters on the input line.
2. Fuel has a low temperature (mis-heating).
3. Circulation valve (wrong modification).
4. Problem with viscosity regulator.
5. Problem with feeding pump (confirm with sounds):

a. calibration of suction inlet or ejection outlet (less likely);
b. relief valve.

It can be also concluded that the result of the simulation has a number equal to 0.9962 (Fig. 4). This CF number represents the degree of agreement of the six marine chief engineer experts according to the rule defined in the expert system. This CF calculates and combines the expert opinions depending on the amount of expertise by years of experience for each expert. The certainty factor has a range between [-1; +1] and (after running the rule) these numbers could be decreased if the diagnose wrong/partially wrong (followed by modification, remove, or add new rules) or increased if it has a correct result. We can summarize that the reliability of the software result is near to the maximal value.

3 CONCLUSIONS

In the case of technically complex marine diesel engines that have multiple diagnostic parameters, it is necessary to minimize the number of the diagnostic parameters. Therefore, the correct selection of the required diagnostic parameters highly determines the efficiency of the developed diagnostic system. The application of an adequate diagnostic system for marine engines offers a good possibility to focus on early recognition of potential problems and prevents catastrophic and costly consequences.

The first aim of our research was to select the most effective diagnostic parameters relating to the subsystem of the marine diesel engines (fuel, lubrication, cooling, air, and exhaust systems) based on statistical studies and research experiments. The main aim of the research was to develop a knowledge-based diagnostic system (based on the selected diagnostic parameters) for the whole engine system to determine the technical condition. The newly developed diagnosis expert system can be applied to every four-stroke marine diesel engine to increase its operational efficiency and reliability.

The article first presented an overview of the marine diesel engine subsystems and their possible failures and effects on the engine operation and condition were introduced. Next, the parameters correlation analysis methods were described to find the direct and indirect relationship between the diagnostic signal and different faults and conditions. Finally, a newly developed diagnosis expert system and a case study for marine diesel engines' technical diagnosis were introduced.

The main added value of the article is the introduction of the newly developed diagnostic expert system, which can be offered to inexperienced users on ships to manage abnormal situations effectively and quickly. Furthermore, this diagnostic tool can be applied to the engines' subsystems to improve the reliability and efficiency of their operation and maintenance.

Our future research plan is to build a bigger knowledge base based on more experts' opinions with different practical experiences and previous diagnoses on similar engine types to improve the recent expert system using artificial intelligence approaches to create a more reliable and accurate diagnostic system.

4 ACKNOWLEDGEMENTS

The research was supported by the Hungarian National Research, Development, and Innovation Office - NKFIH under the project number K 134358.

5 REFERENCES

[1] Witkowski, K. (2019). Research the possibility of obtaining diagnostic information about the ships engine fuel injection system condition based on the analysis of characteristics of heat release. *Journal of KONES Powertrain and Transport*, vol. 26, no. 3, p. 249-256, **DOI:10.2478/kones-2019-0080**.

[2] Witkowski, K. (2017). The correct selection of diagnostic parameters of marine diesel engine and their minimization of as a necessary action in the formation of diagnostic algorithm. *Journal of KONES Powertrain and Transport*, vol. 24, no. 2, p. 287-292, **DOI:10.5604/01.3001.0010.2948**.

[3] Yu, Z., Wang, S., Chen, N. (2022). Thermal fault diagnosis of marine diesel engine based on LSTM neural network algorithm. Vibro*engineering PROCEDIA*, vol. 41, p. 198-203, **DOI:10.21595/vp.2022.22515**.

[4] Radica, G. (2008). Expert system for diagnosis and optimisation of marine diesel engines. *Strojarstvo: Casopis za Teoriju i Praksu u Strojarstvu*, vol. 50, no. 2, p. 105-116.

[5] Rubio, J.A.P., Vera-García, F., Grau, J. (2018). Marine diesel engine failure simulator based on thermodynamic model. *Applied Thermal Engineering*, vol. 144, p. 982-995, **DOI:10.1016/j.applthermaleng.2018.08.096**.

[6] Monieta, J. (2019). Selection of diagnostic symptoms and injection subsystems of marine reciprocating internal combustion engines. *Applied Science*s, vol. 9, no. 8, art. ID 1540, **DOI:10.3390/app9081540**.

[7] Zadrag, R., Kniaziewicz, T. (2015). Identification of diagnostic parameter sensitivity during dynamic processes of a marine engine. *Combustion Engine*s, vol. 162, no. 3, p. 1007-1014.

[8] Lu, J.-B., Liu, Z.-J.,Tulenty, D., Tsvetkova, L., Kot, S. (2021). Implementation of stochastic analysis in corporate decision-making models. *Mathematics*, vol. 9, no. 9, art. ID 1041, **DOI:10.3390/math9091041**.

[9] Dragan, D. (2011). Fault detection of an industrial heat-exchanger: A model-based approach. *Strojniški vestnik - Journal of Mechanical Engineering*, vol. 57, no. 6, p. 477-484, **DOI:10.5545/sv-jme.2010.128**.

[10] Zhao, G., Liu, Z., Chen, L. (2019). A fault diagnosis model of marine diesel engine lubrication system based on improved extreme learning machine. *IOP Conference Series: Earth and Environmental Science*, vol. 300, no. 4, p. 1-7, **DOI:10.1088/1755-1315/300/4/042092**.

[11] Ren, D., Zeng, H., Wang, X., Pang, S., Wang, J. (2020). Fault diagnosis of diesel engine lubrication system based on Bayesian network. *6th International Conference on Control, Automation and Robotics Conference Proceedings*, p. 423-429, **DOI:10.1109/ICCAR49639.2020.9108107**.

[12] Krakowski, R. (2014). Diagnosis modern systems in marine diesel engines. *Journal of KONES Powertrain and Transport*, vol. 21, no. 3, p. 191-198, **DOI:10.5604/12314005.1133203**.

[13] Nahim, H.M., Younes, R., Shraim, H., Ouladsine, M. (2016). Modeling with fault integration of the cooling and the lubricating systems in marine diesel engine: *Experimental validation. IFAC-PapersOnLine*, vol. 49, no. 11, p. 570-575, **DOI:10.1016/j.ifacol.2016.08.083**.

[14] Knežević, V., Orović, J., Stazić, L., Čulin, J. (2020). Fault tree analysis and failure diagnosis of marine diesel engine turbocharger system. *Journal of Marine Science and Engineering*, vol. 8, no. 12, p. 1004-1023, **DOI:10.3390/jmse8121004**.

[15] Bogdanowicz, A. Zadrag, R. (2019). Identification of indicators sensitivity of emissions as a diagnostic parameter during the dynamic process of marine diesel engine, *Diagnostyka*, vol. 20, no. 3, p. 79-86, **DOI:10.29354/diag/109886**.

[16] Puzdrowska, P. (2021). Diagnostic information analysis of quickly changing temperature of exhaust gas from marine diesel engine part I single factor analysis. *Polish Maritime Research*, vol. 28, no. 4, p. 97-106, **DOI:10.2478/pomr-2021-0052**.

[17] Qi, Z., Qi, Y., Hu, G. (2020). A practical approach to detect faults of marine diesel engine. *Journal of Computer and Communications*, vol. 8, p. 12-21, **DOI:10.4236/jcc.2020.88002**.

[18] Niederliński, A. (2018). A new approach for modelling uncertainty in expert systems knowledge bases. *Archives of Control Sciences*, vol. 28, no. 1, p. 19-34, **DOI:10.24425/119075**.

[19] Babič, M., Karabegović, I., Martinčič, S.I., Varga, G. (2019). New method of sequences spiral hybrid using machine learning systems and its application to engineering. In Karabegović, I. (ed.) *New Technologies, Development and Application. Lecture Notes in Networks and Systems*, vol. 42, p. 227-237, **DOI:10.1007/978-3-319-90893-9_28**.

[20] Monieta, J. (2018). Fundamental investigations of marine engines turbochargers diagnostic with use acceleration vibration signals. *AIP Conference Proceedings*, vol. 2029, art. ID 020044, **DOI:10.1063/1.5066506**.

[21] Dong, X.T., Nguyen, M.H. (2021). Experimental study of identifying emission sources of acoustic signals on the cylinder body of a two-stroke marine diesel engine. *Polish Academy of Science Archives of Acoustics*, vol. 46, no. 1, p. 105-119, **DOI:10.24425/aoa.2021.136565**.

[22] Cazanas, R., Sobrino, D., Martínez, E., Kostal, P., Mudriková, A. (2018). Integrating production and maintenance planning as an element of success at the tactical level: A fuzzy control theory approach. *Research Papers Faculty of Materials Science and Technology Slovak University of Technology*, vol. 26, no. 42, p. 109-117, **DOI:10.2478/rput-2018-0013**.

[23] Do, V.T., Chong, U.-P. (2011). Signal model-based fault detection and diagnosis for induction motors using features of vibration signal in two-dimension domain. *Strojniški vestnik - Journal of Mechanical Engineering*, vol. 57, no. 9, p. 655-666, **DOI:10.5545/sv-jme.2010.162**.

[24] Li, Z., Zhao, H., Zeng, R., Xia, K., Guo, Q., Yuhai, L. (2019). Fault identification method of diesel engine in light of Pearson correlation coefficient diagram and orthogonal vibration signals. *Mathematical Problems in Engineering*, vol. 2019, art. ID 2837580, **DOI:10.1155/2019/2837580**.

[25] Kowalik, P. (2014). On an implementation of the method of capacity of information bearers (the Hellwig method) in spreadsheets. *Probability in Action, Politechnika Lubelska*, p. 31-40.

[26] Rebekić, A., Lončarić, Z., Petrović, S., Marić, S. (2015). Pearson's or Spearman's correlation coefficient-which one to use. *Agriculture*, vol. 21, no. 2, p. 47-54, **DOI:10.18047/poljo.21.2.8**.

Vsebina

Strojniški vestnik - Journal of Mechanical Engineering
letnik 68, (2022), številka 0
Ljubljana, oktober 2022
ISSN 0039-2480

Izhaja mesečno

Razširjeni povzetki (extended abstracts)

Nejc Rožman, Marko Corn, Gašper Škulj, Janez Diaci, Primož Podržaj: Rešitve za povečevanje razširljivosti v proizvodnji podprti s tehnologijo veriženja blokov: Pregled literature SI 77
Mateusz Wrzochal, Stanisław Adamczak, Ryszard Domagalski, Grzegorz Piotrowicz, Sylwester Wnuk: Predlog nove naprave za industrijske meritve tornega momenta kotalnih ležajev SI 78
Marcin Trajer, Łukasz Pyclik, Jerzy Robert Sobiecki: Priprava prevlek iz nikljevega aluminida na majhnih luknjah po postopku EDD SI 79
Volodymyr Brazhenko, Yibo Qiu, Jiancheng Cai, Dongyun Wang: Matematični model in analiza toplotnih lastnosti sten letalske kabine pod tlakom SI 80
Hla Gharib, György Kovács: Razvoj novega ekspertnega sistema za diagnostično obravnavo dizelskih motorjev za plovila na osnovi realnočasovnih diagnostičnih parametrov SI 81

Strojniški vestnik - Journal of Mechanical Engineering 68(2022)10, SI 77

Prejeto v recenzijo: 2022-09-02
Prejeto popravljeno: 2022-09-26
Odobreno za objavo: 2022-09-26

Rešitve za povečevanje razširljivosti v proizvodnji podprti s tehnologijo veriženja blokov: Pregled literature

Nejc Rožman* – Marko Corn – Gašper Škulj – Janez Diaci – Primož Podržaj[1]
Univerza v Ljubljani, Fakulteta za strojništvo, Slovenija

Raziskovalci na področju pametnih proizvodnih sistemov so prepoznali prednosti tehnologije veriženja blokov ali bločno-verižne tehnologije. Ta omogoča vzpostavitev zaupljivega okolja v katerem lahko delujejo odprti načini povezovanja proizvodnih sistemov brez posrednikov. Takšno okolje omogoča sodelovanje proizvodnih entitet, ki si med seboj ne zaupajo oziroma predstavljajo konkurenco zato, da bi zadostili naraščajoči kompleksnosti zahtev kupcev.

Vendar pa se obstoječa bločno-verižna omrežja soočajo z omejitvami, ki so opredeljene s kompromisom med razširljivostjo, decentralizacijo in varnostjo. Razširljivost bločno-verižnega omrežja je opredeljena kot sposobnost omrežja, da podpira naraščajoče število transakcij in je nižja v primerjavi s centraliziranimi plačilnimi sistemi. Da bi zmanjšali učinek omejitve razširljivosti, so v literaturi predstavljene različne rešitve za povečevanje razširljivosti tudi na področju pametnih proizvodnih sistemov. Ta raziskava predstavlja pregled literature na področju rešitev za povečevanje razširljivosti v proizvodnji podprti s tehnologijo veriženja blokov.

Izbrana literatura je bila pregledana in razvrščena glede na vrsto predstavljene rešitve za povečevanje razširljivosti. Za vsako vrsto rešitve so poudarjene in obravnavane glavne značilnosti konceptov in povezave med tehnologijo veriženja blokov in proizvodnim sistemom. Glavni ugotovitvi raziskave sta, da so rešitve za povečevanje razširljivosti prvega nivoja bolje zastopane v literaturi in prevladujejo pri splošnih sistemih pametne proizvodnje, medtem ko so rešitve za povečevanje razširljivosti drugega nivoja bolje zastopane pri specifičnih sistemih pametne proizvodnje. Med predlaganimi rešitvami prevladujejo rešitve, ki izboljšujejo konsenzni mehanizem, rešitve zunaj verige ter rešitve ki optimizirajo strukturo verige blokov. Analiza pregledane literature je pokazala, da sta glavna odprta problema pregledanih rešitev pomanjkanje implementacije v industriji in nezadostna analiza trileme bločno-verižne tehnologije v povezavi s praktičnimi omejitvami.

Glavni prispevek predstavljene raziskave je detajlna sistematična analiza pregledane literature na temo tehnologij za povečevanje razširljivosti bločno-verižne tehnologije v okviru pametnih proizvodnih sistemov. Analiza predstavlja nekaj iztočnic za nadaljnje raziskovanje na področju povezovanja tehnologije veriženja blokov in proizvodnih sistemov.

Ključne besede: bločno-verižna tehnologija, proizvodni sistemi, trilema, razširljivost, rešitve prvega nivoja, rešitve drugega nivoja

*Naslov avtorja za dopisovanje: Univerza v Ljubljani, Fakulteta za strojništvo, Aškerčeva 6, 1000 Ljubljana, Slovenija, nejc.rozman@fs.uni-lj.si

Strojniški vestnik - Journal of Mechanical Engineering 68(2022)10, SI 78

Prejeto v recenzijo: 2022-07-08
Prejeto popravljeno: 2022-08-28
Odobreno za objavo: 2022-09-30

Predlog nove naprave za industrijske meritve tornega momenta kotalnih ležajev

Mateusz Wrzochal[1,*] – Stanisław Adamczak[1] – Ryszard Domagalski[1] – Grzegorz Piotrowicz[2] – Sylwester Wnuk[2]
[1] Tehniška univerza v Kielcah, Poljska
[2] Fabryka Lozysk Tocznych-Krasnik S.A., Poljska

V velikem podjetju za proizvodnjo ležajev so začeli uporabljati prototip naprave za preizkušanje tornega momenta kotalnih ležajev. Za novo napravo je značilna inovativna zasnova, ki omogoča preizkušanje širokega razpona dimenzij ležajev, apliciranje znatnih aksialnih obremenitev, dodatne meritve vgradne širine ležajev in, kar je najbolj pomembno, preizkušanje stožčastih ležajev. Pričujoči članek predstavlja zgradbo omenjene naprave in njene možnosti.

Torni moment se do sedaj ni preizkušal, ker ne spada med merila sprejemljivosti kotalnih ležajev. Problem tornega momenta ležajev pa je pomemben z vidika varovanja okolja, saj se z zmanjšanjem tornega upora poveča izkoristek naprav in s tem zmanjšajo izpusti CO_2 v ozračje.

Naprava, ki je predmet tega članka, je eden od osmih zgrajenih testnih sistemov. Nove merilne prakse omogočajo znatno izboljšanje kakovosti izdelanih ležajev ter proizvodnjo nestandardnih ležajev za povečanje zmogljivosti strojev in mehanske opreme. Izhodišče pri razvoju so bile konkretne funkcije in parametri, ki jih mora zagotavljati naprava. Sam proces konstruiranja je trajal več let. Obravnavanih je bilo več različnih rešitev in končno je bila izbrana različica, ki je predstavljena v članku. Med predstavljenimi konstrukcijskimi rešitvami je bilo mogoče izbrati pet originalnih zasnov. Rešitve so primerne tako za celotno preizkuševališče kot za njegove posamezne univerzalne mehanizme, ki bodo uporabni tudi pri drugih napravah s podobno zgradbo. Inovacija pri predstavljenem preizkuševališču je edinstvena zasnova (ta ni običajna za naprave tega tipa), ki omogoča:

i) izvajanje preizkusov s stožčastimi ležaji (podobne naprave se uporabljajo predvsem za krogljične ležaje),
ii) povečanje števila in obsega testnih parametrov, in
iii) višjo točnost meritev.

Naprava je primerna za izvajanje predvidenih nalog in privzeti testni parametri so dosegljivi. Opravljeni preizkusi so pokazali, da točnost meritev izpolnjuje zahteve, na podlagi katerih je potekal konstrukcijski proces.

Zasnova in razvoj preizkuševališča predstavljata le začetek obravnave tornega momenta kot zelo pomembnega parametra kotalnih ležajev. Pomembne bodo tudi raziskave oz. preverjanje vpliva dinamike na rezultate meritev tornega momenta.

Preučiti bo treba spremenljivost rezultatov v času pri konstantnih merilnih pogojih (v pomoč pri določitvi merilne negotovosti), kakor tudi ponovljivost meritev tornega momenta. Najtežji problem ostaja vrednotenje točnosti merilnika tornega momenta. Ne obstajajo namreč standardni preizkušanci z znanim tornim momentom, prav tako pa ni referenčnih merilnikov tornega momenta za primerjanje rezultatov. Prihodnje napore bo zato treba usmeriti v ocenjevanje negotovosti meritev tornega momenta ter poskus razvoja standardnih ležajev z znanim tornim momentom ter primerjalnih postopkov z različnimi napravami in konstrukcijskami rešitvami za določitev referenčnega preizkuševališča.

Možnost meritev tornega momenta v tovarnah bo prinesla znaten tehnološki napredek, saj jo bodo lahko izkoristili konstruktorji in tehnologi za izboljševanje izkoristka kotalnih ležajev.

Ključne besede: kotalni ležaji, torni moment, industrijske meritve, kontrola kakovosti

*Naslov avtorja za dopisovanje: Tehniška univerza v Kielcah, al. Tysiąclecia Państwa Polskiego 7, 25-314, Kielce, Poljska, wrzochalm@gmail.com

Strojniški vestnik - Journal of Mechanical Engineering 68(2022)10, SI 79

Prejeto v recenzijo: 2022-04-19
Prejeto popravljeno: 2022-06-23
Odobreno za objavo: 2022-07-11

Priprava prevlek iz nikljevega aluminida na majhnih luknjah po postopku EDD

Marcin Trajer[1,*] – Łukasz Pyclik[2] _ Jerzy Robert Sobiecki[1]

[1] Tehniška univerza v Varšavi, Fakulteta za materiale in inženiring, Poljska
[2] Šlezijska tehniška univerza, Fakulteta za materiale in inženiring, Poljska

Predmet raziskave sta bila elektroerozijska izdelava (elektroerozijsko vrtanje – EDD) hladilnih lukenj v superzlitini na osnovi niklja ter njen vpliv na trajnost zaščitne prevleke. Nanos prevleke je bil opravljen po postopku aluminizacije iz parne faze (VPA). Postopek nanosa, ki povzroči nasičenje površine dela z aluminijevim dioksidom, se podobno kot EDD uporablja v proizvodnji. Kljub temu, da se omenjene tehnike uporabljajo že desetletja, pa v obstoječi literaturi ni bilo mogoče najti raziskav o njihovih medsebojnih interakcijah. Aluminidne prevleke, ki so bile razvite v šestdesetih letih prejšnjega stoletja, zagotavljajo toplotno in mehansko zaščito za visokoobremenjene dele letalskih motorjev. Površina, bogata z aluminijevim oksidom, s svojo kemijsko in toplotno odpornostjo loči osnovno zlitino od ekstremnih razmer v visokotlačni turbini letalskega motorja. Raziskovalci so dokazali, da lahko difuzijo aluminijevega dioksida v osnovni material med postopkom VPA zmotijo različni dejavniki, kot so stanje površine ter kemijska sestava in kristalna struktura osnovnega materiala. Proces EDD, pri katerem se material odstranjuje s pomočjo taljenja, vpliva na vse omenjene dejavnike. Površina je po obdelavi prekrita s pretaljenim slojem, ki ima drugačno kemijsko sestavo ter pogosto vključuje okside in druge delce. Material se med postopkom EDD raztali in ponovno strdi. Kombiniranje obdelovalnega postopka EDD in aluminizacije za nanos zaščitne prevleke lahko zato zaradi negativnega vpliva stranskih produktov procesa EDD na kakovost prevleke privede do variabilnosti delov. Glavni cilj študije je eksperimentalna verifikacija te hipoteze.

Hipoteza je bila eksperimentalno preverjena. Uporabljeni so bili namenski preizkušanci iz zlitine Inconel 718. Vanje so bile izvrtane tri skupine lukenj različnega premera, temu pa je sledil nanos prevlek in nato oksidacija v zračni atmosferi na temperaturi 1100 °C s 23-urnim ciklom. Sledila je preiskava stanja površine vsake luknje. Končni premer lukenj je bil preverjen z optičnim mikroskopom, preverjeni pa sta bili tudi hrapavost in sestava površine. Prevleka je bila preiskana pred oksidacijskim testom. Za vsako velikost luknje sta bila preverjena debelina in število vključkov. Po oksidaciji je bila analizirana debelina prevleke kot glavni kazalnik njene trajnosti.

Izdelane luknje izkazujejo visoko geometrijsko stabilnost. Dimenzije in geometrija vsake luknje so bile določene z meritvami. Kontrola je bila opravljena po enakem postopku kot v proizvodnji delov. Metalografske preiskave po obdelavi so pokazale pretaljeni sloj v pričakovanem območju. Analiza po nanosu prevleke je razkrila prisotnost vključkov, katerih število rase z manjšanjem premera luknje. Največ vključkov je bilo pri najmanjši luknji. Ti vključki se med oksidacijskim testom pretvorijo v področja intenzivne oksidacije z lokalno stanjšano prevleko. Statistična analiza je pokazala jasno odvisnost med velikostjo pretaljenega sloja in zmanjšanjem debeline prevleke po oksidacijskem testu.

Uporabljeni so bili preizkušanci iz zlitine Inconel 718. Ta nikljeva zlitina je sicer razširjena v industriji, vendar ni primerna za izdelavo delov visokotlačnih turbin. Eksperimente bi zato bilo treba ponoviti z materialom, ki se uporablja za litje delov visokotlačnih turbin. Postopek VPA bi bilo mogoče zamenjati s postopkom CVD. Ta je običajen pri votlih delih visokotlačnih turbin, ki potrebujejo poleg zunanjih tudi notranje prevleke.

Študija obravnava področje na meji med dvema tehnologijama. Vsaka od njiju je dobro raziskana, v praksi pa med njima pogosto prihaja do interakcij, ki še niso bile raziskane ali kvantificirane.

Ključne besede: elektroerozijsko vrtanje, visokotlačna turbina, prevleke

*Naslov avtorja za dopisovanje: Tehniška univerza v Varšavi, Fakulteta za materiale in inženiring, Wołoska 141, 02-507 Varšava, Poljska, marcin.trajer.dokt@pw.edu.pl

Strojniški vestnik - Journal of Mechanical Engineering 68(2022)10, SI 80

Prejeto v recenzijo: 2022-06-20
Prejeto popravljeno: 2022-09-08
Prejeto popravljeno: 2022-09-09

Matematični model in analiza toplotnih lastnosti sten letalske kabine pod tlakom

Volodymyr Brazhenko[1,2] – Yibo Qiu[1] – Jiancheng Cai[1,2,*] – Dongyun Wang[1,2]

[1] Pedagoška univerza v Zhejiangu, Tehniški kolidž, Kitajska
2 Državni laboratorij province Zhejiang za tehnologije in opremo za pametno upravljanje in vzdrževanje v urbanem železniškem transportu, Kitajska

Članek obravnava prenos toplote skozi večslojni trup letalske kabine pod tlakom za oceno njegovih toplotnih lastnosti, ki vplivajo na mikroklimo v letalu. Obravnavani so celotna toplotna upornost, toplotna prehodnost in relativni temperaturni inkrementi. Posebna pozornost je posvečena lastnostim toplotnoizolacijskega sloja.

Ugodje v kabini je ena od glavnih prioritet pri projektiranju sodobnih potniških letal, dosežena pa je predvsem z izboljševanjem kakovosti in učinkovitosti zagotavljanja mikroklimatskih razmer. Na omenjene procese znatno vplivajo toplotne lastnosti sten letala.

Izdelan je bil matematični model in opravljena je bila računalniška analiza toplotne zaščite letalskih kabin pod tlakom. Porazdelitev termodinamičnih lastnosti v izolacijskem sloju s toplotnim »prevodnikom« je bila določena na podlagi enačbe prenosa toplote. Enačbe so bile razrešene numerično pri danih robnih pogojih po metodi končnih razlik. Ravna večslojna toplotna zaščita je bila modelirana ob predpostavki homogenih lastnosti posameznih slojev.

Oblikovan je bil model prenosa toplote skozi večslojno steno z zračno režo, ki omogoča analizo toplotnih lastnosti večslojne konstrukcije stene letalske kabine. Model je pokazal, da toplotna upornost toplotne zaščite neznatno raste z večanjem debeline zračne reže nad 30 mm. Z zmanjšanjem faktorja emisivnosti na mejah zračne reže je dosegljivo do 10-odstotno izboljšanje toplotne upornosti zaščite. Nezadostna debelina toplotnoizolacijskega sloja v coni toplotnega »prevodnika« v hladnih razmerah ter pri letu na večjih višinah povzroči znatno zmanjšanje toplotne zaščite letalske kabine pod tlakom. Toplotna prestopnost se poveča za več kot 40 %, temperaturna razlika med notranjo steno in zrakom v kabini pa se občutno zmanjša.

Članek obravnava prispevek toplotnega toka in vpliv konstrukcijskih parametrov toplotne zaščite na prenos toplote, kar je pomembno za projektiranje letalskih sistemov za klimatizacijo. Študija bo lahko uporabna pri razvoju lahkih izolacijskih materialov, pri študijah možnosti omejevanja nabiranja vlage v izolacijskih materialih ter pri iskanju novih rešitev za zaščito izolacijskih slojev pred vdorom vlage.

Ključne besede: matematično modeliranje, prenos toplote, toplotne lastnosti, letalska kabina pod tlakom, večslojna stena, toplotnoizolacijski sloj

*Naslov avtorja za dopisovanje: Pedagoška univerza v Zhejiangu, Tehniški kolidž, 688 Yingbin Road, Jinhua, Zhejiang Province, Kitajska, cai_jiancheng@foxmail.com

Strojniški vestnik - Journal of Mechanical Engineering 68(2022)10, SI 81

Prejeto v recenzijo: 2022-07-23
Prejeto popravljeno: 2022-09-16
Odobreno za objavo: 2022-09-28

Razvoj novega ekspertnega sistema za diagnostično obravnavo dizelskih motorjev za plovila na osnovi realnočasovnih diagnostičnih parametrov

Hla Gharib – György Kovács*
Univerza v Miskolcu, Fakulteta za strojništvo in informatiko, Inštitut za proizvodne znanosti, Madžarska

Z uvedbo primernih diagnostičnih strategij za motorje plovil je omogočeno zgodnje prepoznavanje potencialnih težav ter preprečevanje katastrofalnih in dragih posledic. Uspešno delovanje diagnostičnih sistemov in naprav za stroje je v veliki meri odvisno od dovršenosti diagnostičnih pristopov. Izbira primernih diagnostičnih parametrov je ključna za odkrivanje okvar in odpovedi v zgodnji fazi, saj se vsak parameter odziva na spremembe strukturnih parametrov motorja na drugačen način in v različni meri. Ti rezultati zagotavljajo dragocene informacije za točno lociranje okvar ter opisujejo odvisnosti med operativnimi in strukturnimi parametri.

Prvi cilj naše raziskave je bila izbira najbolj učinkovitih diagnostičnih parametrov za posamezne podsisteme dizelskih motorjev za plovila (npr. sistemi za dovod goriva, mazanje, hlajenje, dovod zraka in odvod izpušnih plinov) na podlagi statističnih študij in eksperimentov. Glavni cilj raziskave je bil razvoj na znanju temelječega diagnostičnega sistema za opredelitev tehničnega stanja celotnega motorja. Novi diagnostični ekspertni sistem je primeren za povečanje operativne učinkovitosti in zanesljivosti štiritaktnih dizelskih motorjev za plovila.

Vsak diagnostični parameter daje specifičen diagnostični signal, ki je odvisen od občutljivosti parametra na spremembe in na njihovo hitrost. Neposredna in posredna povezava med diagnostičnimi signali in različnimi napakami opredeljujeta primernost parametra za diagnostiko.

V naši raziskavi je bila uporabljena analiza korelacij kot statistični koncept, ki pojasnjuje odvisnosti med dvema ali več spremenljivkami glede na različne tipe podatkov, spremenljivke in merske enote v znanstvenih raziskavah. Koeficiente korelacije je mogoče izračunati na več načinov, namenjeni pa so preverjanju obstoja sorazmerne ali obratno sorazmerne oz. močne ali šibke odvisnosti med dvema spremenljivkama. V raziskavi so bili poleg korelacijskih metod opravljeni tudi poglobljeni razgovori s šestimi strokovnjaki (upravitelji ladijskega stroja) o možnostih uporabe njihovih praktičnih izkušenj in znanja pri razvoju našega novega ekspertnega sistema za diagnostično obravnavo. V ekspertni sistem so bili vgrajeni izbrani najpomembnejši diagnostični parametri in mnenja šestih upraviteljev ladijskega stroja v zvezi s specifičnimi pravili za različna stanja motorjev.

Najprej je podan pregled podsistemov dizelskega motorja za plovila ter njihovih možnih odpovedi in vplivov le-teh na delovanje motorja in njegovo stanje. Nato so opisane metode analize korelacije parametrov za ugotavljanje neposrednih in posrednih odvisnosti med diagnostičnimi signali ter različnimi napakami in stanji. Končno je predstavljen novi diagnostični ekspertni sistem skupaj s študijo primera tehnične diagnostike dizelskih motorjev za plovila.

Glavna dodana vrednost študije je v uvedbi novega diagnostičnega sistema, s katerim se lahko tudi neizkušeni uporabniki na ladjah učinkovito odzivajo v izrednih situacijah. Diagnostično orodje bo mogoče uporabljati na podsistemih motorjev za izboljšanje zanesljivosti ter učinkovitosti delovanja in vzdrževanja dizelskih motorjev za plovila.

Avtorji nameravajo v prihodnje razširiti bazo znanja na podlagi mnenj strokovnjakov z različnimi praktičnimi izkušnjami, kakor tudi nadgraditi ekspertni sistem z umetno inteligenco na podlagi že opravljenih diagnostičnih obravnav podobnih motorjev.

Ključne besede: motorji za plovila, diagnostični parametri, vzdrževanje, nov diagnostični ekspertni sistem, študija primera

*Naslov avtorja za dopisovanje: Univerza v Miskolcu, Fakulteta za strojništvo in informatiko, Inštitut za proizvodne znanosti, Madžarska, altkovac@uni-miskolc.hu

Guide for Authors

All manuscripts must be in English. Pages should be numbered sequentially. The manuscript should be composed in accordance with the Article Template given above. The suggested length of contributions is 10 to 20 pages. Longer contributions will only be accepted if authors provide justification in a cover letter. For full instructions see the Information for Authors section on the journal's website: http://en.sv-jme.eu .

SUBMISSION:

Submission to SV-JME is made with the implicit understanding that neither the manuscript nor the essence of its content has been published previously either in whole or in part and that it is not being considered for publication elsewhere. All the listed authors should have agreed on the content and the corresponding (submitting) author is responsible for having ensured that this agreement has been reached. The acceptance of an article is based entirely on its scientific merit, as judged by peer review. Scientific articles comprising simulations only will not be accepted for publication; simulations must be accompanied by experimental results carried out to confirm or deny the accuracy of the simulation. Every manuscript submitted to the SV-JME undergoes a peer-review process.

The authors are kindly invited to submit the paper through our web site: http://ojs.sv-jme.eu. The Author is able to track the submission through the editorial process - as well as participate in the copyediting and proofreading of submissions accepted for publication - by logging in, and using the username and password provided.

SUBMISSION CONTENT:

The typical submission material consists of:

- A **manuscript** (A PDF file, with title, all authors with affiliations, abstract, keywords, highlights, inserted figures and tables and references),
- Supplementary files:
  - a **manuscript** in a WORD file format
  - a **cover letter** (please see instructions for composing the cover letter)
  - a ZIP file containing **figures** in high resolution in one of the graphical formats (please see instructions for preparing the figure files)
  - possible **appendicies** (optional), cover materials, video materials, etc.

Incomplete or improperly prepared submissions will be rejected with explanatory comments provided. In this case we will kindly ask the authors to carefully read the Information for Authors and to resubmit their manuscripts taking into consideration our comments.

COVER LETTER INSTRUCTIONS:

Please add a **cover letter** stating the following information about the submitted paper:

1. Paper **title**, list of **authors** and their **affiliations**. **One** corresponding author should be provided.
2. **Type of paper**: original scientific paper (1.01), review scientific paper (1.02) or short scientific paper (1.03).
3. A **declaration** that neither the manuscript nor the essence of its content has been published in whole or in part previously and that it is not being considered for publication elsewhere.
4. State the **value of the paper** or its practical, theoretical and scientific implications. What is new in the paper with respect to the state-of-the-art in the published papers? Do not repeat the content of your abstract for this purpose.
5. We kindly ask you to suggest at least two **reviewers** for your paper and give us their names, their full affiliation and contact information, and their scientific research interest. The suggested reviewers should have at least two relevant references (with an impact factor) to the scientific field concerned; they should not be from the same country as the authors and should have no close connection with the authors.

FORMAT OF THE MANUSCRIPT:

The manuscript should be composed in accordance with the Article Template. The manuscript should be written in the following format:

- A **Title** that adequately describes the content of the manuscript.
- A list of **Authors** and their **affiliations**.
- An **Abstract** that should not exceed 250 words. The Abstract should state the principal objectives and the scope of the investigation, as well as the methodology employed. It should summarize the results and state the principal conclusions.
- 4 to 6 significant **key words** should follow the abstract to aid indexing.
- 4 to 6 **highlights;** a short collection of bullet points that convey the core findings and provide readers with a quick textual overview of the article. These four to six bullet points should describe the essence of the research (e.g. results or conclusions) and highlight what is distinctive about it.
- An **Introduction** that should provide a review of recent literature and sufficient background information to allow the results of the article to be understood and evaluated.
- A **Methods** section detailing the theoretical or experimental methods used.
- An **Experimental section** that should provide details of the experimental set-up and the methods used to obtain the results.
- A **Results** section that should clearly and concisely present the data, using figures and tables where appropriate.
- A **Discussion** section that should describe the relationships and generalizations shown by the results and discuss the significance of the results, making comparisons with previously published work. (It may be appropriate to combine the Results and Discussion sections into a single section to improve clarity.)
- A **Conclusions** section that should present one or more conclusions drawn from the results and subsequent discussion and should not duplicate the Abstract.
- **Acknowledgement** (optional) of collaboration or preparation assistance may be included. Please note the source of funding for the research.
- **Nomenclature** (optional). Papers with many symbols should have a nomenclature that defines all symbols with units, inserted above the references. If one is used, it must contain all the symbols used in the manuscript and the definitions should not be repeated in the text. In all cases, identify the symbols used if they are not widely recognized in the profession. Define acronyms in the text, not in the nomenclature.
- **References** must be cited consecutively in the text using square brackets [1] and collected together in a reference list at the end of the manuscript.
- **Appendix(-icies)** if any.

SPECIAL NOTES

Units: The SI system of units for nomenclature, symbols and abbreviations should be followed closely. Symbols for physical quantities in the text should be written in italics (e.g. *v*, *T*, *n*, etc.). Symbols for units that consist of letters should be in plain text (e.g. ms^{-1}, K, min, mm, etc.). Please also see: http://physics.nist.gov/cuu/pdf/sp811.pdf .

Abbreviations should be spelt out in full on first appearance followed by the abbreviation in parentheses, e.g. variable time geometry (VTG). The meaning of symbols and units belonging to symbols should be explained in each case or cited in a **nomenclature** section at the end of the manuscript before the References.

Figures (figures, graphs, illustrations digital images, photographs) must be cited in consecutive numerical order in the text and referred to in both the text and the captions as Fig. 1, Fig. 2, etc. Figures should be prepared without borders and on white grounding and should be sent separately in their original formats. If a figure is composed of several parts, please mark each part with a), b), c), etc. and provide an explanation for each part in Figure caption. The caption should be self-explanatory. Letters and numbers should be readable (Arial or Times New Roman, min 6 pt with equal sizes and fonts in all figures). Graphics (submitted as supplementary files) may be exported in resolution good enough for printing (min. 300 dpi) in any common format, e.g. TIFF, BMP or JPG, PDF and should be named Fig1.jpg, Fig2.tif, etc. However, graphs and line drawings should be prepared as vector images, e.g. CDR, AI. Multi-curve graphs should have individual curves marked with a symbol or otherwise provide distinguishing differences using, for example, different thicknesses or dashing.

Tables should carry separate titles and must be numbered in consecutive numerical order in the text and referred to in both the text and the captions as Table 1, Table 2, etc. In addition to the physical quantities, such as *t* (in italics), the units [s] (normal text) should be added in square brackets. Tables should not duplicate data found elsewhere in the manuscript. Tables should be prepared using a table editor and not inserted as a graphic.

REFERENCES:

A reference list must be included using the following information as a guide. Only cited text references are to be included. Each reference is to be referred to in the text by a number enclosed in a square bracket (i.e. [3] or [2] to [4] for more references; do not combine more than 3 references, explain each). No reference to the author is necessary.

References must be numbered and ordered according to where they are first mentioned in the paper, not alphabetically. All references must be complete and accurate. Please add DOI code when available. Examples follow.

Journal Papers:

Surname 1, Initials, Surname 2, Initials (year). Title. *Journal*, volume, number, pages, DOI code.

[1] Hackenschmidt, R., Alber-Laukant, B., Rieg, F. (2010). Simulating nonlinear materials under centrifugal forces by using intelligent cross-linked simulations. *Strojniški vestnik - Journal of Mechanical Engineering,* vol. 57, no. 7-8, p. 531-538, DOI:10.5545/sv-jme.2011.013.

Journal titles should not be abbreviated. Note that journal title is set in italics.

Books:

Surname 1, Initials, Surname 2, Initials (year). Title. Publisher, place of publication.

[2] Groover, M.P. (2007). *Fundamentals of Modern Manufacturing*. John Wiley & Sons, Hoboken.

Note that the title of the book is italicized.

Chapters in Books:

Surname 1, Initials, Surname 2, Initials (year). Chapter title. Editor(s) of book, book title. Publisher, place of publication, pages.

[3] Carbone, G., Ceccarelli, M. (2005). Legged robotic systems. Kordić, V., Lazinica, A., Merdan, M. (Eds.), Cutting Edge Robotics. Pro literatur Verlag, Mammendorf, p. 553-576.

Proceedings Papers:

Surname 1, Initials, Surname 2, Initials (year). Paper title. Proceedings title, pages.

[4] Štefanić, N., Martinčević-Mikić, S., Tošanović, N. (2009). Applied lean system in process industry. *MOTSP Conference Proceedings*, p. 422-427.

Standards:

Standard-Code (year). Title. Organisation. Place.

[5] ISO/DIS 16000-6.2:2002. *Indoor Air – Part 6: Determination of Volatile Organic Compounds in Indoor and Chamber Air by Active Sampling on TENAX TA Sorbent, Thermal Desorption and Gas Chromatography using MSD/FID.* International Organization for Standardization. Geneva.

WWW pages:

Surname, Initials or Company name. Title, from http://address, date of access.

[6] Rockwell Automation. Arena, from *http://www.arenasimulation.com,* accessed on 2009-09-07.

EXTENDED ABSTRACT:

When the paper is accepted for publishing, the authors will be requested to send an **extended abstract** (approx. one A4 page or 3500 to 4000 characters or approx. 600 words). The instruction for composing the extended abstract are published on-line: http://www.sv-jme.eu/information-for-authors/ .

COPYRIGHT:

Authors submitting a manuscript do so on the understanding that the work has not been published before, is not being considered for publication elsewhere and has been read and approved by all authors. The submission of the manuscript by the authors means that the authors automatically agree to publish the paper uder CC-BY 4.0 Int. or CC-BY-NC 4.0 Int. when the manuscript is accepted for publication. All accepted manuscripts must be accompanied by a Copyright Agreement, which should be sent to the editor. The work should be original work by the authors and not be published elsewhere in any language without the written consent of the publisher. The proof will be sent to the author showing the final layout of the article. Proof correction must be minimal and executed quickly. Thus it is essential that manuscripts are accurate when submitted. Authors can track the status of their accepted articles on https://en.sv-jme.eu/.

PUBLICATION FEE:

Authors will be asked to pay a publication fee for each article prior to the article appearing in the journal. However, this fee only needs to be paid after the article has been accepted for publishing. The fee is 380 EUR (for articles with maximum of 6 pages), 470 EUR (for articles with maximum of 10 pages), plus 50 EUR for each additional page. The additional cost for a color page is 90.00 EUR (only for a journal hard copy; optional upon author's request). These fees do not include tax.

9 770039 248001
ISSN 0039-2480

http://www.sv-jme.eu

Contents

Papers

585 Nejc Rožman, Marko Corn, Gašper Škulj, Janez Diaci, Primož Podržaj:
Scalability Solutions in Blockchain-Supported Manufacturing: A Survey

610 Mateusz Wrzochal, Stanisław Adamczak, Ryszard Domagalski, Grzegorz Piotrowicz, Sylwester Wnuk:
A New Device Proposed for the Industrial Measurement of Rolling Bearing Friction Torque

623 Marcin Trajer, Łukasz Pyclik, Jerzy Robert Sobiecki:
The Nickel Aluminide Coatings Obtained on Small Holes Produced with the EDD Method

635 Volodymyr Brazhenko, Yibo Qiu, Jiancheng Cai, Dongyun Wang:
Thermal Evaluation of Multilayer Wall with a Hat-Stringer in Aircraft Design

642 Hla Gharib, György Kovács:
Development of a New Expert System for Diagnosing Marine Diesel Engines Based on Real-Time Diagnostic Parameters